Distribution Agreement

In presenting this dissertation as a partial fulfillment of the requirements for an advanced degree from Emory University, I hereby grant to Emory University and its agents the non-exclusive license to archive, make accessible, and display my dissertation in whole or in part in all forms of media, now or hereafter known, including display on the World Wide Web. I understand that I may select some access restrictions as part of the online submission of this dissertation. I retain all ownership rights to the copyright of the dissertation. I also retain the right to use in future work (such as articles and books) all or part of this dissertation.

Signature:

_____ _____

Shengye Jin Date

Interfacial Electron Transfer Dynamics from Single Molecules and Quantum Dots Studied by Single-Molecule Fluorescence Spectroscopy

By

Shengye Jin

Doctor of Philosophy

Chemistry

_____

Dr. Tianquan Lian
Advisor

_____

Dr. Michael C. Heaven
Committee Member

_____

Dr. James T. Kindt
Committee Member

Accepted:

_____

Lisa A. Tedesco, Ph.D.

Dean of the James T. Laney School of Graduate Studies

_____

Date

Interfacial Electron Transfer Dynamics from Single Molecules and Quantum Dots Studied by Single-Molecule Fluorescence Spectroscopy

By

Shengye Jin

B.E., Dalian University of Technology, Dalian, China, 2001

M.S., Dalian Institute of Chemical Physics, Chinese Academy of Sciences, Dalian, China, 2004

Advisor: Tianquan Lian, Ph.D.

An Abstract of
A dissertation submitted to the Faculty of the
James T. Laney School of Graduate School of Emory University
in partial fulfillment of the requirements for the degree of
Doctor of Philosophy
in Chemistry
2010

ABSTRACT

Interfacial Electron Transfer Dynamics from Single Molecules and Quantum Dots Studied by Single-Molecule Fluorescence Spectroscopy

By Shengye Jin

Interfacial electron transfer (ET) dynamics from single organic molecules and quantum dots (QDs) to semiconductor nanocrystalline thin films or molecular electron acceptors have been studied by using single-molecule fluorescence spectroscopy.

The photoinduced interfacial ET dynamics in sulforhodamine B (SRhB)-aminosilane-TiO_2/SnO_2 nanoparticle (donor-bridge-acceptor) complexes have been studied on the single molecule level. The presence of the silane bridge enabled the complete sampling of these molecules under single molecule conditions. Shorter fluorescence lifetimes for molecules on TiO_2 and SnO_2 compared to on ZrO_2 were observed and attributed to ET from SRhB to TiO_2 and SnO_2. The single molecule fluorescence lifetimes fluctuated with time and varied among single donor-bridge-acceptor complexes, suggesting that both static and dynamic ET rate distributions contribute to the heterogeneity of ET in this system. Computational modeling of the complexes showed a distribution of molecular conformations, leading to a distribution of electronic coupling strengths and ET rates.

The ET dynamics from single CdSe core/multi-shell QDs to adsorbed Fluorescein (F27) molecules and to TiO_2 nanoparticles have also been studied by single particle spectroscopy. The QDs in both systems showed intermittent ET dynamics modulated by their blinking activities. The excited state lifetime of QDs in the “on” state reflected the ET rate, whereas in the “off” state, QD excitons decayed by fast non-radiative Auger relaxation. Furthermore, interfacial ET provided an additional pathway for generating

"off" states, leading to the intermittent ET dynamics. The ET dynamics from single QDs to TiO_2 rutile (110) and (001) single crystals were also studied. The preliminary results have shown that QDs on rutile (110) had much narrower ET rate distributions compared to QDs on TiO_2 nanoparticles. The ET rates for QDs on rutile (110) and (001) were found to differ, probably due to the different surface structures of these two single crystals.

The exciton quenching dynamics of QDs on ITO were also studied and compared with results for QDs on In_2O_3 and glass. Single QDs on ITO showed suppressed blinking activities and reduced fluorescence lifetimes, which was attributed to negative charging of the QDs. In these negatively charged QDs, the off states were suppressed due to the effective removal of the valence band holes, and their fluorescence lifetimes were shortened because of Auger relaxation processes involving the additional electrons.

Interfacial Electron Transfer Dynamics from Single Molecules and Quantum Dots Studied by Single-Molecule Fluorescence Spectroscopy

By

Shengye Jin

B.E., Dalian University of Technology, Dalian, China, 2001

M.S., Dalian Institute of Chemical Physics, Chinese Academy of Sciences, Dalian, China, 2004

Advisor: Tianquan Lian, Ph.D.

An Abstract of
A dissertation submitted to the Faculty of the
James T. Laney School of Graduate School of Emory University
in partial fulfillment of the requirements for the degree of
Doctor of Philosophy
in Chemistry
2010

ACKNOWLEDGEMENT

First and foremost I would like to express my wholehearted gratitude to my supervisor Dr. Tianquan Lian for his guidance and encouragement during my graduate studies. As my supervisor, Dr. Lian has taught me not only the scientific knowledge but also how to be a good scientist. It is my great honor to be one of his students. I also want to express my sincere appreciation to my committee members, Dr. James Kindt and Dr. Michael Heaven, for their advice and valuable time.

I want to express my great appreciation to my coworker and friend Dr. Abey Issac whom I have been working with for two years. It was a great experience of working with Dr. Issac. He was always positive and has given me many valuable advices and helps both in my studies and in my life.

I highly appreciate all my current and former group members: Dr. Jianqiang Guo, Dr. Chunxing She, Dr. David Stockwell, Zhuangqun Teddy Huang, Chantelle Anfuso, Jier Huang, Nianhui Song, Haiming Zhu, Ye Yang, David Wu, and Dr. Weimin Liu. They are always good collaborators in my work and good friends in my life.

I also want to express my special thanks to Jung-Cheng Hsiang in Dr. Dickson's group at Georgia Institute of Technology, for his great help in programming for my data analysis and thoughtful discussions in my studies.

Finally, I cannot thank enough my entire family. My parents, parents-in-law and my sisters always encourage and support me during my studies in US. My wife, Dan Shi, gives her unconditional love and care to me. She has always been supporting and encouraging me whenever I have difficulties in my research and in my life. Their love and care are the prime source of incentive for me to accomplish more.

Table of Contents

List of Figures

Chapter 1

Chapter 2

Chapter 3

Chapter 5

Chapter 6

List of Tables

Chapter 1. Introduction

1.1 Single-Molecule Fluorescence Spectroscopy and Interfacial Electron Transfer

1.1.1 Single-Molecule Fluorescence Spectroscopy

Single-molecule fluorescence spectroscopy (SMFS) has been recognized as an important spectroscopic technique for almost two decades now.[1-3] Unlike traditional ensemble-averaged measurements, single-molecule techniques allow for the detection of individual molecules (or particles) and are thus able to reveal the hidden dynamic and static heterogeneities masked in ensemble studies. SMFS also provides detailed insights into the photophysical processes or molecular dynamics for a particular system.

Single-molecule fluorescence measurements are mostly carried out in a scanning confocal microscope. Laser light of an appropriate wavelength (λ) is focused to a diffraction limited ($\lambda/2$) spot on the sample surface through the confocal microscope in order to excite the dye molecules. The resulting photoluminescence is collected by the microscope and detected by appropriate detectors. Chromophores with large absorption cross-sections and high fluorescence quantum yields are preferred in order to maximize the signal-to-noise ratio. If the molecules on the sample surface are located far enough away from each other (the average distance between molecules should be $> \lambda/2$), only one molecule is photoexcited at a time, and the fluorescence from only that single molecule is collected. Plots of fluorescence intensity as a function of time (fluorescence intensity trajectories) can then be obtained, revealing dynamics on the millisecond (ms) to second (s) time scale. Furthermore, when using pulsed lasers and time-correlated single photon counting (TCPSC), fluorescence lifetime trajectories can be gathered,

revealing the dynamics on the hundreds of picoseconds (ps) to nanoseconds (ns) time scale. An emission spectrum trajectory of a single molecule can also be constructed by using a spectrometer at the detector.

Overall, SMFS is a powerful tool that has been applied in many studies ranging from biomolecular dynamics[4-6] and biological imaging,[7,8] to interfacial charge transfer dynamics.[9-17] Interfacial electron transfer (ET) processes can lead to changes in single molecule fluorescence intensities that can be detected and analyzed. The studies being presented in this work focus on interfacial ET dynamics from single molecules and single quantum dots. These topics will be introduced and discussed in detail in later sections.

1.1.2 Using SMFS to study interfacial ET

Photoinduced interfacial electron transfer (ET) is a widely studied process due to its applications in solar cells[18-20], photocatalysis[21,22] and molecular electronics[23-25]. The studies on this topic have recently become more intense due to the increasing demand for environmentally clean solar energy sources. Motivated by the desire to understand and optimize the performance of solar conversion devices, the interfacial ET dynamics between molecules, QDs and semiconductor oxides have been extensively investigated.[26-52] In most previous studies, the ET dynamics were measured on the ensemble-averaged level. Typically, transient absorption spectroscopy is used to directly examine charge transfer dynamics through spectroscopic identification of various species, such as ground, excited, reduced and oxidized forms of the electron donors and acceptors, at different delays times ranging from hundreds of femtoseconds (fs) to tens of microseconds (μs).

The interfacial ET dynamics can also be probed by time-resolved fluorescence spectroscopy. The fluorescence decay rate of chromophores in an inactive ET state can be represented by the following equation:

$$\frac{1}{\tau} = k_r + k_{nr} = k_0 \qquad \text{(Eq. 1.1)}$$

where τ is the observed fluorescence lifetime and k_r and k_{nr} are the radiative and nonradiative decay rates, respectively. In the active ET state, the fluorescence lifetimes can be shortened as follows:

$$\frac{1}{\tau'} = k_r + k_{nr} + k_{et} = k_0 + k_{et} \qquad \text{(Eq. 1.2)}$$

where k_{et} is the interfacial ET rate. The ET dynamics can then be resolved by comparing the lifetimes with and without ET activation.

Previous ensemble-averaged measurements have revealed multi-exponential ET dynamics for numerous systems,[26,32-36,38-41,44,45,47,53-76] suggesting a distribution of ET rates which transient absorption and ensemble fluorescence techniques cannot distinguish. However, single-molecule fluorescence spectroscopy has demonstrated the capability to examine the hidden static and dynamic heterogeneities in interfacial ET processes.[9-12 13-15,77] The study of interfacial ET from single molecules or particles explores how the behavior of molecules and particles may differ between each other at different times, how the molecules are affected by their local environments, and how their ET dynamics can affect or be affected by their fluorescence properties. Single-molecule fluorescence spectroscopy thus reveals the details in the interfacial ET dynamics that are obscured by ensemble averaging. For example, the intermittent ET

dynamic from QDs to their molecular adsorbates were only observed and understood through single QD measurements.

The research presented in this work focuses on the ET dynamics from single molecules and single particles (QDs) to various semiconductor oxides and molecular adsorbates. The details of these two ET systems (molecules and QDs) will be introduced separately in the later sections in this chapter.

1.2 Interfacial Electron Transfer from Single Molecules

Figure 1.1 shows the photoinduced processes of dye molecules adsorbed on semiconductor nanoparticles. The dye molecules are electronically excited through light absorption, permitting ET to the conduction band.

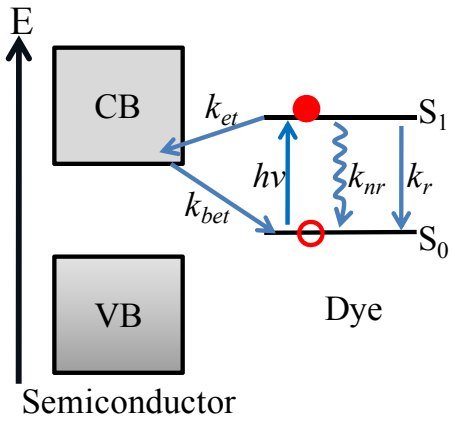

Figure 1.1. Schematic representation of the photoinduced processes of dye molecules sensitized on semiconductor nanoparticles. k_r: radiative decay rate; k_{nr}: intrinsic nonradiative decay rate; k_{et}: rate of ET from excited molecule to semiconductor; k_{bet}: back electron transfer (BET) rate.

One applilcation based on this photoinduced ET process is the dye-sensitized solar cell (DSSC), consisting of two electrodes in a sandwich configuration with electrolyte in between, which is believed to be a low-cost alternative to traditional silicon-based solar cells.[18-20,78-83] TiO_2 is the most commonly used semiconductor film in DSSCs,[18,19,78] and the solar cells based on TiO_2 have shown promising efficiencies. For example, dye-sensitized solar cells utilizing ET from $Ru(dcbpy)_2(NCS)_2$ [called RuN3, dcbpy = (4,4'-dicarboxy-2,2'-bipyridine)] to TiO_2 nanocrystalline thin films have achieved solar-to-electric power conversion efficiencies as high as 10%.[18,84]

Although the ensemble-averaged ET dynamics from dye molecules such as RhB,[85] Courmine[86] and RuN3[18,84] to various semiconductors such as TiO_2,[18,19,78,86] SnO_2,[85,87,88] ZnO,[35,86,88,89] In_2O_3[85,88,89] have been extensively investigated, the single molecule ET dynamics of these dye molecules are still poorly understood. Studying interfacial ET dynamics from single molecules has been an appealing and challenging effort since the first report of observed single molecule ET dynamics in 1997, when Lu and Xie studied ET from single cresyl violet molecules to indium tin oxide (ITO).[9] Their pioneering work demonstrated the capability to detect single molecule ET dynamics using single-molecule fluorescence spectroscopy. A wide distribution of ET rates caused by the inhomogeneity of molecular interactions on the semiconductor surface was observed in their experiments and was used to explain the physical origin of the multiexponential kinetics of ET.

Unfortunately, there are only a few published reports on this topic after their intial work.[10-12,17] The main challenge in conducting these single molecule experiments is the ultrafast ET rate ($\leq$ 10 ps), which significantly quenches the fluorescence and hinders the

observation of single molecules undergoing ET. For the photoinduced processes represented in Figure 1.1, the quantum yield of a dye molecule undergoing ET is:

$$\Phi_f = \frac{K_r}{K_0 + K_{et}} \qquad \text{(Eq. 1.3)}$$

Assuming that the intrinsic lifetime and quantum yield of a dye molecule are 3 ns and 100%, respectively, and the ET time is 10 ps on a given semiconductor, the quantum yield of this dye molecule under ET conditions is estimated to be 0.3%, far beyond the sensitivity of current single-molecule fluorescence spectroscopy techniques. The fluorescence quenching of molecules undergoing ET has been verified by the studies of single RhB molecules on antimony doped tin oxide (ATO).[12] It was noted that the number of observed (bright) molecules on ATO was much smaller than that on glass. Additionally, the ET rates derived from single-molecule measurements were much slower than those derived from ensemble-averaged transient absorption measurements due to incomplete sampling of molecules undergoing fast ET in the single molecule study.

One of the strategies used to enable studies of single molecule ET dynamics is to develop an electron donor-bridge-acceptor complex, where the presence of the bridge slows down the ET rate and allows for the observation of single molecules undergoing ET. Adams et al. have reported using single-molecule spectroscopy to measure the interfacial ET rate in a perylene chromophore-carboxylic acid terminated aliphatic bridge-ITO electrode system.[10] By analyzing the fluctuations in the fluorescence intensity trajectories, ET as well as back ET was resolved on the second time scale. Although their work contributed to the fundamental studies on single molecule ET dynamics, this slow ET rate significantly reduces the practical applications of this ET system.

More recently, Lu and coworkers reported studies on single molecule ET dynamics for cresyl-violet, courmin and porphyrin molecules on TiO_2 nanoparticles.[11,90] These molecules on TiO_2 exhibited vigorous fluctuations in fluorescence intensities, and the ET times estimated by the fluorescence lifetimes were much slower than those measured by ensemble-averaged transient absorption spectroscopy. To explain the discrepancy between single molecule and ensemble average measurements, they suggested a model for the intermittent ET dynamics, according to which the ET rate on TiO_2 fluctuated between fast (on) and slow (off) states. In the "off" state, molecules underwent slow (or no) ET and the fluorescence intensities were high, and thus all detected fluorescence photons originated from the slow injecting states. In the "on" state, however, the molecules were undergoing ultrafast ET, but the fluorescence quantum yield of the fast injecting state was too low to be observed. The physical origin of the fluctuation of the ET rate was attributed to spontaneous thermal motions of the molecules, which led to changes in the electronic coupling between the molecules and substrates.

Based on their intermittent ET model, Lu and coworkers continued their studies by probing the single molecule charge recombination dynamics through the statistics of photon to photon pair times for ZnTCPP on TiO_2 nanoparticles.[90] However, the physical reasons behind their intermittent ET model are still not clear. The proposed model is also unable to explain the complete "disappearance" (fluorescence quenching) of dye molecules observed in other dye/semiconductor ET systems.[12,17]

In this work, we will present our studies on interfacial ET dynamics in electron donor-bridge-acceptor complexes. The ET time is found to be on a few ns time scale, indicating the observation of the majority of molecules undergoing ET using single-

molecule fluorescence spectroscopy. The details of this research project will be discussed in Chapter 3.

1.3 Interfacial Electron Transfer from Single QDs

1.3.1 Introduction

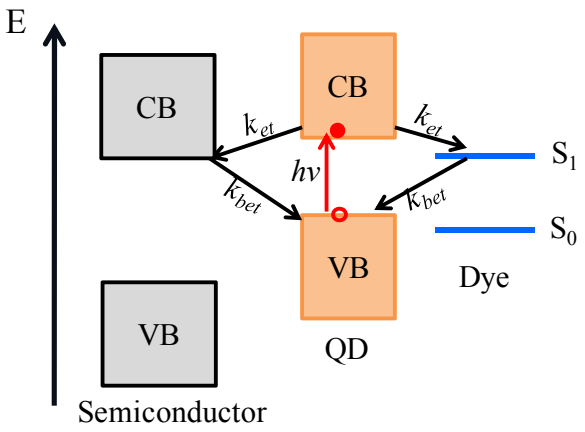

Figure 1.2. Schematic representation of photoinduced ET processes from QDs to semiconductor or molecular adsorbates.

Semiconductor quantum dots (QDs) such as CdS and CdSe can also serve as sensitizers in light conversion devices, because they can transfer electrons to long-band-gap semiconductors such as TiO_2 and SnO_2 and some particular molecules under visible light excitation, as shown in Figure 1.2. Because QDs exhibit special properties that are not available in traditional molecular sensitizers, QD solar cells have also been considered as a promising low-cost alternative to conventional silicon-based cells in recent years.[91-95] The advantages of using QDs as sensitizers are attractive. First, QDs have tunable band gaps which offer the opportunity to improve light harvesting

capabilities over conventional cells.[96-99] Secondly, QDs can generate multi excitons by absorbing only one photon, providing the possibility of improving the efficiency of QD-based light conversion devices.[100-106] This process, known as multi-exciton generation (MEG), does not occur in bulk semiconductors where the extra energy simply dissipates away as heat before it can cause another exciton to form.

For the purpose of improving the performance of QD-based light conversion devices, the interfacial ET dynamics in QD/semiconductor oxide and QD/molecular adsorbate systems have been studied.[44-52] Although previous studies conducted on the ensemble-averaged level have contributed considerably to the current understanding of ET dynamics to and from QDs, the study on the single QD level is also necessary because of the unique fluorescent properties of QDs which may play an important role in QD-based devices.

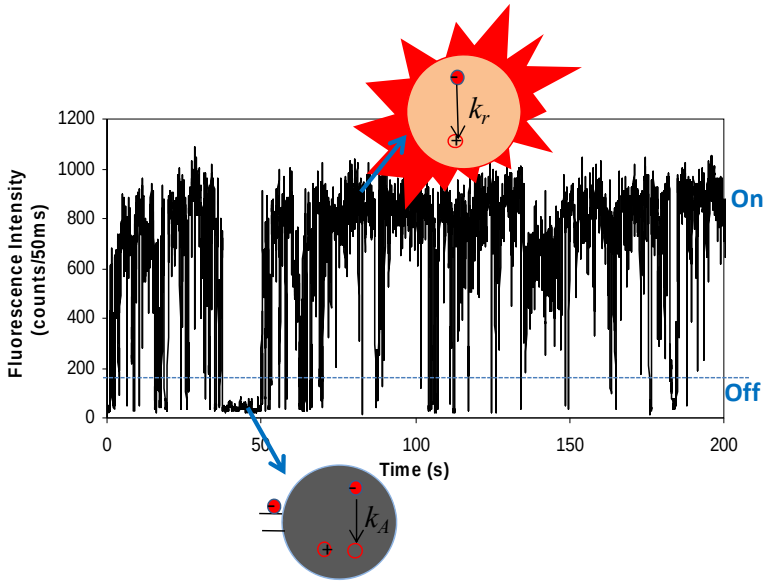

Figure 1.3. A typical fluorescence intensity trajectory of a single QD on glass exhibiting blinking activity. The high intensity (on state) corresponds to the neutral state of the QD and the low intensity (off state) corresponds to a positively charged state of the QD.

A prominent property of QDs is their fluorescence intermittence, known as blinking.[107-128] This phenomenon is buried in ensemble fluorescence detection and can only be probed by using single QD measurements. Shown in Figure 1.3 is a typical fluorescence intensity trajectory of a single CdSe core/multishell QD on glass, presenting a strong fluorescence fluctuation between high intensity (defined as the on state) and low intensity (defined as the off state) levels. This blinking activity is attributed to the photoinduced charging of the QD through the transfer of an electron to the trap states in and around the QD.[107-110,114,118,127,128] As shown in Figure 1.3, the on state is neutral and the QD exciton recombines through a radiative decay pathway, while in the off state the QD is positively charged with an electron in the trap state and a hole in the QD. Under photoexcitation, the exciton recombines through nonradiative fast Auger relaxation, quenching the fluorescence. The physical origins of the blinking activity have been also studied.[117] The formation of positively charged QDs is suggested to result from the generation of multiple excitons, as shown in Figure 1.4. Under continuous illumination, the chance that the QD will produce multiple excitons increases. The formation of multi excitons leads to the exciton-exciton annihilation process, in some cases transferring one electron to the trap state and forming a positively charge QD.

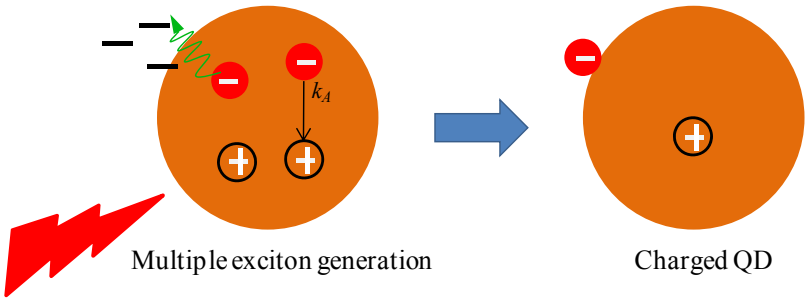

Figure 1.4. The formation of a positively charged QD through multi exciton generation.

QD blinking is not an independent activity, but is related to other photophysical and photochemical processes involving QDs. For example, it has been reported that the photoinduced charging effect can result in spectral diffusion by changing the local electric field of QDs.[119,129-131] Therefore, the presence of QD blinking activities triggers important fundamental questions about the interfacial ET to and from QDs. How does this blinking activity affect the interfacial ET dynamics? How does the interfacial ET influence the fluorescence properties of QDs? Are there any correlations between blinking and interfacial ET dynamics? How do the properties of semiconductor oxide substrates affect the blinking and ET processes?

In an effort to explore the answers for the above mentioned questions, the research presented in this work focuses on the single QD ET and blinking dynamics in QD/molecular adsorbate and QD/semiconductor oxide complexes. The studies on these two types of complexes will be introduced separately in the following sections.

1.3.2 ET from QDs to molecular adsorbates

Interfacial charge transfer from QDs to their molecular adsorbates is currently of intense interest due to its potential application in multiple exciton dissociation. Previous studies on this type of system have indicated the possibility of separating multiple excitons through ultrafast electron or hole transfer from QDs to adsorbed molecules before exciton-exciton annihilation occurs.[45,47-49,132-136] More recently, Lian's group reported their study on multiple exciton dissociation through ultrafast interfacial ET from CdSe QDs to adsorbed methylene blue by transient absorption spectroscopy.[136] They have shown that the excitons in the QDs dissociate by ultrafast electron transfer to

adsorbed molecules with an average time constant of ~ 2 picoseconds, and up to three adsorbed molecules per QD could be reduced by exciton dissociation.

To gain further insight into the dynamics of charge transfer from QDs, ET on the single QD level has also been investigated.[13-15,77] Lian's group reported for the first time single QD ET from CdSe core/multi-shell QDs to adsorbed fluorescein 27 (F27) molecules.[13] In this study, QDs undergoing ET exhibited much stronger fluorescence and lifetime fluctuations than intrinsic QDs (without ET), indicating intermittent ET dynamics. Similar ET dynamics in single CdTe-pyromellitimide complexes were also observed and reported by another group.[14] This fluctuating ET activity was suggested to arise from a change of charge states in the QDs, which may affect the driving force and/or electronic coupling strength of electron transfer to acceptors. However, the origins of the intermittent ET dynamics are still poorly understood, and the correlation between blinking (photoinduced charging) and interfacial ET is still unclear.

In order to further explore the origins of the observed intermittent ET activity, we have conducted a systemic study of ET dynamics in single QD-F27 complexes in which the ET rate was modulated by the number of adsorbed F27 molecules. The details of this study will be presented in Chapter 4.

1.3.3 ET from QDs to semiconductor oxides

Although the QD-based solar cell is considered a promising solar conversion device with some specific advantages over DSSC, current QD solar cells based on the combination of QDs with various semiconductor oxides (such as TiO_2 and SnO_2) only achieve a power-conversion efficiency of 2%,[51,137-140] significantly lower than the 11%

power-conversion efficiency realized by DSSCs.[141-143] This can be partially attributed to the lack of fundamental understanding of the charge transfer and recombination dynamics between QDs and semiconductor nanocrystalline films and their controlling factors. For example, the ET rate from sensitized CdSe QDs to TiO_2 nanocrystalline thin films ranges from hundreds of picoseconds to a few nanoseconds for different QD sizes. These ET rates are much lower than those seen in DSSCs and QD/molecular adsorbate ET systems. Therefore, further investigations of ET dynamics from QDs to semiconductor oxides are highly desirable.

In an effort to improve the efficiency of QD based solar cells, most previous studies have focused on surface chemistry that may help improve the QD coverage on substrates,[144] fabrication of hybrid nanostructures which can increase the efficiency of electron transfer and transportation,[20,138,139] and exploration of the controlling factors that modulate QD ET dynamics.[44,45,145,146] For example, Kamat's group has reported a modulation of the ET rate from CdSe QDs to TiO_2 by tuning the size of the QDs and changing the medium alkalinity.[44,145] However, there are still very few reports on interfacial ET dynamics from single QDs to semiconductor oxides.

In this work, we present our study on interfacial ET dynamics from single CdSe core/multishell QDs to TiO_2 nanoparticles and rutile single crystals. The details of this investigation will be discussed in Chapter 5.

1.3.4 Fluorescence and ET dynamics of QDs on conducting materials

Besides QD-based light conversion devices, another important application of QDs is QD light-emitting-devices (QD-LED),[147-150] which also involve charge transfer between

QDs and their substrates. This device utilizes the electroluminescence of QDs under bias voltage, where the use of QDs as the light source offers specific advantages such as high color purity and durability.[151] The most popular conducting materials used in these devices are ITO, FTO (fluorine doped tin oxide) and gold. QDs on these conducting materials exhibit significantly different optical properties.[128,152,153,154] For example, blinking suppression and lifetime reduction have been observed for single QDs on nanostructured metal substrates.[128,152,153] The reduction in lifetime was attributed to an increase of the radiative decay rate caused by the enhancement of the electromagnetic field strength on roughened metal surfaces. The suppression of blinking in QDs may be caused by a shortened ionized period through fast charge recombination processes and/or an enhancement of the radiative decay rate, which enables the observation of charged QDs. More recently, CdSe/CdS core/shell QDs were reported to be negatively charged on ITO under negative bias voltage.[154] Upon photoexcitation, negative trions (an exciton and an electron) were formed and the QD lifetimes were greatly reduced.

In order to understand how the optical properties can be altered for QDs in a device environment, we studied fluorescence and lifetime dynamics of single QDs on an ITO surface, where both charging and ET are allowed. We observed that the QDs on ITO presented suppressed blinking dynamics and the photoinduced interfacial ET from QDs to ITO was reduced due to the negative charging of the QDs. The details of this study will be discussed in Chapter 6.

1.4 Summary

In summary, the interfacial electron transfer dynamics from single molecules and single QDs have been investigated by using single-molecule fluorescence spectroscopy.

These studies on the single molecule or single particle level are essential because they can reveal static and dynamic heterogeneities that remain hidden in ensemble measurements and provide detailed insights into the electron transfer process. Studies of interfacial ET from single molecules have been enabled by developing a donor-bridge-acceptor complex, and have revealed broad distributions and dynamic fluctuations of ET rates for various molecules on TiO_2 and SnO_2, which explains the non-single exponential ET kinetics observed in ensemble measurements. In QD ET systems, intermittent ET dynamics from QDs to molecular adsorbates and semiconductor oxides have been observed though single QD measurements. The intermittent ET dynamics are correlated with single QD blinking (charging) activity, which can only be examined on the single QD level. Additionally, QDs on electric conducting materials have also been investigated on both the single particle and ensemble levels, presenting unique fluorescence and lifetime properties.

The rest of this work will be organized as follows: Chapter 2 summarizes the experimental techniques and procedures, including the preparation and characterization of organic chemicals, quantum dot samples and semiconductor nanocrystalline thin films. Chapter 3 introduces the single molecule interfacial electron transfer dynamics in donor-bridge-acceptor complexes. Chapter 4 contains the detailed investigation of electron transfer dynamics from single CdSe core/multishell QDs to adsorbed fluorescein 27 molecules. Chapter 5 covers studies of interfacial electron transfer dynamics from single CdSe core/multishell QDs to TiO_2 nanoparticles and rutile (110) and (001) single crystals. Finally, the studies of fluorescence and lifetime properties of single QDs on ITO are presented in Chapter 6.

References:

(1) Xie, X. S. *Accounts of Chemical Research* **1996**, *29*, 598.

(2) Xie, X. S.; Trautman, J. K. *Annual Review of Physical Chemistry* **1998**, *49*, 441.

(3) Moerner, W. E. *Journal of Physical Chemistry B* **2002**, *106*, 910.

(4) Lu, H. P.; Xun, L.; Xie, X. S. *Science* **1998**, *282*, 1877.

(5) Myong, S.; Rasnik, I.; Joo, C.; Lohman, T. M.; Ha, T. *Nature* **2005**, *37*, 1321.

(6) Luo, G.; Wang, M.; Konigsberg, W. H.; Xie, X. S. *PNAS* **2007**, *104*, 12610.

(7) Zhuang, X. *Nature Photonics* **2009**, *3*, 365.

(8) Moerner, W. E. *PNAS* **2007**, *104*, 12596.

(9) Lu, H. P.; Xie, X. S. *Journal of Physical Chemistry B* **1997**, *101*, 2753.

(10) Holman, M. W.; Liu, R.; Adams, D. M. *J, Am. Chem. Soc.* **2003**, *125*, 12649.

(11) Biju, V.; Micic, M.; Hu, D.; Lu, H. P. *Journal of the American Chemical Society* **2004**, *126*, 9374.

(12) Goh, W.; Guo, J.; Yuan, R.; Lian, T. "Single molecule study of Rhodamine/ATO nanoparticle junctions"; Proceedings of SPIE-The International Society for Optical Engineering, (Physical Chemistry of Interfaces and Nanomaterials IV), 2005.

(13) Issac, A.; Jin, S.; Lian, T. *J. Am. Chem. Soc.* **2008**, *130*, 11280.

(14) Cui, S.-C.; Tachikawa, T.; Fujitsuka, M.; Majima, T. *J. Phys. Chem. C* **2008**, *112*, 19625.

(15) Jin, S.; Lian, T. *Nano Letters* **2009**, *9*, 2448.

(16) Jin, S.; Song, N.; Lian, T. *Acs Nano* **2010**, *4*, 1545.

(17) Jin, S.; Issac, A.; Stockwell, D.; Yin, F.-C.; Kindt, J.; Batista, V. S.; Robert, S.; Lian, T. *J. Phys. Chem. B* **2010**, *ASAP*.

(18) O'Regan, B.; Gratzel, M. *Nature* **1991**, *353*, 737.

(19) Bach, U.; Lupo, D.; Comte, P.; Moser, J. E.; Weissortel, F.; Salbeck, J.; Spreitzer, H.; Gratzel, M. *Nature* **1998**, *395*, 583.

(20) Huynh, W. U.; Dittmer, J. J.; Alivisatos, A. P. *Science* **2002**, *295*, 2425.

(21) Kamat, P. V.; Meisel, D. *Semiconductor Nanoclusters - Physical, Chemical, and Catalytic Aspects*; Elsevier: Amsterdam, 1997; Vol. 103.

(22) Serpone, N.; Pelizzetti, E. *Photocatalysis, Fundamentals and Applications*; John Wiley & Sons, 1989.

(23) Colvin, V. L.; Schlamp, M. C.; Alivisatos, A. P. *Nature* **1994**, *370*, 354.

(24) Aviram, A.; Ratner, M. A. *Chemical Physics Letters* **1974**, *29*, 277.

(25) Nitzan, A. *Annual Review of Physical Chemistry* **2001**, *52*, 681.

(26) Asbury, J. B.; Hao, E.; Wang, Y.; Ghosh, H. N.; Lian, T. *J. Phys. Chem. B* **2001**, *105*, 4545.

(27) Tachibana, Y.; Moser, J. E.; Graetzel, M.; Klug, D. R.; Durrant, J. R. *J. Phys. Chem.* **1996**, *100*, 20056.

(28) Benko, G.; Myllyperkio, P.; Pan, J.; Yartsev, A. P.; Sundstrom, V. *J. Am. Chem. Soc* **2003**, *125*, 1118.

(29) Burfeindt, B.; Hannapel, T.; Storck, W.; Willig, F. *J. Phys. Chem.* **1996**, *100*, 16463.

(30) Kuciauskas, D.; Monat, J. E.; Villahermosa, R.; Gray, H. B.; Lewis, N. S.; McCusker, J. K. *J. Phys. Chem. B* **2002**, *106*, 9347.

(31) Piotrowiak, P.; Galoppini, E.; Wei, Q.; Meyer, G. J.; Wiewior, P. *J. Am. Chem. Soc.* **2003**, *125*, 5278.

(32) Bauer, C.; Boschloo, G.; Mukhtar, E.; Hagfeldt, A. *International Journal of Photoenergy* **2002**, *4*, 17.

(33) Gaal, D. A.; Hupp, J. T. *Journal of the American Chemical Society* **2000**, *122*, 10956.

(34) Iwai, S.; Hara, K.; Murata, S.; Katoh, R.; Sugihara, H.; Arakawa, H. *J. Chem. Phys.* **2000**, *113*, 3366.

(35) Rensmo, H.; Keis, K.; Lindstrom, H.; Sodergren, S.; Solbrand, A.; Hagfeldt, A.; Lindquist, S. E.; Wang, L. N.; Muhammed, M. *Journal of Physical Chemistry* **1997**, *101*, 2598.

(36) Martini, I.; Hodak, J.; Hartland, G. V.; Kamat, P. V. *J. Chem. Phys.* **1997**, *107*, 8064.

(37) Liu, D.; Fessenden, R. W.; Hug, G. L.; Kamat, P. V. *J. Phys. Chem. B* **1997**, *101*, 2583.

(38) Kilsa, K.; Mayo, E. I.; Kuciauskas, D.; Villahermosa, R.; Lewis, N. S.; Winkler, J. R.; Gray, H. B. *J. Phys. Chem. A* **2003**, *107*, 3379.

(39) Hashimoto, K.; Hiramoto, M.; Lever, A. B.; Sakata, T. *J. Phys. Chem.* **1988**, *92*, 1016.

(40) Bedja, I.; Hotchandani, S.; Kamat, P. V. *J. Phys. Chem.* **1994**, *98*, 4133.

(41) Bell, T. D.; Pagba, C.; Myahkostupov, M.; Hofkens, J.; Piotrowiak, P. *J. Phys. Chem. B* **2006**, *110*, 25314.

(42) Rehm, J. M.; McLendon, G. L.; Nagasawa, Y.; Yoshihara, K.; Moser, J.; Gratzel, M. *J. Phys. Chem.* **1996**, *100*, 9577.

(43) Furube, A.; Katoh, R.; Hara, K.; Murata, S.; Arakawa, H.; Tachiya, M. *J. Phys. Chem. B* **2003**, *107*, 4162.

(44) Robel, I.; Kuno, M.; Kamat, P. V. *J. Am. Chem. Soc.* **2007**, *129*, 4136.

(45) Huang, J.; Stockwell, D.; Huang, Z.; Mohler, D. L.; Lian, T. *J. Am. Chem. Soc.* **2008**, *130*, 5632.

(46) Huang, J.; Huang, Z.; Jin, S.; Lian, T. *J. Phys. Chem. C* **2008**, *112*, 19734.

(47) Boulesbaa, A.; Issac, A.; Stockwell, D.; Huang, Z.; Huang, J.; Guo, J.; Lian, T. *J. Am. Chem, Soc.* **2007**, *129*, 15132.

(48) Burda, C.; Green, T. C.; Link, S.; El-Sayed, M. A. *J. Phys. Chem. B* **1999**, *103*, 1783.

(49) Logunov, S.; Green, T.; Marguet, S.; El-Sayed, M. A. *J. Phys. Chem. A* **1998**, *102*, 5652.

(50) Blackburn, J. L.; Ellingson, R. J.; Micic, O. I.; Nozik, A. J. *Journal of Physical Chemistry B* **2003**, *107*, 102.

(51) Robel, I.; Subramanian, V.; Kuno, M.; Kamat, P. V. *J. Am. Chem. Soc.* **2006**, *128*, 2385.

(52) Sykora, M.; Petruska, M. A.; Alstrum-Acevedo, J.; Bezel, I.; Meyer, T. J.; Klimov, V. I. *Journal of the American Chemical Society* **2006**, *128*, 9984.

(53) Anderson, N. A.; Ai, X.; Lian, T. *J. Phys, Chem. B* **2003**, *107*, 14414.

(54) Ghosh, H. N.; Asbury, J. B.; Lian, T. *J. Phys. Chem. B* **1998**, *102*, 6482.

(55) Huang, H.; Dorn, A.; Bulovic, V.; Bawendi, M. G. *Appl. Phys. Lett. FIELD Full Journal Title:Applied Physics Letters* **2007**, *90*, 023110/1.

(56) Martini, I.; Hodak, J. H.; Hartland, G. V. *J. Phys. Chem. B* **1998**, *102*, 9508.

(57) Martini, I.; Hodak, J. H.; Hartland, G. V. *J. Phys. Chem. B* **1999**, *103*, 9104.

(58) Martini, I.; Hodak, J. H.; Hartland, G. V. *J. Phys. Chem. B* **1998**, *102*, 607.

(59) Ghosh, H. N.; Asbury, J. B.; Weng, Y.; Lian, T. *J. Phys. Chem. B* **1998**, *102*, 10208.

(60) Haque, S. A.; Tachibana, Y.; Klug, D. R.; Durrant, J. R. *J. Phys. Chem. B* **1998**, *102*, 1745.

(61) Kamat, P. V.; Bedja, I.; Hotchandani, S.; Patterson, L. K. *Journal Of Physical Chemistry* **1996**, *100*, 4900.

(62) Heimer, T. A.; Heilweil, E. J.; Bignozzi, C. A.; Meyer, G. J. *J. Phys. Chem. A* **2000**, *104*, 4256.

(63) Haque, S. A.; Tachibana, Y.; Willis, R. L.; Moser, J. E.; Graetzel, M.; Klug, D. R.; Durrant, J. R. *J. Phys. Chem. B* **2000**, *104*, 538.

(64) Nelson, J.; Haque, S. A.; Klug, D. R.; Durrant, J. R. *Phys. Rev. B: Condens. Matter Mater. Phys.* **2001**, *63*, 205321.

(65) Barzykin, A. V.; Tachiya, M. *Journal of Physical Chemistry B* **2004**, *108*, 8385.

(66) Palomares, E.; Clifford, J. N.; Haque, S. A.; Lutz, T.; Durrant, J. R. *Chemical Communications (Cambridge, United Kingdom)* **2002**, 1464.

(67) Palomares, E.; Clifford, J. N.; Haque, S. A.; Lutz, T.; Durrant, J. R. *Journal of the American Chemical Society* **2003**, *125*, 475.

(68) Clifford, J., N.; Palomares, E.; Nazeeruddin, M., K.; Thampi, R.; Gratzel, M.; Durrant, J., R. *Journal of the American Chemical Society* **2004**, *126*, 5670.

(69) Hasselmann, G. M.; Meyer, G. J. *J. Phys. Chem. B* **1999**, *103*, 7671.

(70) Guo, J.; She, C.; Lian, T. *J. Phys. Chem. B.* **2005**, *109*, 7095.

(71) Weng, Y.-X.; Wang, Y.-Q.; Asbury, J. B.; Ghosh, H. N.; Lian, T. *J. Phys. Chem. B* **2000**, *104*, 93.

(72) Desilvestro, J.; Gratzel, M.; Kavan, L.; Moser, J. *J. Am. Chem. Soc.* **1985**, *107*, 2988.

(73) Vlachopoulos, N.; Liska, P.; Augustynski, J.; Gratzel, M. *J. Am. Chem. Soc.* **1988**, *110*, 1216.

(74) Argazzi, R.; Bignozzi, C. A.; Heimer, T. A.; Castellano, F. N.; Meyer, G. J. *Inorganic Chemistry* **1994**, *33*, 5741.

(75) Ford, W. E.; Rodgers, M. A. J. *J. Phys. Chem.* **1994**, *98*, 3822.

(76) Vinodgopal, K.; Hua, X.; Dahlgren, R. L.; Lappin, A. G.; Patterson, L. K.; Kamat, P. V. *Journal Of Physical Chemistry* **1995**, *99*, 10883.

(77) Jin, S.; Song, N.; Lian, T. *ACS Nano* **2010**, *4*, 1545.

(78) Gratzel, M. Mesoporous oxide junctions and nanostructured solar cells. In *Curr. Opin. Colloid Interface Sci.*, 1999; Vol. 4; pp 314.

(79) Brabec, C. J.; Sariciftci, S. N. *Monatshefte fuer Chemie* **2001**, *132*, 421.

(80) Brabec, C. J. *Solar Energy Materials and Solar Cells* **2004**, *83*, 273.

(81) Krebs, F. C.; Alstrup, J.; Spanggaard, H.; Larsen, K.; Kold, E. *Solar Energy Materials and Solar Cells* **2004**, *83*, 293.

(82) Spanggaard, H.; Krebs, F. C. *Solar Energy Materials and Solar Cells* **2004**, *83*, 125.

(83) Shaheen, S. E.; Brabec, C. J.; Sariciftci, N. S.; Padinger, F.; Fromherz, T.; Hummelen, J. C. *Applied Physics Letters* **2001**, *78*, 841.

(84) Nazeeruddin, M. K.; Kay, A.; Rodicio, I.; Humphrybaker, R.; Muller, E.; Liska, P.; Vlachopoulos, N.; Gratzel, M. *J. Am. Chem. Soc.* **1993**, *115*, 6382.

(85) Huang, J.; Stockwell, D.; Boulesbaa, A.; Guo, J.; Lian, T. *J. Phys. Chem. C* **2008**, *112*, 5203.

(86) Stockwell, D.; El-Sayed Mostafa, A.; Lian, T. *J.Phys. Chem. C, accepted* **2010**.

(87) Ferrere, S.; Zaban, A.; Gregg, B. A. *Journal of Physical Chemistry B* **1997**, *101*, 4490.

(88) Hara, K.; Horiguchi, T.; Kinoshita, T.; Sayama, K.; Sugihara, H.; Arakawa, H. *Solar Energy Materials and Solar Cells* **2000**, *64*, 115.

(89) Sayama, K.; Sugihara, H.; Arakawa, H. *Chem. Mater.* **1998**, *10*, 3825.

(90) Yuanmin Wang; Xuefei Wang; Sujit Kumar Ghosh; Lu, H. P. *J. Am. Chem. Soc.* **2009**, *131,* , 1479.

(91) Hodes, G. *J. Phys. Chem. C* **2008**, *112*, 17778.

(92) Kamat, P. *J. Phys. Chem. C* **2008**, *112*, 18737.

(93) Shalom, M.; Dor, S.; Ruhle, S.; Grinis, L.; Zaban, A. *J. Phys. Chem. C* **2009**, *113*, 3895.

(94) de Mello Donega, C.; Hickey, S. G.; Wuister, S. F.; Vanmaekelbergh, D.; Meijerink, A. *J. Phys. Chem. B* **2003**, *107*, 489.

(95) Niitsoo, O.; Sarkar, S. K.; Pejoux, C.; Ruhle, S.; Cahen, D.; Hodes, G. *J. Photochem. Photobiol. A* **2006**, *181*, 306.

(96) Hodes, G. *Isr. J. Chem.* **1993**, *33*, 95.

(97) Sasha, G.; Gary, H. *J. Phys. Chem. A* **1994**, *98*, 5338.

(98) Nozik, A. J. *Physica E: Low-Dimensional Systems & Nanostructures (Amsterdam, Netherlands)* **2002**, *14*, 115.

(99) Wang, Z. L. *J. Phys. Chem. A* **2000**, *104*, 1153.

(100) Schaller, R. D.; Klimov, V. I. *Phys. Rev. Lett.* **2004**, *92*, 186601.

(101) Ellingson, R. J.; Beard, M. C.; Johnson, J. C.; Yu, P.; Micic, O. I.; Nozik, A. J.; Shabaev, A.; Efros, A. L. *Nano Letters* **2005**, *5*, 865.

(102) Luther, J. M.; Beard, M. C.; Song, Q.; Law, M.; Ellingson, R. J.; Nozik, A. J. *Nano Letters* **2007**, *7*, 1779.

(103) Schaller, R. D.; Sykora, M.; Pietryga, J. M.; Klimov, V. I. *Nano Letters* **2006**, *6*, 424.

(104) Trinh, M. T.; Houtepen, A. J.; Schins, J. M.; Hanrath, T.; Piris, J.; Knulst, W.; Goossens, A. P. L. M.; Siebbeles, L. D. A. *Nano Letters* **2008**, *8*, 1713.

(105) Klimov, V. I. *Annual Review of Physical Chemistry* **2007**, *58*, 635.

(106) Murphy, J. E.; Beard, M. C.; Norman, A. G.; Ahrenkiel, S. P.; Johnson, J. C.; Yu, P.; Micic, O. I.; Ellingson, R. J.; Nozik, A. J. *Journal of the American Chemical Society* **2006**, *128*, 3241.

(107) Efros, A. L.; Rosen, M. *Physical Review Letters* **1997**, *78*, 1110.

(108) Shimizu, K. T.; Neuhauser, R. G.; Leatherdale, C. A.; Empedocles, S. A.; Woo, W. K.; Bawendi, M. G. *Physical Review B: Condensed Matter and Materials Physics* **2001**, *63*, 205316/1.

(109) Krauss, T. D.; O'Brien, S.; Brus, L. E. *Journal of Physical Chemistry B* **2001**, *105*, 1725.

(110) Nirmal, M.; Dabbousi, B. O.; Bawendi, M. G.; Macklin, J. J.; Trautman, J. K.; Harris, T. D.; Brus, L. E. *Nature* **1996**, *383*, 802.

(111) Empedocles, S.; Bawendi, M. *Acc. Chem. Res.* **1999**, *32*, 389.

(112) Fisher, B. R.; Eisler, H.-J.; Stott, N. E.; Bawendi, M. G. *J. Phys. Chem. B* **2004**, *108*, 143.

(113) Chung, I.; Bawendi, M. G. *Phys. Rev. B:* **2004**, *70*, 165304/1.

(114) Kuno, M.; Fromm, D. P.; Johnson, S. T.; Gallagher, A.; Nesbitt, D. J. *Phys. Rev. B:* **2003**, *67*, 125304/1.

(115) Kuno, M.; Fromm, D. P.; Hamann, H. F.; Gallagher, A.; Nesbitt, D. J. *J. Chem. Phys.* **2001**, *115*, 1028.

(116) Kuno, M.; Fromm, D. P.; Gallagher, A.; Nesbitt, D. J.; Micic, O. I.; Nozik, A. J. *Nano Letters* **2001**, *1*, 557.

(117) Peterson, J. J.; Nesbitt, D. J. *Nano Lett.* **2009**, *9*, 338.

(118) Zhang, K.; Chang, H.; Fu, A.; Alivisatos, A. P.; Yang, H. *Nano Letters* **2006**, *6*, 843.

(119) Montiel, D.; Yang, H. *J. Phys. Chem. A* **2008**, *112*, 9352.

(120) Pelton, M.; Smith, G.; Scherer, N. F.; Marcus, R. A. *Proc. Natl. Acad. Sci. U. S. A.* **2007**, *104*, 14249.

(121) Tang, J.; Marcus, R. A. *J. Chem. Phys.* **2006**, *125*, 044703/1.

(122) Tang, J.; Marcus, R. A. *J. Chem. Phys.* **2005**, *123*, 054704/1.

(123) Tang, J.; Marcus, R. A. *Phys. Rev. Lett.* **2005**, *95*, 107401/1.

(124) Tang, J.; Marcus, R. A. *J. Chem. Phys.* **2005**, *123*, 204511/1.

(125) Issac, A.; von Borczyskowski, C.; Cichos, F. *Phys.l Rev. B* **2005**, *71*, 161302/1.

(126) Schlegel, G.; Bohnenberger, J.; Potapova, I.; Mews, A. *Phys. Rev. Lett.*. **2002**, *88*, 137401.

(127) Verberk, R.; van Oijen, A. M.; Orrit, M. *Physical Review B: Condensed Matter and Materials Physics* **2002**, *66*, 233202/1.

(128) Shimizu, K. T.; Woo, W. K.; Fisher, B. R.; Eisler, H. J.; Bawendi, M. G. *Physical Review Letters* **2002**, *89*, 117401/1.

(129) Empedocles, S. A.; Bawendi, M. G. *Journal of Physical Chemistry B* **1999**, *103*, 1826.

(130) Empedocles, S. A.; Bawendi, M. G. *Science* **1997**, *278*, 2114.

(131) Neuhauser, R. G.; Shimizu, K. T.; Woo, W. K.; Empedocles, S. A.; Bawendi, M. G. *Physical Review Letters* **2000**, *85*, 3301.

(132) Rossetti, R.; Beck, S. M.; Brus, L. E. *J. Am. Chem. Soc.* **1984**, *106*, 980.

(133) Rossetti, R.; Brus, L. E. *J. Phys. Chem.* **1986**, *90*, 558.

(134) Ramsden, J. J.; Gratzel, M. *Chem. Phys. Lett.* **1986**, *132*, 269.

(135) Henglein, A. *Pure & Appl. Chem.* **1984**, *56*, 1215.

(136) Huang, J.; Huang, Z.; Yang, Y.; Zhu, H.; Lian, T. *J. Am. Chem. Soc.* **2010**, *132*, 4858.

(137) Tachibana, Y.; Akiyama, H. Y.; Ohtsuka, Y.; Torimoto, T.; Kuwabata, S. *Chemistry Letters* **2007**, *36*, 88.

(138) Kongkanand, A.; Tvrdy, K.; Takechi, K.; Kuno, M.; Kamat, P. V. *Journal of the American Chemical Society* **2008**, *130*, 4007.

(139) Brown, P.; Kamat, P. V. *Journal of the American Chemical Society* **2008**, *130*, 8890.

(140) Farrow, B.; Kamat, P. V. *Journal of the American Chemical Society* **2009**, *131*, 11124.

(141) Cahen, D.; Hodes, G.; Graetzel, M.; Guillemoles, J. F.; Riess, I. *J. Phys. Chem.* **2000**, *104*, 2053.

(142) Graetzel, M. *Nature* **2001**, *414*, 338.

(143) Graetzel, M. *Nature (London, United Kingdom)* **2003**, *421*, 586.

(144) Sambur, J. B.; Parkinson, B. A. *Journal of the American Chemical Society*, *132*, 2130.

(145) Chakrapani, V.; Tvrdy, K.; Kamat, P. V. *Journal of the American Chemical Society* **2010**, *132*, 1228.

(146) Boulesbaa, A.; Huang, Z.; Wu, D.; Lian, T. *Journal of Physical Chemistry C* **2010**, *114*, 962.

(147) Colvin, V. L.; Schlamp, M. C.; Alivisatos, A. P. *Nature* **1994**, *370*, 354.

(148) Coe, S.; Woo, W.-K.; Bawendi, M. G.; Bulović, V. *Nature* **2002**, *420*, 800.

(149) Anikeeva, P. O.; Madigan, C. F.; Coe-Sullivan, S. A.; Steckel, J. S.; Bawendi, M. G.; Bulovic, V. *Chem. Phys. Lett.* **2006**, *424*, 120.

(150) Anikeeva, P. O.; Halpert, J. E.; Bawendi, M. G.; Bulovic, V. *Nano Lett.* **2007**, *7*, 2196.

(151) Anikeeva, P. O.; Halpert, J. E.; Bawendi, M. G.; Bulovic, V. *Nano Lett.* **2009**, *9*, 2532.

(152) Ray, K.; Badugu, R.; Lakowicz, J. R. *Journal of the American Chemical Society* **2006**, *128*, 8998.

(153) Ito, Y.; Matsuda, K.; Kanemitsu, Y. *Physical Review B* **2007**, *75*, 033309.

(154) Jha, P. P.; Guyot-Sionnest, P. *ACS Nano* **2009**, *3*, 1011.

Chapter 2. Experimental Section

The samples used in this work are based on metal oxide nanocrystalline thin films which are sensitized by organic dye molecules or quantum dots (QDs). The synthesis of semiconductor colloid and the preparation of thin films are based on the published procedures, but also modified slightly for single-molecule study. Some organic dye molecules are conjugated to facilitate the single molecule measurements. The single-molecule studies are conducted by single-molecule fluorescence spectroscopy which consists of laser source, confocal microscope and time-correlated single photon counting. This chapter summarizes the procedures for sample preparations and introduces the experimental setup for single-molecule measurements.

2.1. Preparation of Semiconductor Colloid and Nancrystalline Thin Films

2.1.1. Preparation of SnO_2 Colloid and Thin Films

Colloidal SnO_2 are synthesized according to a published procedure.[1,2] 0.085 mol $SnCl_4$ (99.9%, Aldrich) was first injected into 20 mL of HCl (37 wt. %) by syringe and dispersed by sonication for at least 30 minutes. The resulting solution was added drop-wise into 500 mL of water under rapid stirring at 0 ^oC. After stirring for additional 30 min, aqueous ammonia (25%) was added to the solution until a pH value of 3.5-4.0 was reached, which led to precipitation of SnO_2 nanoparticles. The solution was allowed to settle overnight in the dark. The white precipitate was washed at least 3 times with

distilled water, and then 300 mL of water was added and the pH value was adjusted to 9.5-10. The suspension was stirred vigorously overnight and dialyzed against ~10 L of water at pH 10 for at least two days. The resulting transparent SnO_2 colloid was then refluxed for 4 h. 150 ml of this colloid was poured into an autoclave and heated firstly at 150 ^oC for 1 h, and then at 270 ^oC for 16 h. Solid SnO_2 nanoparticles were obtained by rotary evaporation of the solution under vacuum. 0.01g/mL of SnO_2 nanoparticle water solution was spin coated on a cover glass slide (Fisher Scientific) and sintered in air at 550 ^oC for 2.5 hours to produce SnO_2 nanocrystalline thin film. The films are transparent. The atomic force microscopy (AFM) image of the SnO_2 nanocrystalline thin film is shown in Figure 2.1, demonstrating a homogenous coverage of SnO_2 nanoparticles on the glass cover slip.

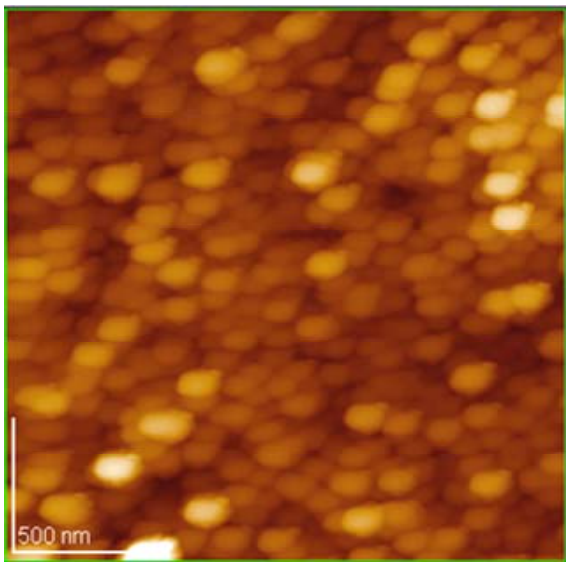

Figure 2.1. AFM image of a SnO_2 nanocrystalline thin film.

2.1.2. Preparation of TiO_2 Colloid and Thin Films

TiO_2 colloidal nanoparticles and thin films were prepared by following reported methods.[3] 250 mL of water and 80 mL of acetic acid were added to a 1000 mL round bottom flask and cooled to 0°C. A mixture of 10 mL of 2-propanol and 37 mL of Ti(IV) isopropoxide (Aldrich, 97%) was dropped slowly to the water acetic acid bulk solution over a 30-40 min period under vigorous stirring and dry N_2 purge. After stirring overnight, the transparent colloid was poured into a 1000 ml beaker and heated in 80°C hot water bath for 3-4 h under vigorous stirring. The colloid was autoclaved at 230 °C for 12 h, and then stirred for 4 days. The colloidal solution was spin coated on glass cover slips and then sintered at 550 ^oC for 2.5 h in air to form nanocrystalline thin films. The AFM image of the TiO_2 nanocrystalline thin film is shown in Figure 2.2, demonstrating a homogenous coverage of TiO_2 nanoparticles on the glass cover slip.

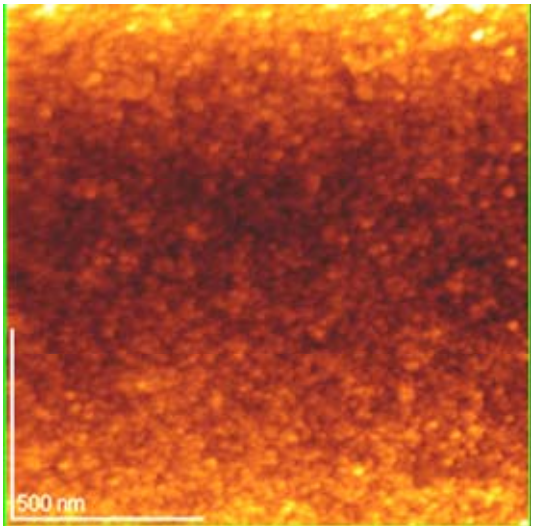

Figure 2.2. An AFM image of a TiO_2 nanocrystalline thin film.

2.1.3. Preparation of ZnO Colloid and Thin Films

ZnO nanoparticle colloids were prepared according to a published procedure.[4] 10 mmol $Zn(Ac)_2$ (Aldrich) was added to 5 mL absolute ethanol and cooled to 0°C. Separately, 14 mmol $LiOH \cdot H_2O$ was dissolved in 95 mL ethanol at room temperature, cooled to 0°C, and slowly added to the Zn(II) solution under vigorous stirring at 0°C. The mixture was thoroughly washed with ~250 ml hexane and centrifuged to remove the supernatant liquid. The ZnO precipitant was dissolved in ethanol to make ZnO colloid and was washed with hexane twice more. The ZnO nanoparticle colloid solution was spin coated on glass cover slip and then sintered at 550 ^{o}C for 2.5 h in air to produce nanocrystalline thin films. The AFM image of the ZnO nanocrystalline thin film is shown in Figure 2.3, demonstrating a homogenous coverage of ZnO nanoparticles on the glass cover slip.

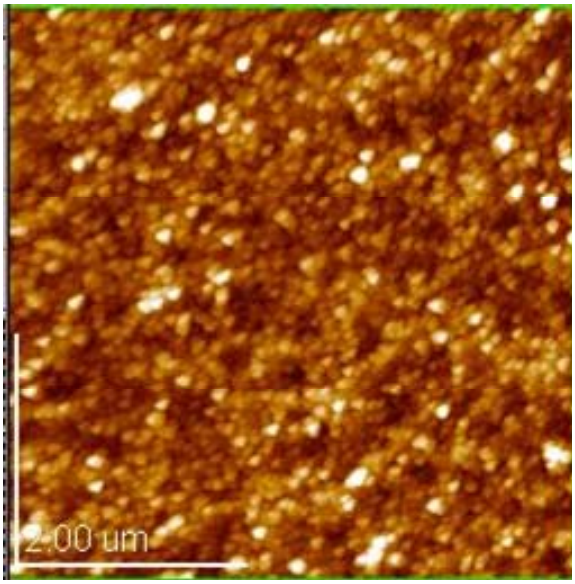

Figure 2.3. An AFM image of ZnO nanocrystalline thin film.

2.1.4. Preparation of ZrO2 Colloid and Thin Films

ZrO_2 nanoparticles were obtained from Degussa Corporation. ZrO_2 powder (2 g) was ground in a mortar with distilled water (4 mL), acetylacetone (10 μL) and 5 drops of Triton X-100 to break up the aggregate into a dispersed paste.[5] The paste was washed several times by water. A final diluted ZrO_2 nanoparticle water solution (~0.01 g/mL) was spin coated on glass cover slips. The films were then sintered at 550 ^oC for 2.5 h in air.

2.1.5. Preparation of In_2O_3 Colloid and Thin Films

In_2O_3 nanoparticle colloids were synthesized according to a published procedure.[6,7] Briefly, 1 g (~3.4 mmol) of $InCl_3 \cdot 4H_2O$ (97%, from Aldrich) was dissolved in 14 ml of H_2O (Millipore, 18.3 MΩ/cm) in an ice bath under vigorous stirring. After stirring 30 minutes, aqueous ammonia (25%) was added to adjust the pH to ~8, which led to the precipitation of indium hydroxide. The resulting precipitation was centrifuged and dried in vacuum for 10 minutes. The precipitation was mixed with H_2O, and then spin coated on glass cover slip and sintered at 550 ^oC for 2.5 h in air to produce nanocrystalline thin films.

2.2. Fabrication of Electron Donor-Bridge-Acceptor Complex

2.2.1 Synthesis of Silane Conjugated Sulforhodamine B

Silane conjugated sulforhodamine B (SRhB-Silane) was synthesized through the reaction between sulforhodamine B acid chloride (Fluka, referred as SRhB) and 3-aminopropyltrimethoxysilane (referred as aminosilane, 97%, from Aldrich) according to a literature procedure.[8] The chemical reaction is presented in Figure 2.4. 0.012g of SRhB and 0.01g of 4-dimethylaminopyridine were added into 3 mL of dry pyridine (Sigma,

99%), and after stirring for 30 min, 10 µl of aminosilane was injected and allowed to react for 3 hours. The product was purified by eluting through a silica gel column (100-200 mesh, 60 Å, Sigma-Aldrich, eluent: 5/1 chloroform/methanol solvent). The measured mass/charge ratio was 762.29127, consistent with the calculated value of 762.29088 for $[C_{36}H_{51}O_9N_3S_2Si+ H]^+$. Compared to SRhB, the UV-VIS absorption peak of SRhB-Silane was red-shifted by 7 nm (Figure 2.5 A), and its fluorescence lifetime in ethanol solution was unchanged (3.1ns, Figure 2.5 B).

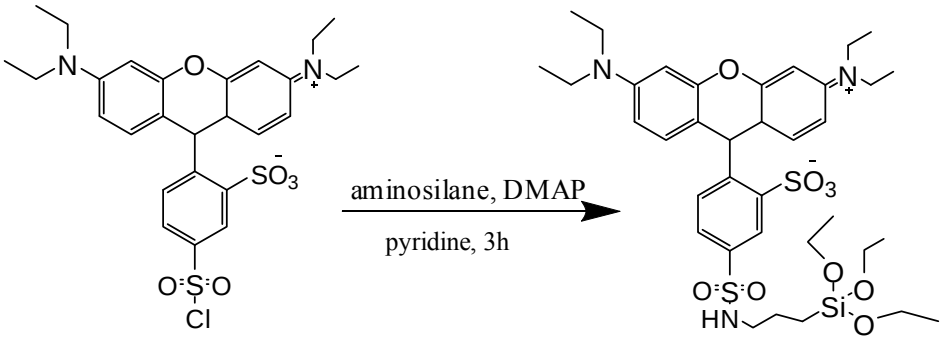

Figure 2.4. The chemical reaction scheme for silane conjugated sulforhodamine B

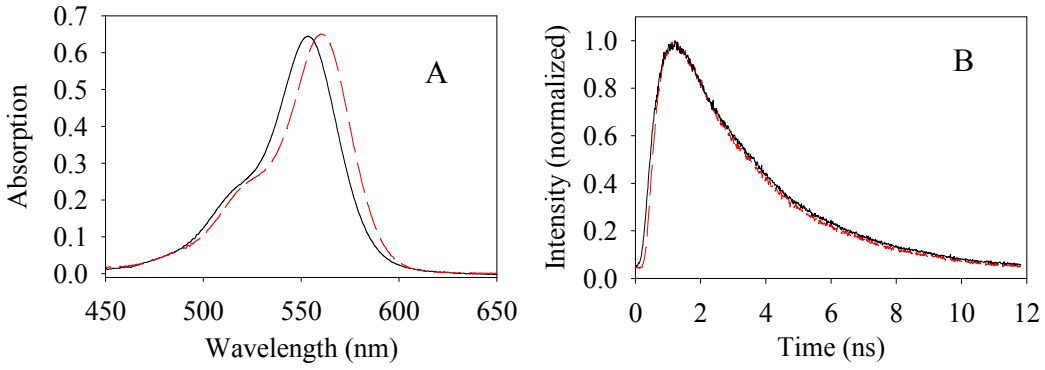

Figure 2.5. (A) UV-VIS absorption of SRhB (black solid line) and Silane-SRhB (red dashed line) in ethanol and (B) ensemble fluorescence decay of SRhB (black solide line) and Silane-SRhB (red dashed line) in water.

2.2.2 Fabrication of Electron Donor-Bridge-Acceptor Complex

To study the electron transfer dynamics from single organic molecules, the SRhB-Silane molecules were immobilized on semiconductor nanocrystalline thin films through the reaction shown in Figure 2.6, to form an electron donor-bridge-nanoparticle acceptor complex. A drop (~20 μL) of SRhB-Silane water (Millipore, 18.2 MΩcm) solution was dropped on the surfaces of substrates (SnO_2, TiO_2 or ZrO_2 nanocrystalline thin films, or glass cover slip). After drying in the dark, the substrates were heated at 120 ^oC for 10 minutes and then washed with water to remove unreacted SRhB-Silane molecules. Here we refer SRhB-Silane immobilized on different substrates as SRhB-silane-SnO_2 (or ZrO_2,TiO_2, Glass). The concentrations of the SRhB-Silane solution used were ~10^{-4}, ~10^{-8}, ~10^{-11}-10^{-12} M for the samples for transient absorption, ensemble average fluorescence and single molecule fluorescence measurements, respectively. Fluorescence (single molecule and ensemble averaged) and transient absorption measurements were performed with nanocrystalline thin films prepared on glass cover slip and sapphire windows respectively.

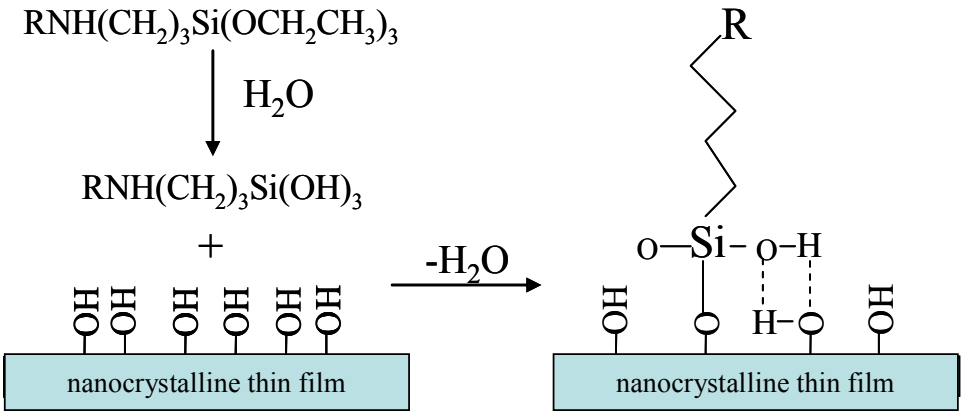

Figure 2.6. The reaction scheme for the immobilization of SRhB-Silane molecule on semiconductor nanocrystalline thin film. R represents the SRhB molecule.

2.3 Fabrication of QD ET Complexes

2.3.1 QD-F27 Complex

The QDs used in this work for QD-F27 complex were purchased from Ocean NanoTech, LLC, USA. They consist of a CdSe core, a multi-shell of $CdS_{3ML}ZnCdS_{2ML}ZnS_{2ML}$ and octadecylamine capping ligands. The absorption spectrum of the QDs in heptane solution is shown as the blue line in Figure 2.7 B. The first exciton peak of the QDs is at 605 nm, which is red-shifted from the first exciton peak (574 nm) of the CdSe core. Fluorescein 27 (F27) was purchased from Exciton, USA. The structure of the molecule is shown in Figure 2.7 A. The QD-F27 complexes were prepared by adding solid F27 dye into QD heptane solution. The mixture was then sonicated for ~30 min and kept in dark for overnight. The mixture was finally filtered to remove undissolved F27 dyes. Since the F27 is not soluble in heptane, all dissolved dyes were believed to attach on the surfaces of QDs, as shown in the inset in Figure 2.7 B. Figure 2.7 B shows the UV-VIS. absorption spectrum of QD-F27 complexes at different dye-to-QD ratios.

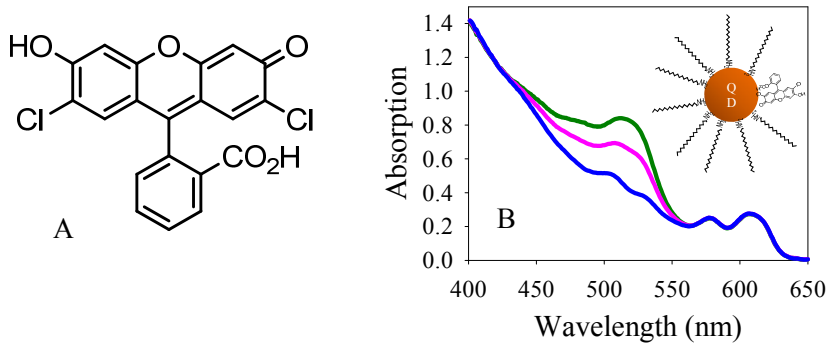

Figure 2.7. (A) the chemical structure of fluorescein 27 (F27). (B) UV-vis. absorption spectrum of QDs (blue line) and QD-F27 complexes at different dye-to-QD ratios (high

ratio: green line; low ratio: pink line). The inset is the schematic structure of a QD-F27 complex.

2.3.2 QD-TiO_2 Nanoparticle Complex

The QDs used in this work for QD-TiO_2 nanoparticle complexes were water soluble and purchased from Ocean NanoTech, LLC, USA. They consist of a CdSe core, a multi-shell of $CdS_{2ML}ZnCdS_{1ML}ZnS_{1ML}$ and octadecylamine capping ligands. The QDs were finally covered by polymers with carboxylic functional groups. The first exciton peak is at 580 nm. Figure 2.8 shows the SEM image of the QDs. The size of the QD is estimated to be 5.7 ± 0.7 nm.

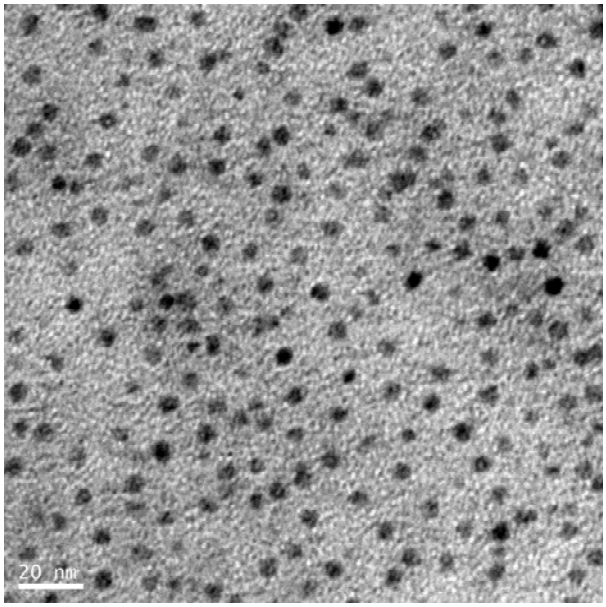

Figure 2.8. A SEM image of CdSe core multi shell QDs, whose first exciton absorption peak is at 580 nm.

To prepare the QD-TiO_2 nanoparticle complex, the QD solution was spin coated on TiO_2 nanocrystalline thin films or directly on glass cover slips, and then dried in air and

washed by water to remove weakly absorbed QDs on the surfaces. The concentration of the QD solution is 10 pM for single QD detection and ~0.1 μM for averaged ensemble fluorescence measurements. QDs were believed to attach on the TiO_2 nanoparticle surfaces through the carboxylic functional groups.

2.3.3 QD-In_2O_3 and ITO Complexes

The QDs used for QD-In_2O_3 and ITO (tin-doped indium oxide) complexes were the same as in QD-F27 complex. The ITO coated cover slips (15-30 ohms, 18×18 mm^2, ~10% doping) were purchased from SPI Supplies. The ITO films were first washed by 2-propanol, dried in air and rapidly scanned over a flame for a few seconds to remove any adsorbed organic materials before use. The flame treatment process did not change the resistance of ITO. To prepare samples for single QDs study, a QD heptane solution with a concentration of ~10 pM was spin-coated on ITO, In_2O_3, or glass cover slips. For ensemble averaged measurement the samples were prepared by spin-coating a QD solution with a concentration of ~0.1 μM.

2.4 Single-Molecule Fluorescence Spectroscopy

2.4.1. Time-Correlated Single Photon Counting (TCSPC) Technique

Photon counting is an intensity measurement technique based on the quantum nature of light. TCSPC technique detects and count individual photons from the signal rather than measuring. The advantages of single photon counting (SPC) over traditional analog method of measurements are:

(i) SPC is insensitive to the drift and noise associated with the instrument.

(ii) Digital nature of SPC simplifies both the acquisition as well as analysis of the data. Schematic representation of the data acquisition from TCSPC technique is shown below in Figure 2.9.

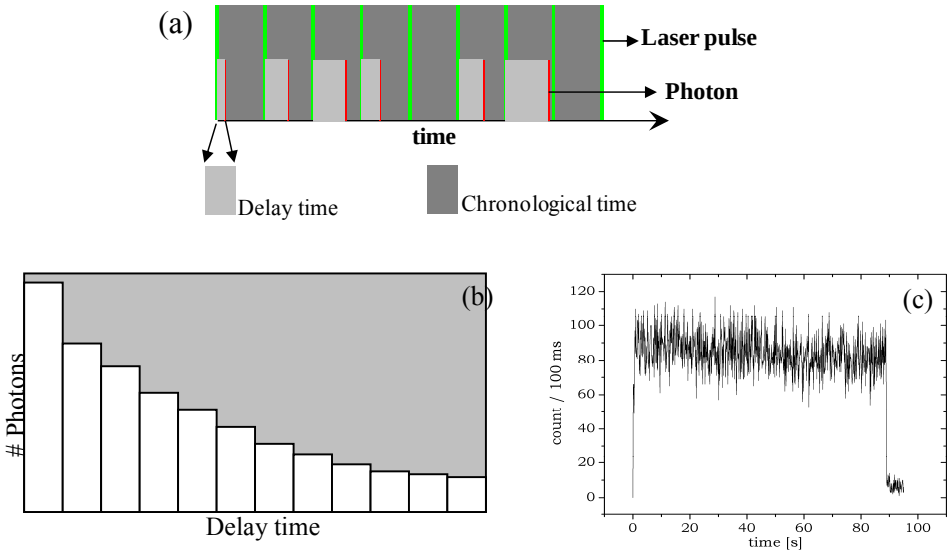

Figure 2.9. Photon counting method of TCSPC technique. (a) Photon counting module monitors the time interval between laser pulse and detected photon (delay time). The output of a TCSPC measurement are (b) a histogram of delay times and (c) fluorescence intensity trajectory (number of photons per integration time).

Figure 2.10 shows the major components of a TCSPC system. A brief description of the functions of the components is discussed below:

Laser: The light source used for the excitation of the chromophore is a pulse laser. Moreover, every excitation pulse also sends a 'start' signal to the Time to Amplitude Converter (TAC), which measures time interval between excitation pulse and the detected photon before the next excitation pulse.

Detector: Fluorescence from the sample is collected by the confocal microscope and focused to the detector. In our case the detector used is an Avalanche Photo Diode

(APD). APD converts the photon counts to voltage. However, the output of APD includes the electronic noise as well. The resulting 'signal + noise' is being sent to the stop discriminator.

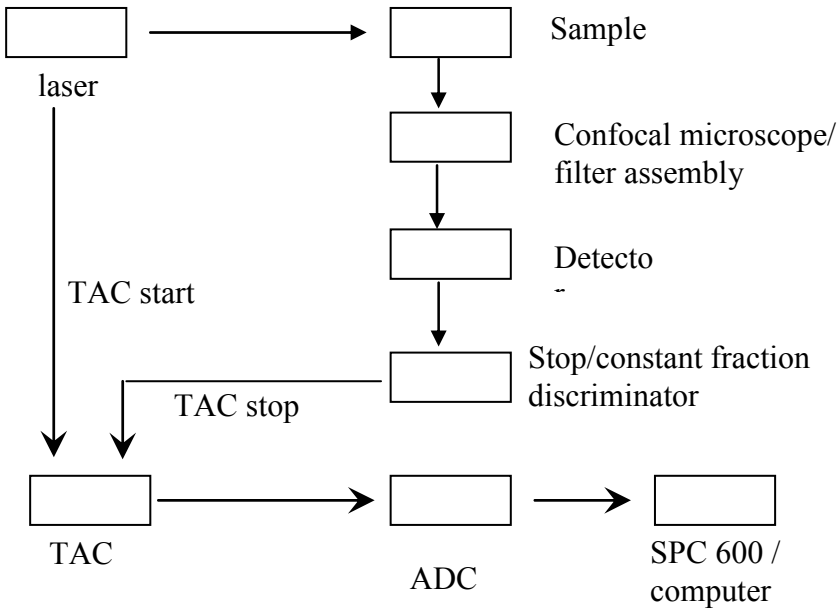

Figure 2.10. Block diagram of TCSPC set-up.

Stop discriminator: This unit differentiates the signal from the detector. If the signal level is below the given threshold, it will be completely ignored while the signal level above the threshold will be recognized. The threshold level is decided by the noise level of the detector. However, there is a finite probability of detecting multiple photons at the same time. This problem can be resolved electronically by setting an upper limit. An electronic unit called Constant Fraction Discriminator (CFD) generates a TAC stop signal only if the signal level is between upper and lower limit (Figure 2.11).

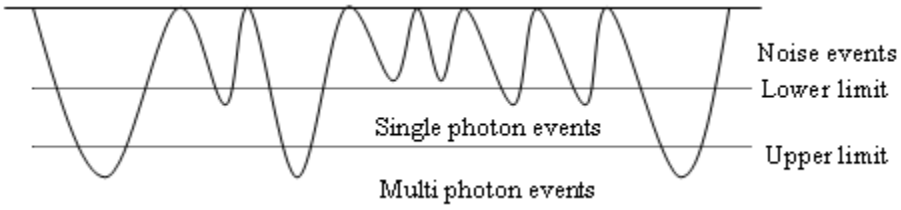

Figure 2.11. CFD discriminate single photon events from noise level and multi photon events.

Time to Amplitude Converter (TAC): When TAC receives the stop signal, it generates an analog output pulse whose amplitude very precisely represents the time that has elapsed between start and stop signals.

Analog to Digital Converter (ADC): ADC measures the amplitude of the pulse from the TAC to determine into which of the time slots in the decay curve, as shown in Figure 2.9, this particular photon to be recorded. Repeated excitation and detection cycle develops a histogram of delay times (Figure 2.9).

2.4.2. Single-Molecule Detection

Single-molecule detection is carried out with a home built scanning confocal microscope (SCM). The working principle of the microscope is depicted in Figure 2.12. The excitation source is a mode locked Ti:sapphire laser (Tsunami, spectra physics) operated at 700~1000 nm at 82 MHz repetition rate (Tsunami oscillator pumped by 10 W Millennia Pro, Spectra-Physics). For single QD studies, the output is passed through a pulse picker (Conoptics, USA) to reduce the repetition rate by a factor of 9. 350~500 nm laser pulses are generated when the Tsunami output is passed through a frequency doubling beta-BaB_2O_4 (BBO) crystal. The sample placed on a piezo scanner is illuminated by the laser beam focused through the objective (Olympus). The information

about the specimen (e.g. fluorescence) is obtained by point by point scanning of the laser beam across the specimen. The laser beam is focused to a diffraction-limited spot (λ/2 diameter) to excite dye molecules on the surface of a glass cover slip or a nanocrystalline thin film. The illuminated area and its image lie in conjugate planes. A pinhole in the image plane transmits signal only from the focal plane of the objective. This is called confocal ray path. Signal from out of the focal area are obstructed by the pinhole and do not contribute to the image formation. Signal from the sample is collected by the same objective and focused to the avalanche photodiode (APD). Photon by photon counting is achieved with the TSCPC module. The instrument response function for the fluorescence lifetime measurement had a full-width-at-half-maximum of ~500 ps.

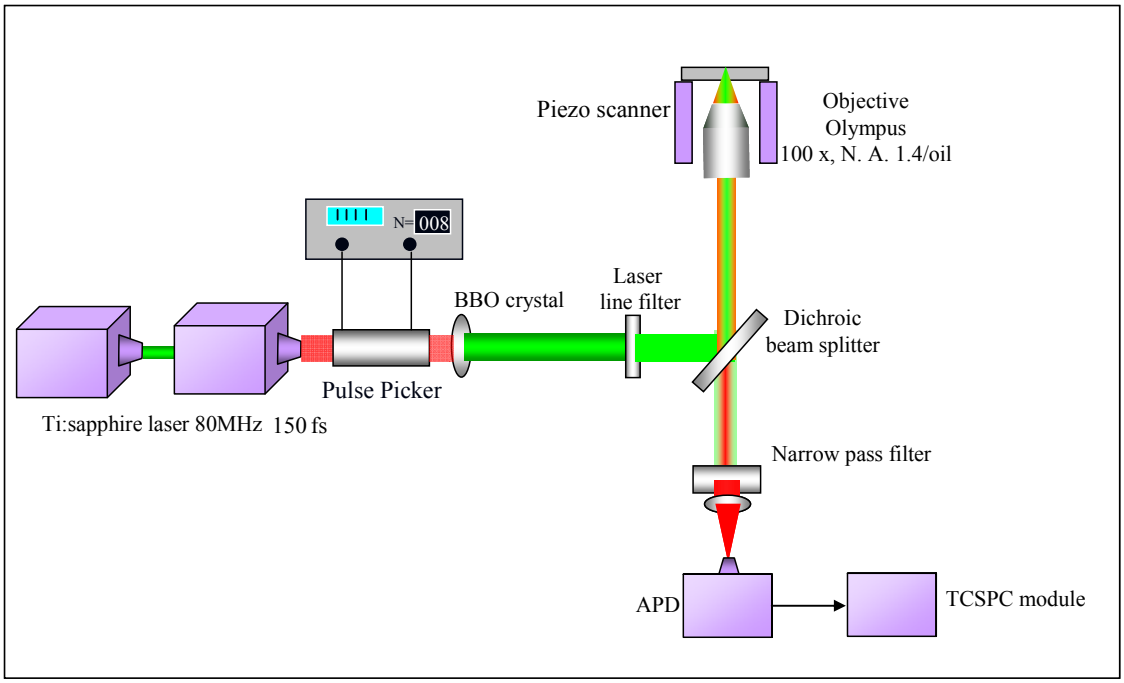

Figure 2.12. Confocal microscope setup attached with TCSPC module.

Scanning of the sample is done with a piezo scanner. Figure 2.13 A shows a raster scanned single molecules fluorescence image of single SRhB molecules on glass cover

slip. Each peak in the image indicates a single molecule. When focusing the excitation laser out of the confocal plane, a wide-field-illuminated fluorescence image of single SRhB molecules on glass cover slip is obtained by using a CCD camera (Roper Scientific, VersArray 512B), as shown in Figure 2.13 B.

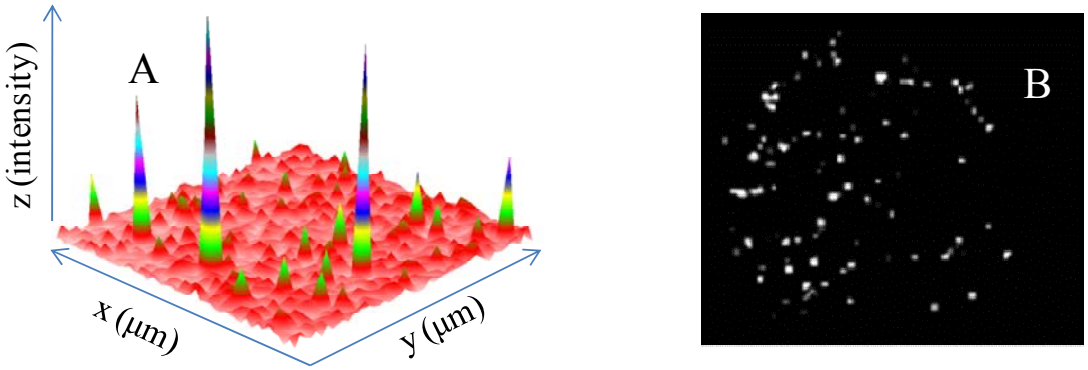

Figure 2.13. (A) Raster scanned single molecule fluorescence image of single SRhB molecules on glass cover slip. (B) A wide-field-illuminated fluorescence image (25 μm × 25 μm) of SRhB molecules on glass cover slip.

References:

(1) Rockenberger, J.; zum Felde, U.; Tischer, M.; Troger, L.; Haase, M.; Weller, H. J. of Chem. Phys. 2000, 112, 4296.

(2) Nutz, T.; Felde, U. Z.; Haase, M. J. Chem. Phys. 1999, 110, 12142.

(3) Zaban, A.; Ferrere, S.; Sprague, J.; Gregg, B. A. J. Phys. Chem. B 1997, 101, 55.

(4) Meulenkamp, E. A. J. of Phys. Chem. B 1998, 102, 7764.

(5) Nazeeruddin, M. K.; Kay, A.; Rodicio, I.; Humphrybaker, R.; Muller, E.; Liska, P.; Vlachopoulos, N.; Gratzel, M. J. Am. Chem. Soc. 1993, 115, 6382.

(6) Poznyak, S. K.; Golubev, A. N.; Kulak, A. I. Surface Science 2000, 454-456, 396.

(7) Poznyak, S. K.; Kulak, A. I. Electrochimica Acta 2000, 45, 1595.

(8) Chan, E. W. L.; Yousaf, M. N. J. Am. Chem. Soc. 2006, 128, 15542.

Chapter 3. Single-Molecule Interfacial Electron Transfer Dynamics in Donor-Bridge-Nanoparticle Acceptor Complexes

3.1 Introduction

Interfacial electron transfer (ET) has been intensively investigated for decades because of its important role in biological processes, chemical reactions, and solar cells.[1-6] Recently, ET in dye sensitized semiconductor nanoparticle films has become more interesting due to its potential applications in solar energy devices,[7-9] waste catalytic treatment[5,10] and molecular electronics.[11-13] Photo induced interfacial ET can occur from the singlet excited state of certain dye molecules to the conduction band (CB) of semiconductor such as TiO_2 and SnO_2 after photoexcitation (Figure 3.1). The interfacial ET dynamics have usually been measured by transient absorption and/or time-resolved fluorescence spectroscopy on the ensemble level in most previous studies. Using these techniques, dominant interfacial ET processes in various dye-semiconductor combinations are reported to occur on the femotosecond (fs) to hundreds of picoseconds (ps) time scale and the corresponding kinetics show multi-exponential behavior.[6,14-26,21-38,31,32,38,39,39-47] The multi-exponential kinetics indicate a broad range of ET rates, which may have any of following origins: 1) static heterogeneities in the energetics of the adsorbate and semiconductor; 2) static heterogeneities in the electronic coupling between the adsorbate and semiconductor; and 3) dynamic fluctuation of the energetics and electronic coupling. Unfortunately, it is difficult to investigate the possible inhomogeneities using only ensemble measurements, which usually obscure the static and dynamic information on ET. Therefore, to probe the inhomogeneitie in the ET

process, single molecule spectroscopy,[48] which can study one molecule at a time, is the best approach.

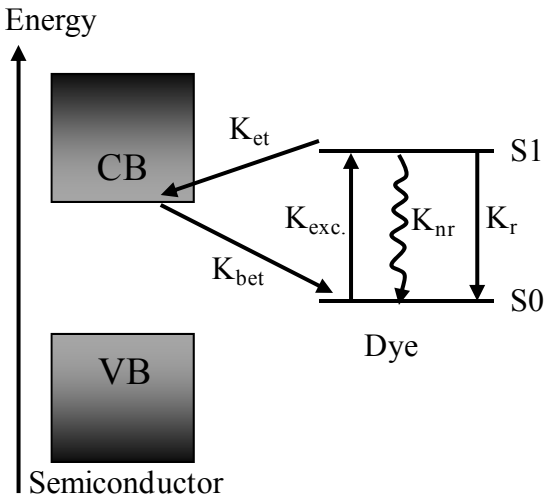

Figure 3.1. Schematic representation of photo induced ET processes for dye molecules sensitized on semiconductor nanoparticles. $K_{exc.}$: excitation rate; K_r: radiative decay rate; K_{nr}: nonradiative decay rate; K_{et}: ET rate; K_{bet}: BET rate.

Single-molecule fluorescence spectroscopy has been used to study ET processes in molecules,[49,50] in conjugated polymers,[51] at interfaces[52-55] and in biological systems.[56-62] However, studying ET processes by single-molecule fluorescence is still technically challenging, because ET shortens the fluorescence lifetime and reduces the fluorescence quantum yield of the dye molecules. As shown in Eq. 3.1-3.3,

$$\tau = \frac{1}{K_r + K_{nr}} = \frac{1}{K_0} \qquad \text{(Eq. 3.1)}$$

$$\tau' = \frac{1}{K_0 + K_{et}} \qquad \text{(Eq. 3.2)}$$

$$\Phi_f = \frac{K_r}{K_0 + K_{et}} \qquad \text{(Eq. 3.3)}$$

where τ (τ') is the fluorescence lifetime without (with) ET and Φ_f is the fluorescence quantum yield, the ET rate can be estimated by measuring the excited state fluorescence lifetime of molecules with and without ET, assuming that K_r and K_{nr} are the same in both cases. When ET occurs, both the lifetimes and the fluorescence intensities of the dye molecules will decrease. Many ensemble-average studies have shown that for organic dye molecules (such as rhodamine and coumarin) that are directly attached to metal oxides (such as TiO_2, SnO_2 and ZnO), the interfacial ET was often on the ps or faster time scale.[18,63-66] Assuming an intrinsic lifetime of 3 ns and a quantum yield of 100%, based on Eq. 3.1~3.3, a dye molecule undergoing ultrafast ET on a time scale of < ~10 ps has a calculated emission yield of < 0.3%, which is well below the detection sensitivity of current single-molecule techniques. Consequently, these ET events cannot be directly observed, hindering unbiased samplings of fast injecting molecules and/or direct observation of fast ET rate by single molecule fluorescence spectroscopy.[4-6]

So far, there have been only a few published reports of single molecule interfacial ET.[52-55] Lu and Xie first report a study on single-molecule interfacial ET for cresyl violet on ITO ($Sn:In_2O_3$).[52] Shorter fluorescence lifetimes were observed for crysyl violet on ITO compared to on glass, which was attributed to ET from the dye's excited state to ITO. Although the fluorescence decays of single molecules on ITO were found single exponential, the lifetimes were widely distributed, suggesting a static inhomogeneous distribution of ET rates. Our previous study of RhB molecule on ATO (Sb: SnO_2) also reported a similar static heterogeneous distribution of ET rates.[54] It was noted that the number of observed (bright) molecules on ATO was much smaller than that on glass, and ET rate from single-molecule measurements were much slower than those obtained from

ensemble-averaged transient absorption measurements due to incomplete sampling of molecules undergoing fast ET in the single molecule study. More recently, Lu et al observed long single molecule fluorescence lifetimes and vigorous fluctuations (blinking) of fluorescence intensities in a study of cresyl violet, courmin and porphyrin on TiO_2 nanoparticles.[55,67] The observed long lifetimes were inconsistent with ultrafast ET dynamics measured by ensemble-averaged transient absorption and fluorescence measurements. To explain the single molecule results, they proposed an intermittent ET activity model in which the single molecules on TiO_2 were separated into "on" and "off" states. In the "off" state, molecules underwent slow (or no) ET and the fluorescence intensities were high, so that all detected fluorescence photons originated from the slow injecting states. In the "on" state, on the other hand, the molecules were undergoing ultrafast ET dynamics, but the fluorescence quantum yield of the fast injecting state was too low to be observed. The switching between "on" and "off" states was inferred from the fluctuations in emission intensity.

Modulating interfacial ET rates by inserting spacers between the chromophore and the semiconductor nanoparticles has also been a subject of considerable interest.[33,68-72] It offers a way to potentially optimize the efficiency of dye-sensitized solar cells,[72] and to test the electronic coupling dependencies of the interfacial ET rate[68-70] and molecular conductance.[73] The presence of the molecular spacer reduces the ET rate, and hence decreases the degree of fluorescence quenching, allowing the study of the ET process by single-molecule fluorescence spectroscopy.

In this chapter, we describe a study of single molecule ET dynamics in a donor-bridge-acceptor complex. In order to observe the dye molecules undergoing ET, we apply

a molecular spacer between dye molecules and semiconductor surfaces to control the ET rate. Specifically, we used an aminosilane whose amino group was conjugated with an organic dye molecule while the silane group was immobilized on a semiconductor nanoparticle surface to construct the donor-bridge-acceptor complex. For dye molecule, Sulforhodamine B chloride was chosen at the dye molecule for its high quantum yield (Φ_f = ~0.6),[74] robust structure and the ability to conjugate with aminosilane. SnO_2 and TiO_2 nanoparticles were used as the electron acceptor because ET from related Rhodamine B molecules to these substrates has been well studied by ensemble-averaged ultrafast spectroscopic techniques.[63] We experimentally show that, for a donor-bridge-acceptor architecture, the study of ET in an individual complex is possible by using single-molecule fluorescence spectroscopy. The single-molecule measurements show consistent results with the ensemble-averaged measurements, indicating an unbiased sampling of all molecules. Both static and dynamic heterogeneity in the interfacial ET process are revealed by the single-molecule study.

3.2 Results and Discussion

3.2.1 Ensemble-Averaged Electron Transfer Dynamics

The ensemble-averaged ET dynamics from organic dye molecule Rhodamine B (RhB) to various semiconductors (SnO_2, In_2O_3 and ZnO) have been studied recently by transient absorption in the visible and mid-IR.[63] The ET process can be represented by following scheme:

$$RhB^{*} + Nano \xrightarrow{K_{et}} RhB^{+} + Nano^{-} \xrightarrow{K_{bet}} RhB + Nano \quad \text{(Scheme 3.1)}$$

where RhB, RhB* and RhB^+ represent RhB molecules in the ground, excited and oxidized states, respectively. The ET process was monitored by the decay of RhB excited state absorption and stimulated emission, the formation of RhB cation and injected electrons in SnO_2. Figure 3.2 A shows the transient absorption spectrum of SRhB molecules sensitized on SnO_2 nanoparticles. Because the UV-vis absorption spectrum of SRhB is only slight red-shifted (~7nm) from RhB, the observed features in the transient absorption measurement of SRhB can be assigned following those for RhB. The spectral evolution shows the decay of the excited SRhB (absorption at 460nm and stimulated emission at 570-650nm) and the formation of SRhB cation (~494 nm) in the first 10 ps, indicating electron transfer from SRhB excited state to SnO_2. Then the decrease of amplitude of the cation absorption after 10 ps is due to the recombination of the cation with injected electrons to reform SRhB molecules in the ground state. The ET dynamics from SRhB to TiO_2 nanoparticles was also studied by transient absorption measurement. Unfortunately, we could not obtain clear spectrum due to the quickly bleaching of SRhB molecules under photo excitation. However ET processes to TiO_2 nanoparticles from other directly attached organic chromophores was also reported to be on the picosecond or faster time scales. [2,75]

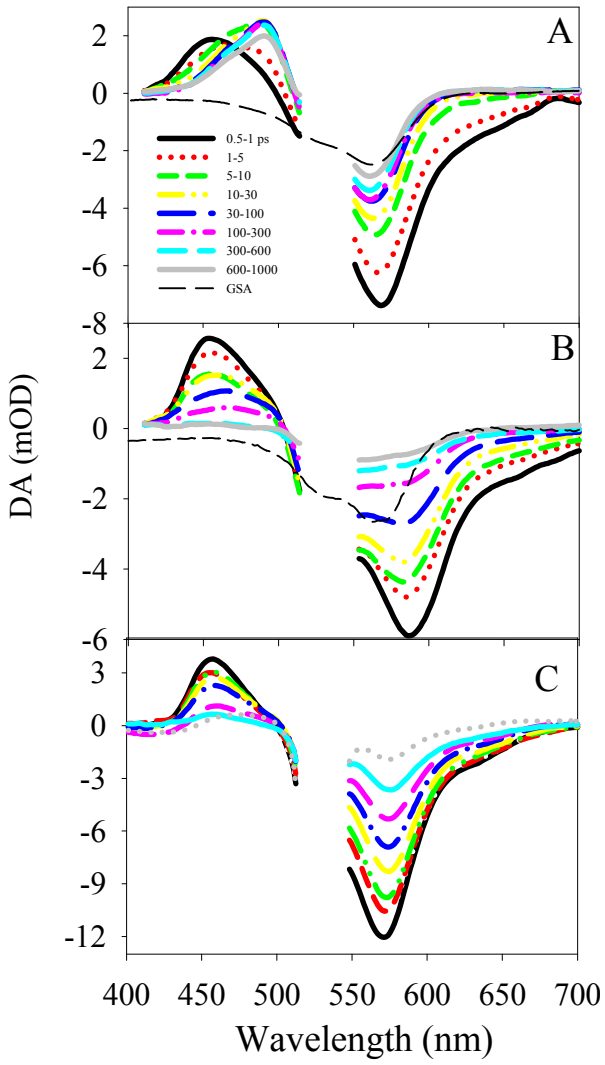

Figure 3.2. Transient absorption spectra of (A) SRhB-SnO_2, (B) SRhB-Silane-SnO_2 and (C) SRhB-Silane-TiO_2 recorded at indicated delay time (in unit of ps) following 532 nm excitation. Also plotted along the negative vertical axis is the ground-state absorption (GSA) of SRhB-SnO_2 and SRhB-Silane-SnO_2 (dashed black lines). The transient spectra consist of the bleach of ground-state absorption at 550 nm, stimulated emission at 570-650 nm and excited state absorption at ~460 nm in (A), (B) and (C). The cation absorption at ~494 nm is also observable in (A), indicating the presence of interfacial ET.

The photoinduced ET from SRhB to SnO_2 and TiO_2 nanoparticles should be significantly slowed down in the donor-bridge-acceptor complex. The transient absorption spectra of SRhB-Silane-SnO_2 and SRhB-Silane-TiO_2 are shown in Figure 3.2 B and C. Unlike the dyes directly sensitized on SnO_2, the decays of excited state absorption (~460 nm) and stimulated emission (570-650 nm) did not result in the formation of SRhB cation (absorption at ~494 nm) on the same time scale. Instead, they lead to regeneration of the ground state molecules as indicated by the recovery of the ground state bleach. The presence of an isosbestic point at 510 nm provides the evidence that the transient spectra at this region consist of two species (excited absorption at 460 nm and ground state bleach) which are formed instantaneously and decay with the same kinetics. The excited state decay occurred in a few hundreds of picoseconds, much shorter than the 3 ns excited state lifetime of isolated SRhB in solution. This decay is attributed to the quenching between excited dye molecules on SnO_2 and TiO_2 films, similar to that observed for RhB/ZrO_2 system where ET is not energetically allowed.[63] The ET rate is slower than the quenching rate among excited molecules, and then unable to be observed by transient absorption measurement. For SRhB-Silane-TiO_2, we did not observe significantly bleaching of SRhB molecules under photo excitation due to the slow ET process.

Ensemble-averaged fluorescence decay measurement can be more informative to probe such slower ET process. To reduce chromophore self-quenching effect, we measured ensemble-averaged ET dynamics by TCSPC, which can be performed at much lower dye coverage and excitation power. SRhB-Silane water solution with a concentration as low as ~10^{-8} M was used to immobilize on glass, ZrO_2, SnO_2 and TiO_2

nanoparticle thin films for ensemble fluorescence decay measurements. Their fluorescence decays are shown in Figure 3.3. The fluorescence decays of SRhB-Silane-ZrO_2 and SRhB-Silane-Glass are very similar, whereas they are slower than those of SRhB-Silane-SnO_2 and SRhB-Silane-TiO_2. ZrO_2 has high conduction band edge position, ET from SRhB to ZrO_2 is not energetically allowed, and the refractive index and film morphology of ZrO_2 nanoparticle film are similar to SnO_2 and TiO_2, and hence the effects of dielectric constant on the radiative lifetime of the molecules on these surfaces are similar[76]. The energy transfer from dye to semiconductors is not possible because of the negligible absorption of SnO_2 and TiO_2 at wavelength longer than 500 nm. Therefore we attribute the faster fluorescence decay of SRhB-Silane-SnO_2/TiO_2 to the ET from dye molecules to SnO_2 and TiO_2 nanoparticles.

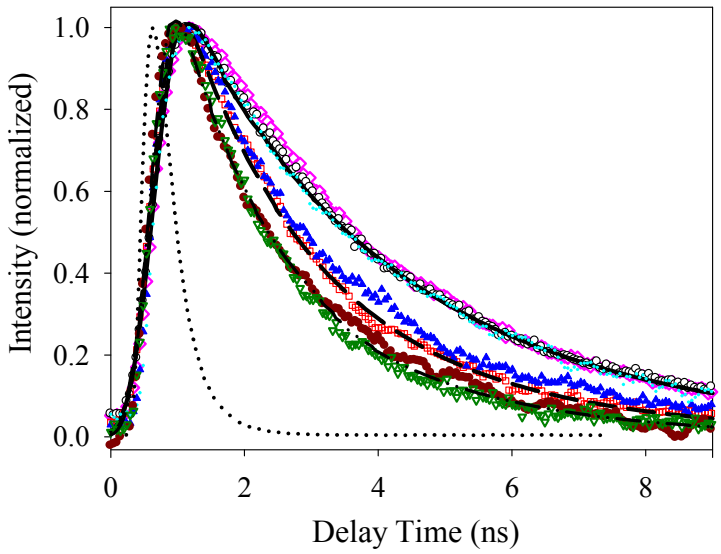

Figure 3.3. Ensemble-averaged fluorescence decays of SRhB-Silane on glass (pink open diamonds), ZrO_2 (black open circles), SnO_2 (red open squares) and TiO_2 (green open triangles) and the instrument response function of these measurements (black dotted line). Multi-exponential fits for the data on ZrO_2 (black solid line), SnO_2 (black dashed line)

and TiO_2 (back dotted-dash line) are also shown. Averaged fluorescence decays constructed from the sum of single SRhB-Silane decays on ZrO_2 (cyan filled diamonds), SnO_2 (blue filled triangles) and TiO_2 (dark red solid circles) are also shown.

Table 3.1. Bi-exponential fitting parameters for fluorescence decay of SRhB-Silane on ZrO_2, SnO_2 and TiO_2. a_i and τ_i are amplitudes and time constants of i^{th} (=1,2) exponents, and τ_{ave} is the amplitude weighted average time constant, as defined in Eq. (3.5) . The errors indicate one standard deviation.

	$a_{1\,(\%)}$	τ_1 (ns)	$a_{2\,(\%)}$	τ_2 (ns)	τ_{ave} (ns)
SRhB-Silane-ZrO_2	0.45 ±0.02	4.3 ±0.2	0.55 ±0.02	2.7 ±0.1	3.4 ±0.4
SRhB-Silane-SnO_2	0.36 ±0.01	3.7 ±0.2	0.64 ±0.02	1.8 ±0.04	2.5 ±0.2
SRhB-Silane-TiO_2	0.64 ±0.02	2.4 ±0.2	0.36 ±0.01	1.0 ±0.03	1.9 ±0.2

The ensemble-averaged fluorescence decays of SRhB-Silane-ZrO_2/SnO_2/TiO_2 are well fit by bi-exponential kinetics, *E(t)*:

$$E(t) = a_1 e^{-t/\tau_1} + a_2 e^{-t/\tau_2} \qquad \text{(Eq. 3.4)}$$

where a_i and τ_i are amplitudes and time constants of the i^{th} (=1,2) exponential component. The amplitude weighted lifetime is then calculated:

$$\tau_{ave} = \frac{a_1\tau_1 + a_2\tau_2}{a_1 + a_2} \qquad \text{(Eq. 3.5)}$$

For SRhB-Silane-ZrO_2, a bi-exponential kinetics indicates a broad distribution of intrinsic lifetimes ($1/K_0$), which prevents an accurate determination ET rate by comparing lifetimes on ET active and inactive substrates according to Eq. 3.1 and 3.2. To estimate

the ET rate, the amplitude weighted lifetime of 3.4 ns is taken as $1/K_0$, and then the ET rates on SnO_2 and TiO_2 are calculated to be 0.11 and 0.23 ns^{-1}. The ET time of SRhB directly sensitized on SnO_2 nanoparticles is a few ps. It has been reported that the ET rate decayed exponentially as the number of chemical bonds separating the chromophore and semiconductor increases: [77]

$$K_{ET}' = K_{ET} e^{-n} \qquad \text{(Eq. 3.6)}$$

where n is the number of chemical bonds. For the SRhB-Silane-SnO_2/TiO_2 complexes, there are 9 bonds separating the conjugated region of the chromophore and the SnO_2/TiO_2. Based on Eq. 3.6 we estimate an ET time in this donor-bridge-acceptor system of ~ 10 ns, similar to that estimated from the measured fluorescence lifetimes.

3.2.2 Wide Field Imaging of Single Molecules

The above ensemble-averaged transient absorption measurements have indicated that the ET times of SRhB molecules directly on SnO_2 and TiO_2 are on ps time scale. Such fast ET rate significantly quenches the fluorescence of molecules and hence hinders the study of the ET process on single-molecule level. To confirm that the ultrafast ET activity is also present under single-molecule condition, we compared samples of SRhB directly sensitized on SnO_2, TiO_2 and glass. The samples were prepared with similar number densities of SRhB molecules. Figure 3.4 show the wide-field-illuminated fluorescence image of these samples. The numbers of observable single molecules on SnO_2 (Figure 3.4 B) and TiO_2 (Figure 3.4 C) are much less than on glass (Figure 3.4 A), confirming that on SnO_2 and TiO_2 the fluorescence of SRhB molecule is significantly quenched due to ET on the ps time scale. It is interesting to note that the lifetimes of

observable bright molecules on SnO_2 and TiO_2 are around 3 ns, similar to the lifetimes of the molecules on glass, as shown in Figure 3.5. Under single-molecule condition, the molecules detected by emission measurements only account for a few percent of the initial excited state population, and these molecules either inject electrons at a slow rate (<< 1/(3ns)) or do not undergo ET at all. Similar observation has been reported before for RhB molecules on Sb:SnO_2 (ATO).[54]

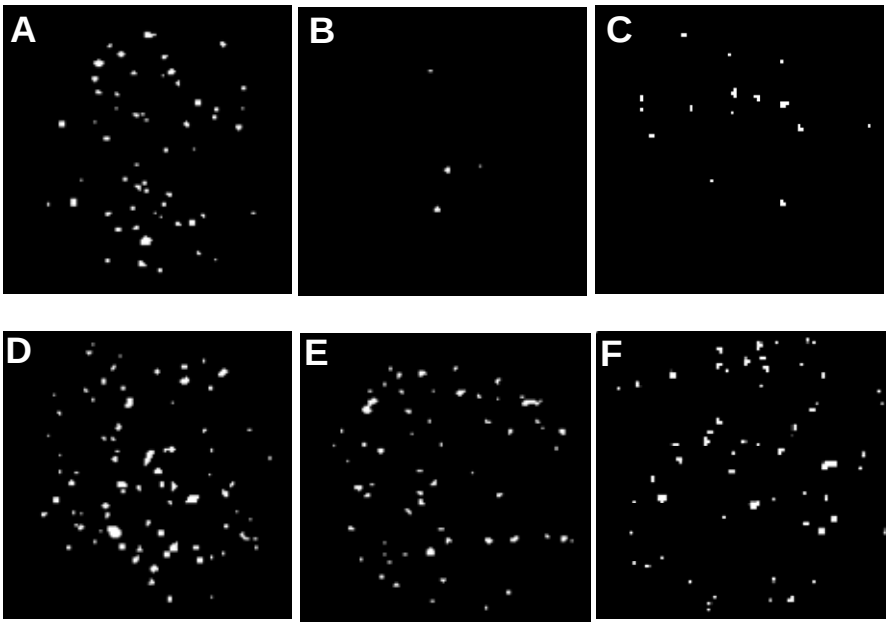

Figure 3.4. Wide-field-illuminated fluorescence images (25 μm × 25 μm) of similar amount of single SRhB molecules dropped on glass (A), SnO_2 film (B) and TiO_2 film (C), and similar amount of single SRhB-Silane molecules immobilized on ZrO_2 (D), SnO_2 (E) and TiO_2 (F) nanocrystalline thin films. All images are obtained under the same condition ($\lambda_{exc.}$: 500 nm; $P_{exc.}$ = 400 W/cm^2).

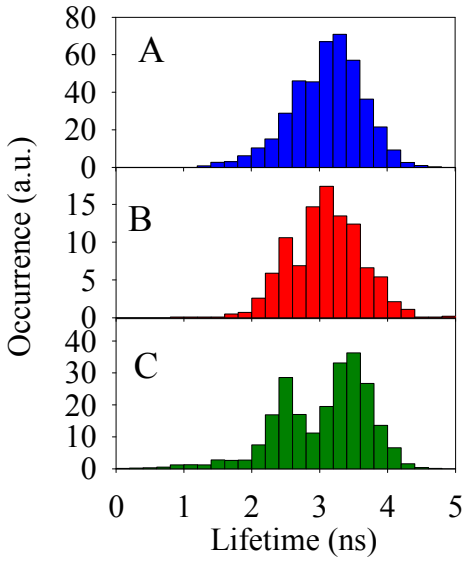

Figure 3.5. Lifetime histograms of single SRhB molecules on glass (A) and observable single SRhB molecules on SnO_2 (B) and TiO_2 (C)

However, for SRhB-Silane-SnO_2 and TiO_2 complexes, their fluorescence lifetimes are long (slow ET rates), and hence enable the study using single-molecule spectroscopy. As shown in the wide-field-illuminated single molecule fluorescence images of SRhB-Silane molecules immobilized on ZrO_2 (Figure 3.4 D), SnO_2 (Figure 3.4 E) and TiO_2 (Figure 3.4 F) (prepared with similar number densities of SRhB-Silane molecules), the number of observable molecules are similar on these three substrates, indicating unbiased sampling of most molecules on ET active substrates. This is further supported by the comparison between ensemble and single molecule fluorescence decays. As shown in Figure 3.3, the fluorescence decays constructed by the sum of 68, 103 and 67 single SRhB-Silane molecules on ZrO_2, SnO_2 and TiO_2, respectively, are very close to their corresponding ensemble-averaged fluorescence decays, confirming a near complete sampling of all molecules under single-molecule condition. Therefore, the single

molecule ET dynamics to be discussed below represents the dynamics of the whole ensemble.

3.2.3. Single-Molecule Dynamics on ZrO_2

The ensemble fluorescence decays of SRhB-Silane on different substrates are non-single exponential, indicating the inhomogeneous distributions of lifetimes and ET rates. To quantify these distributions and understand their origins, fluorescence lifetimes of single SRhB-Silane molecules were measured on ET inactivated substrate ZrO_2 and ET activated substrates SnO_2 and TiO_2.

The results of 68 single SRhB-Silane molecules on ZrO_2 are fist discussed. Figure 3.6 shows two typical single molecule fluorescence and lifetime trajectories on ZrO_2 as well as their corresponding lifetime histograms. The fluorescence intensity trajectory was constructed by the number of photons within a bin time of 0.1 s. The delay time histograms of photons within 2 second bin time were constructed and fit by single exponential function to obtain the lifetime trajectories with 0.5 s step size. It is to note that the lifetimes were calculated after background subtractions, as shown in Figure 3.6 E. The background trace was constructed with the photons within 2 s after the molecule was photo bleached. To determine accuracy of lifetime measurement in this study, a plot of chi-square of single exponential fit as a function of lifetime for a total of ~800 photons for a single SRhB-Silane-SnO2 is shown in Figure 3.6 F. This corresponded to the lowest number of total photons in a 2 s window and represented the largest uncertainty in lifetime determination. The change in chi-square increases by ~20% when lifetime deviates from the best fit value by ~200 ps. A bin size of 200 ps was used to construct the

lifetime histograms. The lifetimes at different bins are considered as a real change. For example, we compare in Figure 6E the fluorescence decay curve for two points (P1 and P2) in the lifetime trajectory shown in Figure 6C. The best fit lifetime values of these points are 3.3 and 2.8 ns respectively, and their decay curves can be differentiated.

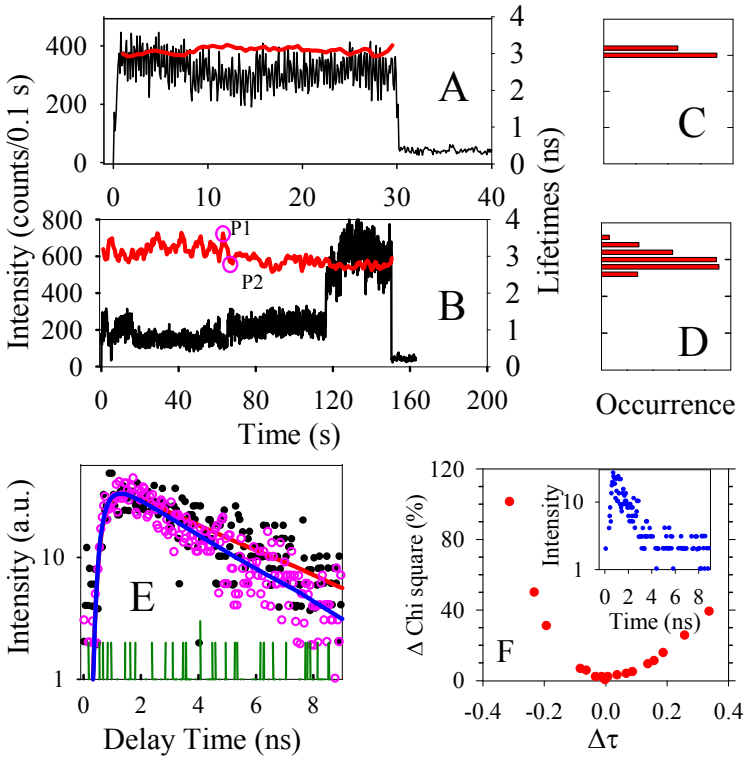

Figure 3.6. Typical fluorescence intensity (black) and lifetime (red) trajectories of two single SRhB-Silane molecules on ZrO_2 (A and B), and their corresponding lifetime histogram (C and D, respectively). The delay time histograms of the points P1 and P2 in C are plotted in panel E. Solid lines are their corresponding single exponential fit. Green trace is their background. The change of chi-square of exponential fit to a fluorescence decay curve (shown in inset) as a function of lifetime for a SRhB-Silane-SnO_2 complex is shown in panel F. This represents the smallest number of fluorescence photons (~800) in a 2 s window and the largest uncertainty in lifetime obtained from fit.

The lifetime distributions of the single molecules shown in Figure 3.6 A and B are shown in Figure 3.6 C and D, respectively. The average single molecule lifetime is calculated as:

$$\tau_{ave} = \frac{\sum_i p_i \tau_i}{\sum_i p_i} \qquad \text{(Eq. 3.7)}$$

where p_i, and τ_i are the occurrence and lifetime in the lifetime histogram for each molecule, respectively. To quantify the fluctuation of the lifetime trajectory, the standard deviation (STDEV) σ of the lifetime distribution is calculated as:

$$\sigma = \sqrt{\frac{\sum_i p_i (\tau_i - \tau_{ave})^2}{(\sum_i p_i - 1)}} \qquad \text{(Eq. 3.8)}$$

The histogram of the average lifetimes of all studied single SRhB-Silane molecules on ZrO_2 is shown in Figure 3.7 A. The average lifetime varies from 2.4 to 4.6 ns with a peak at 3.2 ns. However, because lifetime fluctuates over the duration of measurement for each molecule, the distribution of average lifetime doesn't adequately describe the ensemble distribution of lifetime. Therefore, we added up the lifetime histograms of all single molecules. The resulting total lifetime histogram shown in Figure 3.7 D should reflect the distribution of lifetime of the whole ensemble. The distribution can be well described by a Gaussian function with a center at 3.3 ns and a FWHM of 0.9 ns. It is worth to note that although the ensemble average fluorescence decay of this sample can be fit phenomenologically by bi-exponential decay (see Figure 3.3), this fit doesn't describe the underlining heterogeneous distributions. Through the study of single molecules, these distributions can be revealed.

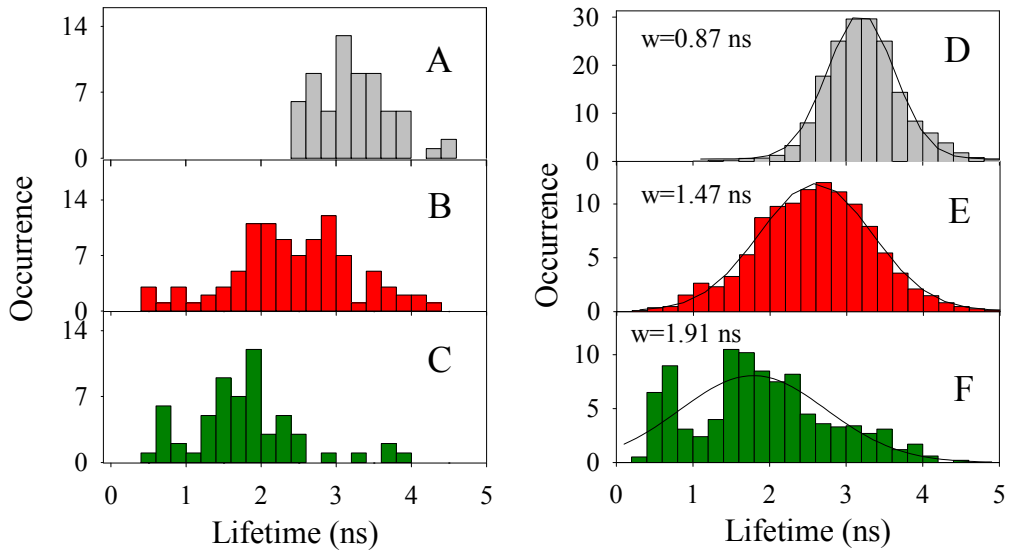

Figure 3.7. (A, B and C) Histograms of average single molecule lifetimes of SRhB-Silane on ZrO_2, SnO_2 and TiO_2, respectively. (D, E, F) Also plotted are the histograms of total single molecule lifetimes of SRhB-Silane on ZrO_2, SnO_2 and TiO_2, respectively. The total lifetime histograms are the sum of lifetime histrograms of all single molecules. The solid line in panels D, E and F are the gauss fits of the lifetime distributions. The FWHM is shown beside.

The lifetime STDEV of single SRhB-Silane molecules on ZrO_2 is shown in Figure 3.8 A. Most (90%) molecules show small fluctuations of lifetime (σ < 0.4). For the molecules on ZrO_2 where the ET is inactive, their lifetimes depend on the radiative and nonradiative rates. The observed lifetime distribution of single molecule is caused by the fluctuation of either radiative or nonradiative rates. It has been reported that the nonradiative decay rate of rhodamine B is determined by polarity and rigidity of medium because of the presence of twisted intramolecular charge-transfer (TICT) excited states.[78,79] Its quantum yield was about 1 in a rigid environment and radiative decay time

was about 5 ns in alcohols.[74] Based on Eq. 3.1 and 3.3, the fluctuation of nonradiative rate will lead to positive correlation between lifetime and fluorescence intensity. However, there is no correlation between the fluctuations in lifetime and intensity for molecules on ZrO_2. For example, the molecule in Figure 3.6 B shows a sudden change of fluorescence intensity at ~ 115 s, but the lifetime trajectory still keeps at a constant level. Therefore, the observed distribution and fluctuation of lifetimes should not be due to a fluctuation in nonradiative decay rate. For a fluorescence molecule at an interface, its radiative lifetime depends on the refractive index of the media and the orientation of the molecule relative to interface normal.[76,80] A distribution of single molecule lifetimes on glass due to variation of orientation has been observed in previous studies.[54,76] We attribute the observed lifetime distribution to the distribution and fluctuation of the orientation of SRhB-Silane molecules relative to surface normal. As we will discuss below, the presence of the bridge introduces conformation flexibility in the donor-bridge-acceptor system studied here.

About 25% of the molecules show significant fluctuation of fluorescence intensities, as the molecule shown in Figure 3.6 B, while their lifetime trajectories are stay at constant levels. These intensity fluctuations are similar to other single molecules on non-ET active substrates, and have been attributed to spectral diffusion and formation of non-emissive states[48,81-84]

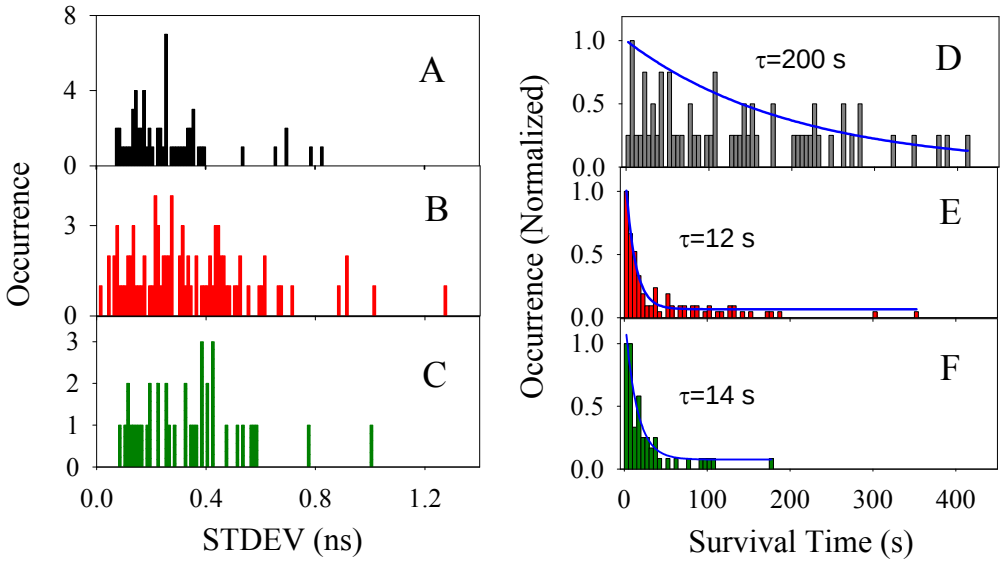

Figure 3.8. The histograms of lifetime STDEV (A, B and C) and the histograms of survival times (D, E and F) of single SRhB-Silane molecules on ZrO_2, SnO_2 and TiO_2, respectively. The blue solid lines in panel D, E and F are the single exponential fits of the histograms.

3.2.4. Single-Molecule Dynamics on SnO_2 and TiO_2

103 and 67 single SRhB-Silane molecules on ET activate substrates, SnO_2 and TiO_2, respectively, were studied by single-molecule fluorescence spectroscopy. The fluorescence intensity and lifetime trajectories were constructed for each single molecule. There are 9 of molecules on SnO_2 and 15 on TiO_2 which were photo bleached within 2-3 s, and their lifetime STDEV were not able to be calculated. A few typical fluorescence intensity and lifetime trajectories of single SRhB-Silane molecules on SnO_2 and TiO_2 are shown in Figure 3.9 and 3.10, respectively. Compared to ZrO_2, the molecules on SnO_2 and TiO_2 exhibit significantly different characteristics due to the presence of interfacial ET pathway. The main differences include:

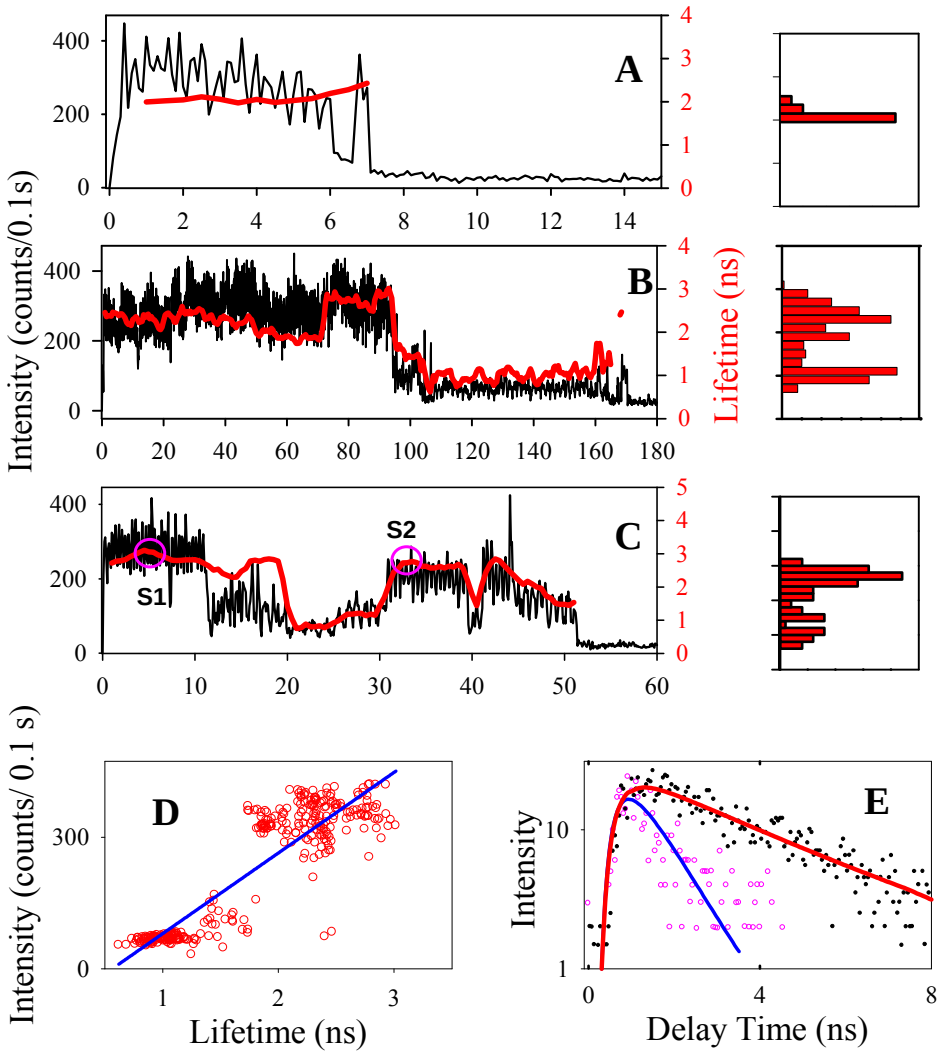

Figure 3.9. Typical fluorescence intensity (black) and lifetime (red) trajectories of single SRhB-Silane molecules on SnO_2 (A, B and C). The fluorescence intensity as a function of lifetime of the molecule in panel B as well as its linear fit (blue solid line) is plotted in panel D. The fluorescence decays and their single exponential fits of selected points P1 (black circles) and P2 (red circles) in trajectory in panel C are shown in panel E.

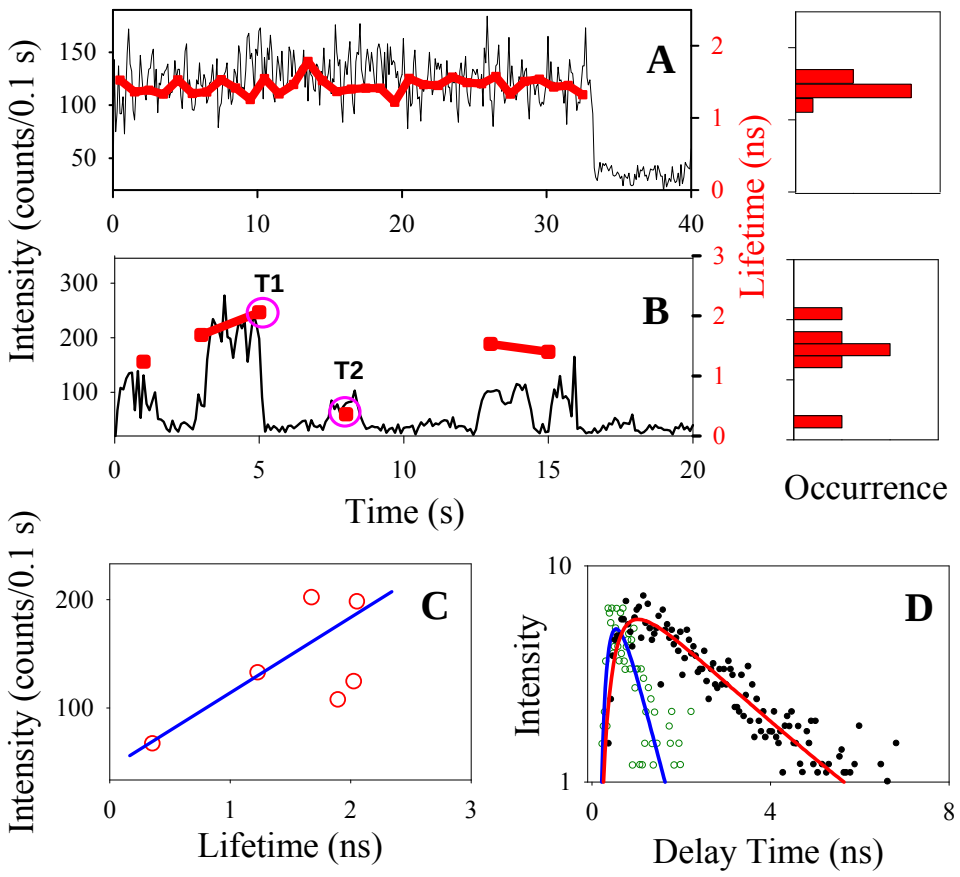

Figure 3.10. Typical fluorescence intensity (black) and lifetime (red) trajectories of single SRhB-Silane molecules on TiO_2 (A and B). The fluorescence intensity as a function of lifetime of the molecule in panel B as well as its linear fit (blue solid line) is plotted in panel C. The fluorescence decays and their single exponential fits (solid lines) of selected points P1 (black circles) and P2 (green circles) in trajectory in panel B are shown in panel D.

i) The lifetimes on SnO_2 and TiO_2 are shorter and the lifetime distributions become broader. For molecules on SnO_2 and TiO_2 the average lifetime histograms have peaks centered at ~2.6 ns on SnO_2 (Figure 3.7 B) and ~1.7 ns on TiO_2 (Figure 3.7 C), and lifetimes are distributed from 600 ps to 4ns on both substrates. The total lifetime

histograms show Gaussian distributions with center and FWHM of ~2.6 ns and 1.5 ns on SnO_2 (Figure 3.7 E), and ~1.8 ns and 1.9 ns on TiO_2 (Figure 3.7 F). The lifetime distributions indicate that on SnO_2 and TiO_2, the single molecule lifetimes become shorter and the distribution widths are much broader compared to ZrO_2. The shorter single molecule fluorescence lifetimes of SRhB-Silane on SnO_2 and TiO_2 can be attributed to the presence ET activity. Additionally, the distributions exhibit clear dependence of single molecule lifetime on the substrate, showing a trend of decreasing lifetime and broadening distribution from ZrO_2 to TiO_2. All these observations from single molecule measurements are consistent with those of ensemble-averaged measurements. A broadened distribution of lifetimes on SnO_2 and TiO_2 suggests additional broadening due to the distribution of ET rates.

ii) The single molecules on SnO_2 and TiO_2 exhibit larger fluctuation of lifetime and positive correlation between lifetime and florescence intensity. The trajectories can be separated into two categories. In the first category, the single molecules show small fluctuation of lifetimes similar to those on ZrO_2. This category includes 60% of molecules on SnO_2 and 65% of molecules on TiO_2, whose STDEVs (σ) are < 0.4 (Figure 3.8 A, B and C). Shown in Figure 3.9 A and 3.10 A are examples of such single molecules on SnO_2 and TiO_2, respectively. In the second class of single molecules, there exist large fluctuations of lifetimes. This category includes 40% of molecules on SnO_2 and 35% of molecules on TiO_2, whose σ are > 0.4 (Figure 3.8 A, B and C). A few typical molecules are shown in Figure 3.9 B and C and 3.10 B. In these trajectories, lifetime decrease is companied by a decrease in fluorescence intensity, as shown in Figure 3.9 D and Figure 3.10 C, suggesting a fluctuation of nonradiative decay rate. The larger

fluctuation of lifetime can be attributed to the fluctuation of ET rates in these donor-bridge-acceptor complexes. An increase in ET rate should reduce fluorescence lifetime as well as fluorescence quantum yield, accounting for the observed correlation between lifetime and intensity fluctuation.

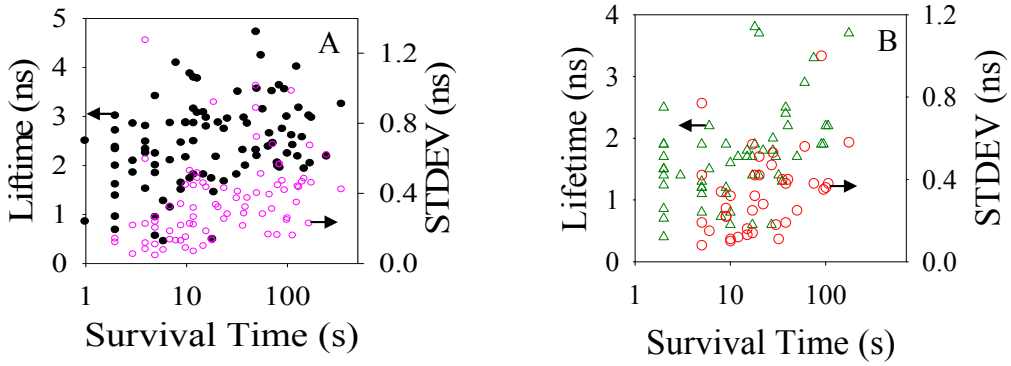

Figure 3.11. The average lifetimes and standard deviations as a function of their survival times for single molecules on SnO_2 (A) and TiO_2 (B).

iii) The single molecules on SnO_2 and TiO_2 have shorter survival times. The survival time of the single molecule is defined as the duration time until the molecule is irreversible photo bleached. The histograms of survival times of single molecules on ZrO_2, SnO_2 and TiO_2 are plotted in Figure 3.8 D, E and F, respectively. The histograms are fit by single exponential function with time constants of 200, 12, and 14 s on ZrO_2, SnO_2 and TiO_2, respectively, indicating that the average survival times of single molecules on SnO_2 and TiO_2 are ~15 times shorter than on ZrO_2. The shortening of survival times are attributed to the ET from SRhB-Silane molecule to SnO_2 and TiO_2, which generates oxidized SRhB radical that is unstable in air. For molecules with short survival times, their average fluorescence lifetimes appear to be shorter and their

fluctuations (as measured by standard deviation) appear to be smaller, as shown in Figure 3.11 A and B. It is unclear whether the limited survival time in these trajectories has prevented the sampling of their fluctuation.

3.2.5 Distributions of ET Rates on SnO_2 and TiO_2

To resolve the ET rate distributions of single SRhB-Silane molecules on different substrates, the total rate (K_0 = 1/lifetime) distributions are plotted in Figure 3.12. The fluorescence decay rate distribution $I(k_0)$ of single molecules on ZrO_2 in Figure 3.12 A indicates the variation of K_0 among different molecules and at different times. For molecules on SnO_2 and TiO_2, the fluorescence decay rate is given by $K=K_0+K_{et}$. The measured decay rate distributions $H(K)$ of single molecules on SnO_2 and TiO_2 in Figure 3.12 B and C are dependent on both the distributions of the interfacial ET rates ($F(K_{et})$) and the intrinsic decay rates $I(k_0)$ of molecules:

$$H(k) = \int_0^\infty I(k_0)F(k-k_0)dk_0 \qquad \text{(Eq. 3.9)}$$

Thus the ET rate distribution can be obtained from the measured $H(k)$ and $I(k_0)$ according to Eq. 3.9. The ET rate distributions of molecules on SnO_2 and TiO_2 are shown in Figure 3.12 D and E, respectively. The average ET rates are calculated to be 0.18 ns^{-1} on SnO_2 and 0.46 ns^{-1} on TiO_2.

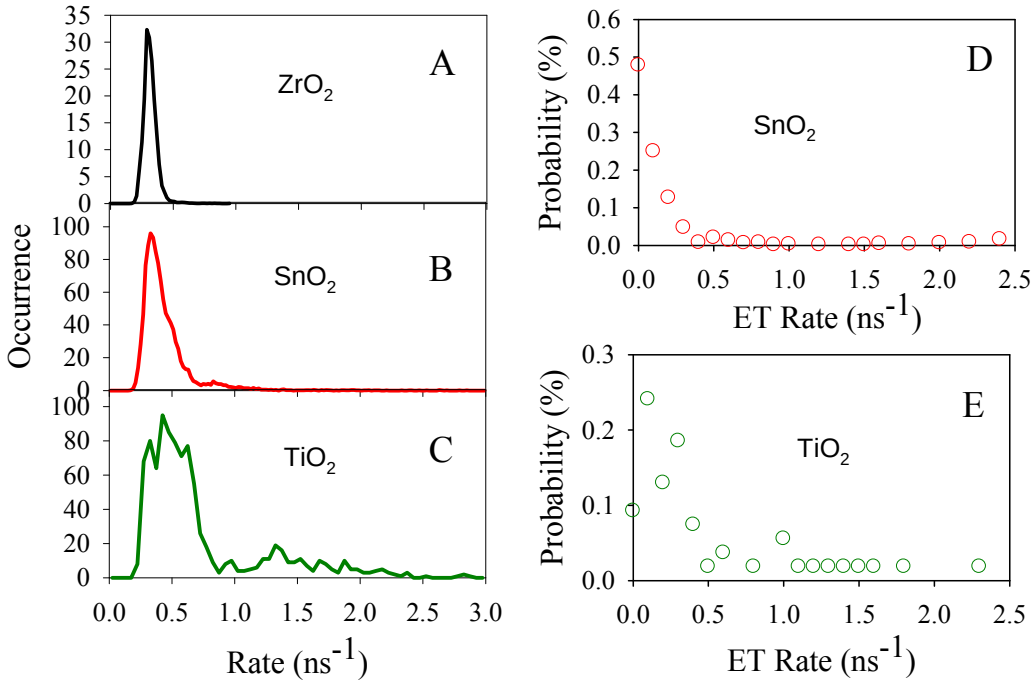

Figure 3.12. The total rate distributions of single molecule on ZrO_2 (A), SnO_2 (B) and TiO_2 (C). Also plotted are the ET rate distributions of single molecules on SnO_2 (D) and TiO_2 (E).

The IET process has been theoretically explained by Marcus theory. Briefly, in the nonadiabatic limit, the total ET rate can be expressed as the sum of ET rates to all possible accepting states in the semiconductor:[85-88]

$$k_{ET} = \frac{2\pi}{h}\int_{-\infty}^{\infty} dE\rho(E)\left|\overline{H}(E)\right|^2 \frac{1}{\sqrt{4\pi\lambda k_B T}}\exp\left[-\frac{(\lambda + \Delta G_0 - E)^2}{4\lambda k_B T}\right] \qquad \text{(Eq. 3.10)}$$

where $\Delta G^0 = E(S^+/S^*) - E_{CB}$ is the energy difference between conduction band edge (E_{CB}) and the redox potential of adsorbate excited state ($E(S^+/S^*)$); $\rho(E)$ is the density of state at energy E from the conduction band edge; $H_{DA}(E)$ is the average electronic coupling between the adsorbate excited state and different k states in the semiconductor

at the same energy E; λ is the total reorganization energy. According to Eq. 3.10, the interfacial ET rate depends on the energy difference between conduction band edge and redox potential of adsorbate excited state, the density of accepting states in the semiconductor, the electronic coupling and reorganization energy. Distribution of reorganization energy was reported in a previous study of raman spectrum of single TiO_2 particles sensitized by dye molecules.[89] In addition, static and dynamic heterogeneity of the driving force and electronic coupling strength can also lead to the observed distribution and fluctuation of ET rates. The driving force is determined by the energy of accepting states in the semiconductor and excited state oxidation potential of dye. The former is dependent on conduction band edge position, which has been shown to be sensitive to surface charge, such as protonation state.[90,91] Single molecule spectral diffusion has been observed and can lead to shift of the energy of LUMO orbital and the excited state oxidation potential.[48,81] The electronic coupling is strongly related to the molecule-substrate interaction. A distribution of site specific molecule-substrate interactions can give rise to a broad distribution of ET rates. In the donor-bridge-acceptor system, ET from SRhB to SnO_2 can occur either through super-exchange via the silane bridge units or through space. For both pathways, the coupling strength is sensitive to the conformation of the donor-bridge-acceptor complex.

3.2.6 Computational Modeling of Interfacial ET

The observed distribution and fluctuation of single molecule lifetimes suggests static and dynamic heterogeneity in IET rates and/or radiative decay rates. As have mentioned above, the presence of silane bridge can introduce additional conformational flexibility in

the complex and hence enhance the fluctuation of ET rate. To investigate the origin of this heterogeneity, we have performed molecular dynamics (MD) simulations of SRhB-Silane on hydrated (110) surfaces of rutile SnO_2 at room temperature. This computational simulation work was conducted by Robert C. Snoeberger III and Professor Victor S. Batista at Yale University. The results are summarized in this section.

Computational Structural Models

The attachment of the aminosilane linker to the SnO_2 surface (110) was modeled at the density functional theory (DFT) level. The surface was represented by a slab supercell composed of 108 [SnO_2] units (*i.e.*, 3 layers of Sn^{4+} ions and 9 layers of O^{2-} ions) with a vacuum spacer of 10 Å along the direction of the normal separating the periodic slabs. The surface bridging O^{2-} ions were capped with hydrogen atoms and the silane molecule was adsorbed in a bridging mode between two penta-coordinated Sn^{4+} ions on the surface (see Figure 3.13). The DFT calculations were performed using the Vienna Ab initio Simulation Package (VASP).[92-94] Vanderbilt Ultrasoft pseudopotentials were used to describe the core electrons. A 400 eV energy cutoff was used to truncate the plane-wave basis. Electron exchange and correlation were described using the PW91 generalized gradient approximation (GGA) functional. A 5×1×1 Monkhorst-Pack *k*-point sampling was used to integrate over the Brillouin zone.

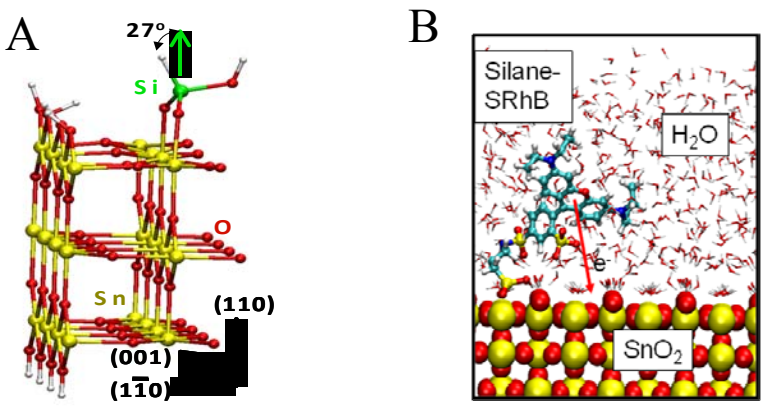

Figure 3.13. (A) Attachment of the silane linker to the SnO_2 surface as described at the DFT PW91 level of theory; and (B) Snapshot of SRhB-silane on the (110) surface of SnO_2 exposed to room-temperature humidity conditions. Color key: O (red), C (light blue), N (blue), H (white), Si (light yellow), Sn (gray yellow).

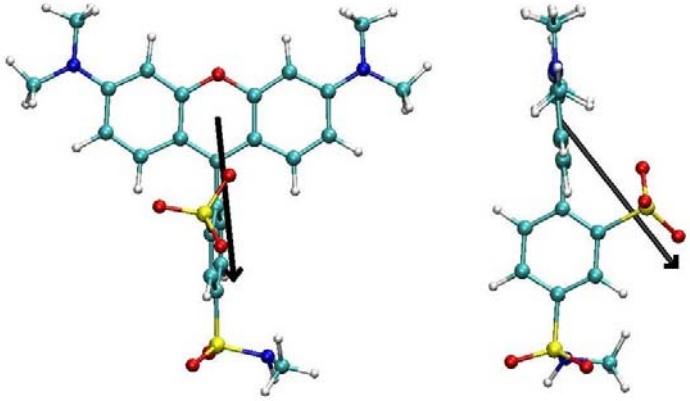

Figure 3.14. Orientation of the $S_1 \leftarrow S_0$ transition dipole moment (black arrow) of SRhB-Silane obtained at the TDDFT-B3LYP/6-31G (d) level of theory.

The minimum energy structure of the SRhB-Silane adsorbate, with the silane linker truncated as a methyl group, was obtained at the DFT B3LYP/6-31G(d) level as implemented in the Gaussian 03 suite of computational chemistry software.[7] The vertical

excitations and transition dipole moments for the first three singlet excited state ($S_1 - S_3$) were computed at the time-dependent (TD) DFT level of theory. Figure 3.14 shows the $S_1 \leftarrow S_0$ transition dipole moment. In the plane of the molecule, the transition dipole moment points toward the aminosilane linker (Figure 3.14 A) while in the direction normal to the molecular plane, the transition dipole moment points towards the sulfonate group (Figure 3.14 B). The orientation of the transition dipole can, therefore, be correlated with the orientation of the sulfonate group. For example, when θ_e (angle between transition dipole and the SnO_2 surface normal) > 90º the sulfonate group is pointing toward the surface, and when $\theta_e < 90^\circ$ the sulfonate group is pointing away from the surface. Furthermore, when $\theta_e \approx 180^\circ$, the sulfonate group is below the three conjugated rings relative to the surface, while $\theta_e \approx 0^\circ$ the three conjugated rings are below the sulfonate group and in close contact with the surface.

Molecular Dynamics Simulations

An ensemble of thermal configurations was generated according to a molecular dynamics (MD) simulation at 300 K performed with the molecular dynamics package NAMD.[95] SRhB-Silane was described by the Amber[96] force field with nuclear atomic charges parametrized according to the Electro Static Potential (ESP) charges obtained by fitting the DFT-B3LYP electrostatic potential calculated with Gaussian 03. The SnO_2 charges and van der Waals parameters were obtained from the work of Bandura *et al*.[97] A 2 nm thick layer of surface waters were included in the dynamics. All MD simulations were subject to the constraints of fixed configurations for the SnO_2 units and siloxane linker group at the *ab initio* minimum energy configuration obtained at the DFT-PW91 level.

Computations of Interfacial Electron Transfer Rate

The time scale $\tau_{et} = \hbar/\gamma$ of interfacial ET was estimated from the broadening γ of the initially populated electronic state in the adsorbate molecule, when coupled to the conduction band[98]

$$\gamma = \sum_i p_i \left| E_d - \varepsilon_i \right| \qquad \text{(Eq. 3.11)}$$

where p_i is the population of the i^{th} orbital with energy ε_i and

$$E_d = \sum_i p_i \varepsilon_i \qquad \text{(Eq. 3.12)}$$

is the energy of the initial state. Figure 3.15 shows the computed distribution of ET times, τ_{et}, obtained from an ensemble of 50,000 configurations of the SRhB-Silane-SnO_2 system at room temperature, sampled from 100 independent MD trajectories for 1 ns. The distribution of ET times in Figure 3.15 is broad, with an average injection time of 27.5 ns The analysis of injection times, as correlated to the orientation and separation of the adsorbate from the surface, indicates that most of the broadening of the distribution shown in Figure 3.15 is due to the effect of conformational flexibility on the electronic couplings responsible for electron injection.

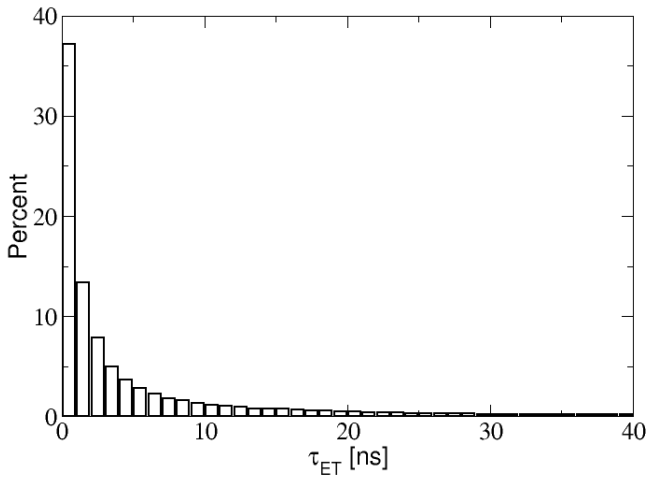

Figure 3.15. Distribution of IET times obtained as described in the text for an ensemble of 50,000 configurations of the SRhB-silane(H_2O)n/SnO_2 supercell, sampled according to room temperature MD simulations.

Computations of Fluorescence Decay Times

The radiative lifetimes τ_r ($1/K_r$) of the adsorbate was estimated as follows,[99]

$$\tau_r = \tau_\infty \left(\frac{L_{\parallel}(z)}{L_\infty} \sin^2(\theta_e) + \frac{L_{\perp}(z)}{L_\infty} \cos^2(\theta_e) \right)^{-1}, \qquad \text{(Eq. 3.13)}$$

by scaling the radiative lifetime of the molecule in solution τ_∞ by the multiplicative factor that depends on the angle θ_e between the emission dipole and the surface normal, and the ratios of radiation power perpendicular and parallel to the interface $\frac{L_{\parallel}}{L_\infty}$ and $\frac{L_{\perp}}{L_\infty}$ that depend on the adsorbate-surface distance and the difference of refractive indices of the media at the interface. Our calculation of these ratios assumes that the wavelength of the incident light λ_1 ~500 nm is much longer than the distance z~1 nm of the adsorbate from the surface. Therefore,

$$\frac{L(z)}{L_\infty} = l_0 + l_1(\frac{4\pi z}{\lambda_1}) + ... \approx l_0, \qquad \text{(Eq. 3.14)}$$

where l_0 depends on the ratio of refractive indices of the two media at the interface.[8] Figure 3.16 shows the ensemble distribution of angles θ_e and adsorbate-surface distances obtained for the ensemble of thermal configurations generated by molecular dynamics simulations of SRhB-Silane anchored to a SnO_2 surface (110). Figure 3.16 shows that the distribution of angles is centered at ~140° ± 20°, indicating that the orientation of the adsorbate with sulfonate group pointing toward the semiconductor surface remains quite constrained for a wide range of configurations. The broad distribution of adsorbate-surface separations, in the 4–18 Å range, indicates that, even with a relatively constrained orientation, the flexibility of the aminosilane linker allows the linker to get partially solvated and separate from the surface. Most of the underlying broadening is due to the partial solvation of the adsorbate on the hydrated SnO_2 surface and is not observed in analogous MD simulations of SRhB-Silane attached to dry SnO_2, where the dominant interactions force SRhB-Silane to remain in close contact with the SnO_2 surface.

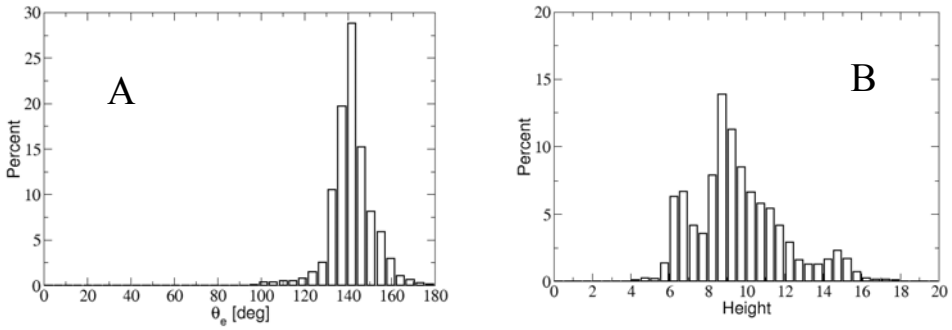

Figure 3.16. (A) Distributions of angles between the transition dipole moment of SRhB-Silane and the SnO_2 surface normal. (B) Distance distribution of adsorbate (center of mass)-surface, separation measured in Å.

The value of the intramolecular nonradiative decay time $\tau_{nr} = \frac{\tau_{sol}}{(1-\Phi)}$ was estimated to be 7.7 ns from the measured total lifetime of $\tau_{sol} = 3.1$ ns SRhB in ethanol and a reported fluorescence quantum yield $\Phi = 0.6$ of rhodamine B in ethanol. The total intrinsic decay rate K_0 $(1/\tau)$ (without IET) is the sum of radiative ($K_r=1/\tau_r$) and intramolecular nonradiative ($K_{nr}=1/\ \tau_{nr}$) decay rates. Figure 3.17 A and B shows distributions of intrinsic lifetimes τ on ZrO_2 and SnO_2, computed according to Eq. (3.1), using the distribution of angles reported in Figure3.16. In the computations, the refractive indices of ZrO_2, SnO_2 and water were 2.006, 2.130 and 1.333, respectively.[100] The value of τ_∞ =11.9 ns was set to fit the experimental lifetime of SRhB-Silane on ZrO_2. The intrinsic lifetimes for molecules with transitions dipole moment parallel and perpendicular to the surface are 3.9 and 2.9 ns on ZrO_2 and 4.1 and 3.1 ns on SnO_2. The calculated average intrinsic lifetimes of SRhB-Silane attached to ZrO_2/H_2O and SnO_2/H_2O surfaces are ~3.2 and ~3.4 ns.

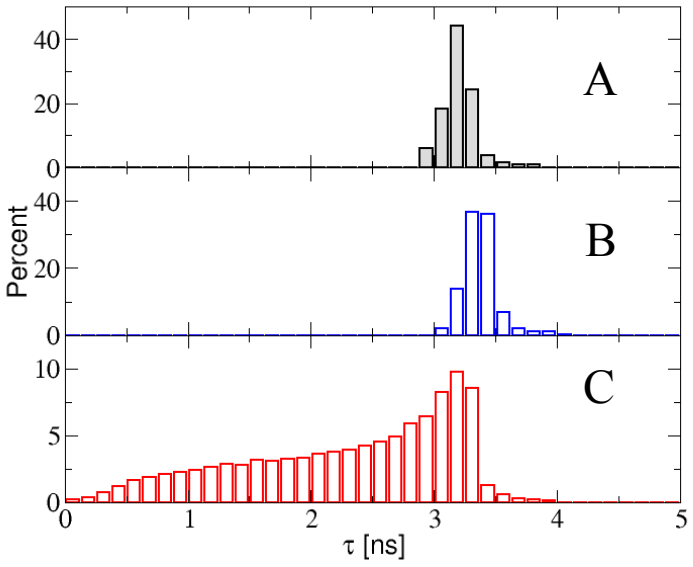

Figure 3.17. Distributions of intrinsic lifetimes τ (without ET), obtained according to Eq. 3.1 for SRhB-Silane molecules attached to ZrO_2 (A) and SnO_2 (B), along with the calculated distribution of observed fluorescence lifetimes τ' (with ET) for SRhB-Silane molecules attached to SnO_2 (C).

The observed fluorescence lifetimes τ' with ET on SnO_2 were computed as follows,

$$\tau' = \left(\frac{1}{\tau} + \frac{1}{\tau_{et}} \right)^{-1} \qquad \text{(Eq. 3.15)}$$

Figure 3.17 C shows the distribution of lifetime τ'. The distribution of lifetimes was computed by randomly sampling values of τ and τ_{et} according to their corresponding distributions. The contribution of a specific randomly sampled τ' to the distribution was weighted by its quantum yield Φ' defined as

$$\Phi' = \frac{\tau'}{\tau_r} \qquad \text{(Eq. 3.16)}$$

The distributions of intrinsic fluorescence lifetimes for SRhB-Silane on ZrO_2 and SnO_2 are quite comparable. However, due to the effect of interfacial ET into SnO_2 (not observed in ZrO_2), the distribution of fluorescence lifetimes with ET for SRhB-Silane on SnO_2 is shifted by about 1 ns to shorter times. The average lifetime is decreased from ~3.4 ns to ~2.3 ns. The distribution on SnO2 with ET is broader when compared to the distribution on ZrO_2. These computational results are partially consistent with the experimental observations, as shown in Figure 3.7 E, where the distribution lifetimes for SRhB-Silane on SnO_2 is broaden and shifted to shorter times (also by ~1 ns) when compared to the distribution of lifetimes for SRhB-Sialne on ZrO_2. The simulations,

however, predict a broader distribution most likely due to the inherent limitations of the computational method applied for estimations of electron injection times.

3.3 Summary

The photoinduced interfacial electron transfer processes in donor-bridge-acceptor (SRhB-Saline-SnO_2 and TiO_2 nanoparticles) complexes have been investigated in this chapter on both ensemble-averaged and single-molecule levels. Ultrafast pump-probe transient absorption measurements showed that in the absence of the spacer ET from SRhB to SnO_2 occurs on the a few picoseconds time scale. However, in the presence of aminosilane spacer, ET times from SRhB to SnO_2 and TiO_2 were slowed to the ns time scale, which were observed by ensemble-averaged fluorescence measurements. The ensemble-averaged fluorescence measurements indicated a substrate dependent ET dynamics. The ET rate increases in the order of ZrO_2, SnO_2 and TiO_2. Wide-field-illuminated single molecule fluorescence images of SRhB molecules (without spacer) on SnO_2, TiO_2 and glass showed that only a few number of molecules on ET activate substrates were observable under single-molecule condition, indicating incomplete sampling of molecules undergoing ultrafast ET on SnO_2 and TiO_2. However, the wide-field-illuminated fluorescence images of SRhB-Silane on SnO_2, TiO_2 and ZrO_2 showed similar numbers of observable single molecules, indicating an unbiased sampling of donor-bridge-acceptor complexes. Furthermore, the fluorescence decays from the sum of single molecule were shown to be in agreement with their corresponding ensemble-averaged fluorescence decays for SRhB-Silane-SnO_2 and TiO_2, suggesting that the single molecules studied by single-molecule spectroscopy represented the whole population.

On the single molecule level, SRhB-Silane-ZrO_2 shows a Gaussian distribution of lifetimes with a center of 3.2 ns and a FWHM of 0.9 ns. The distribution of lifetimes was attributed to the distribution of orientations of the molecules relative to surface normal, which leads to variation of radiative decay rates. The lifetime distributions of SRhB-Silane-SnO_2 and SRhB-Silane-TiO_2 were centered at 2.6 and 1.8 ns with FWHM of 1.5 and 1.9 ns, respectively. Shortened lifetime and broadened distribution were attributed to the presence of ET activity in these complexes, which introduced an additional nonradiative decay channel. It was showed that both static distribution and dynamic fluctuation of ET rates were presenting. The reasons for the distribution and fluctuation of ET rates are not clear. Computational model of the complexes showed a distribution of molecular conformation, which led to a distribution of electronic coupling strengths and ET rates. It was likely that the conversion between these conformations led to the fluctuation of ET rate and fluorescence lifetime on the single molecule level.

Our study showed that interfacial ET can be studied by single molecule spectroscopy. Single molecule ET studies can determine the distribution of ET rates that underlies the nonsingle-exponential kinetics observed in ensemble average measurements. Furthermore, they provide detailed insight to the nature of static and dynamic heterogeneities that are difficult to be revealed by ensemble average studies alone.

References:

(1) Miller, R. J. D.; McLendon, G. L.; Nozik, A. J.; Schmickler, W.; Willig, F. *Surface electron transfer processes*; VCH publishers, Inc.: New York, 1995.

(2) Hagfeldt, A.; Gratzel, M. *Chem. Rev.* **1995**, *95*, 49.

(3) Kamat, P. V. *Chem. Rev.* **1993**, *93*, 267.

(4) Kamat, P. V. *Progress In Reaction Kinetics* **1994**, *19*, 277.

(5) Kamat, P. V.; Meisel, D. *Semiconductor Nanoclusters - Physical, Chemical, and Catalytic Aspects*; Elsevier: Amsterdam, 1997; Vol. 103.

(6) Asbury, J. B.; Hao, E.; Wang, Y.; Ghosh, H. N.; Lian, T. *J. Phys. Chem. B* **2001**, *105*, 4545.

(7) O'Regan, B.; Gratzel, M. *Nature* **1991**, *353*, 737.

(8) Bach, U.; Lupo, D.; Comte, P.; Moser, J. E.; Weissortel, F.; Salbeck, J.; Spreitzer, H.; Gratzel, M. *Nature* **1998**, *395*, 583.

(9) Huynh, W. U.; Dittmer, J. J.; Alivisatos, A. P. *Science* **2002**, *295*, 2425.

(10) Serpone, N.; Pelizzetti, E. *Photocatalysis, Fundamentals and Applications*; John Wiley & Sons, 1989.

(11) Colvin, V. L.; Schlamp, M. C.; Alivisatos, A. P. *Nature* **1994**, *370*, 354.

(12) Aviram, A.; Ratner, M. A. *Chemical Physics Letters* **1974**, *29*, 277.

(13) Nitzan, A. *Annual Review of Physical Chemistry* **2001**, *52*, 681.

(14) Bauer, C.; Boschloo, G.; Mukhtar, E.; Hagfeldt, A. *International Journal of Photoenergy* **2002**, *4*, 17.

(15) Anderson, N. A.; Ai, X.; Lian, T. *J. Phys, Chem. B* **2003**, *107*, 14414.

(16) Gaal, D. A.; Hupp, J. T. *Journal of the American Chemical Society* **2000**, *122*, 10956.

(17) Iwai, S.; Hara, K.; Murata, S.; Katoh, R.; Sugihara, H.; Arakawa, H. *J. Chem. Phys.* **2000**, *113*, 3366.

(18) Ghosh, H. N.; Asbury, J. B.; Lian, T. *J. Phys. Chem. B* **1998**, *102*, 6482.

(19) Huang, H.; Dorn, A.; Bulovic, V.; Bawendi, M. G. *Appl. Phys. Lett. FIELD Full Journal Title:Applied Physics Letters* **2007**, *90*, 023110/1.

(20) Rensmo, H.; Keis, K.; Lindstrom, H.; Sodergren, S.; Solbrand, A.; Hagfeldt, A.; Lindquist, S. E.; Wang, L. N.; Muhammed, M. *Journal of Physical Chemistry* **1997**, *101*, 2598.

(21) Martini, I.; Hodak, J.; Hartland, G. V.; Kamat, P. V. *J. Chem. Phys.* **1997**, *107*, 8064.

(22) Martini, I.; Hodak, J. H.; Hartland, G. V. *J. Phys. Chem. B* **1998**, *102*, 9508.

(23) Martini, I.; Hodak, J. H.; Hartland, G. V. *J. Phys. Chem. B* **1999**, *103*, 9104.

(24) Martini, I.; Hodak, J. H.; Hartland, G. V. *J. Phys. Chem. B* **1998**, *102*, 607.

(25) Ghosh, H. N.; Asbury, J. B.; Weng, Y.; Lian, T. *J. Phys. Chem. B* **1998**, *102*, 10208.

(26) Liu, D.; Fessenden, R. W.; Hug, G. L.; Kamat, P. V. *J. Phys. Chem. B* **1997**, *101*, 2583.

(27) Haque, S. A.; Tachibana, Y.; Klug, D. R.; Durrant, J. R. *J. Phys. Chem. B* **1998**, *102*, 1745.

(28) Kamat, P. V.; Bedja, I.; Hotchandani, S.; Patterson, L. K. *Journal of Physical Chemistry* **1996**, *100*, 4900.

(29) Heimer, T. A.; Heilweil, E. J.; Bignozzi, C. A.; Meyer, G. J. *J. Phys. Chem. A* **2000**, *104*, 4256.

(30) Haque, S. A.; Tachibana, Y.; Willis, R. L.; Moser, J. E.; Graetzel, M.; Klug, D. R.; Durrant, J. R. *J. Phys. Chem. B* **2000**, *104*, 538.

(31) Nelson, J.; Haque, S. A.; Klug, D. R.; Durrant, J. R. *Phys. Rev. B: Condens. Matter Mater. Phys.* **2001**, *63*, 205321.

(32) Barzykin, A. V.; Tachiya, M. *Journal of Physical Chemistry B* **2004**, *108*, 8385.

(33) Palomares, E.; Clifford, J. N.; Haque, S. A.; Lutz, T.; Durrant, J. R. *Chemical Communications (Cambridge, United Kingdom)* **2002**, 1464.

(34) Palomares, E.; Clifford, J. N.; Haque, S. A.; Lutz, T.; Durrant, J. R. *Journal of the American Chemical Society* **2003**, *125*, 475.

(35) Clifford, J. N.; Palomares, E.; Nazeeruddin, M. K.; Thampi, R.; Graetzel, M.; Durrant, J. R. *Journal of the American Chemical Society* **2004**, *126*, 5670.

(36) Hasselmann, G. M.; Meyer, G. J. *J. Phys. Chem. B* **1999**, *103*, 7671.

(37) Guo, J.; She, C.; Lian, T. *J. Phys. Chem. B.* **2005**, *109*, 7095.

(38) Weng, Y.-X.; Wang, Y.-Q.; Asbury, J. B.; Ghosh, H. N.; Lian, T. *J. Phys. Chem. B* **2000**, *104*, 93.

(39) Kilsa, K.; Mayo, E. I.; Kuciauskas, D.; Villahermosa, R.; Lewis, N. S.; Winkler, J. R.; Gray, H. B. *J. Phys. Chem. A* **2003**, *107*, 3379.

(40) Desilvestro, J.; Gratzel, M.; Kavan, L.; Moser, J. *J. Am. Chem. Soc.* **1985**, *107*, 2988.

(41) Vlachopoulos, N.; Liska, P.; Augustynski, J.; Gratzel, M. *J. Am. Chem. Soc.* **1988**, *110*, 1216.

(42) Hashimoto, K.; Hiramoto, M.; Lever, A. B.; Sakata, T. *J. Phys. Chem.* **1988**, *92*, 1016.

(43) Argazzi, R.; Bignozzi, C. A.; Heimer, T. A.; Castellano, F. N.; Meyer, G. J. *Inorganic Chemistry* **1994**, *33*, 5741.

(44) Ford, W. E.; Rodgers, M. A. J. *Journal of Physical Chemistry* **1994**, *98*, 3822.

(45) Bedja, I.; Hotchandani, S.; Kamat, P. V. *J. Phys. Chem.* **1994**, *98*, 4133.

(46) Vinodgopal, K.; Hua, X.; Dahlgren, R. L.; Lappin, A. G.; Patterson, L. K.; Kamat, P. V. *Journal Of Physical Chemistry* **1995**, *99*, 10883.

(47) Bell, T. D.; Pagba, C.; Myahkostupov, M.; Hofkens, J.; Piotrowiak, P. *J. Phys. Chem. B* **2006**, *110*, 25314.

(48) Xie, X. S. *Accounts of Chemical Research* **1996**, *29*, 598.

(49) Vallee, R. A. L.; Cotlet, M.; Hofkens, J.; De Schryver, F. C.; Muellen, K. *Macromolecules* **2003**, *36*, 7752.

(50) Zhang, L.; Liu, R.; Holman, M. W.; Nguyen, K. T.; Adams, D. M. *J. Am. Chem. Soc.* **2002**, *124*, 10640.

(51) Park, S.-J.; Gesquiere, A. J.; Yu, J.; Barbara, P. F. *Journal of the American Chemical Society* **2004**, *126*, 4116.

(52) Lu, H. P.; Xie, X. S. *Journal of Physical Chemistry B* **1997**, *101*, 2753.

(53) Holman, M. W.; Liu, R.; Adams, D. M. *J, Am. Chem. Soc.* **2003**, *125*, 12649.

(54) Goh, W.; Guo, J.; Yuan, R.; Lian, T. "Single molecule study of Rhodamine/ATO nanoparticle junctions"; Proceedings of SPIE-The International Society for Optical Engineering, (Physical Chemistry of Interfaces and Nanomaterials IV), 2005.

(55) Biju, V.; Micic, M.; Hu, D.; Lu, H. P. *Journal of the American Chemical Society* **2004**, *126*, 9374.

(56) Yang, H.; Luo, G.; Karnchanaphanurach, P.; Louie, T.-M.; Rech, I.; Cova, S.; Xun, L.; Xie, X. S. *Science (Washington, DC, United States)* **2003**, *302*, 262.

(57) Edman, L.; Mets, U.; Rigler, R. *Proceedings of the National Academy of Sciences of the United States of America* **1996**, *93*, 6710.

(58) Wennmalm, S.; Edman, L.; Rigler, R. *Proceedings of the National Academy of Sciences of the United States of America* **1997**, *94*, 10641.

(59) Heinlein, T.; Knemeyer, J.-P.; Piestert, O.; Sauer, M. *Journal of Physical Chemistry B* **2003**, *107*, 7957.

(60) Sauer, M. *Angewandte Chemie, International Edition* **2003**, *42*, 1790.

(61) Piestert, O.; Barsch, H.; Buschmann, V.; Heinlein, T.; Knemeyer, J.-P.; Weston, K. D.; Sauer, M. *Nano Letters* **2003**, *3*, 979.

(62) Neuweiler, H.; Schulz, A.; Boehmer, M.; Enderlein, J.; Sauer, M. *Journal of the American Chemical Society* **2003**, *125*, 5324.

(63) Huang, J.; Stockwell, D.; Boulesbaa, A.; Guo, J.; Lian, T. *J. Phys. Chem. C* **2008**, *112*, 5203.

(64) Tachibana, Y.; Haque, S. A.; Mercer, I. P.; Durrant, J. R.; Klug, D. R. *J. Phys. Chem. B* **2000**, *104*, 1198.

(65) Rehm, J. M.; McLendon, G. L.; Nagasawa, Y.; Yoshihara, K.; Moser, J.; Gratzel, M. *J. Phys. Chem.* **1996**, *100*, 9577.

(66) Kitamura, T.; Ikeda, M.; Shigaki, K.; Inoue, T.; Anderson, N. A.; Ai, X.; Lian, T.; Yanagida, S. *Chemistry of Materials* **2004**, *16*, 1806.

(67) Yuanmin Wang; Xuefei Wang; Sujit Kumar Ghosh; Lu, H. P. *J. Am. Chem. Soc.* **2009**, *131,* , 1479.

(68) Guo, J.; She, C.; Lian, T. *J. Phys. Chem. C* **2007**, *111*, 8979.

(69) Anderson, N. A.; Ai, X.; Chen, D.; Mohler, D. L.; Lian, T. *Journal of Physical Chemistry B* **2003**, *107*, 14231.

(70) Asbury, J. B.; Hao, E.; Wang, Y.; Lian, T. *J. Phys. Chem. B* **2000**, *104*, 11957.

(71) Galoppini, E. *Coord. Chem. Rev.* **2004**, *248*, 1283.

(72) Durrant, J. R.; Haque, S. A.; Palomares, E. *Coordination Chemistry Reviews* **2004**, *248*, 1247.

(73) Cui, X. D.; Primak, A.; Zarate, X.; Tomfohr, J.; Sankey, O. F.; Moore, A. L.; Moore, T. A.; Gust, D.; Harris, G.; Lindsay, S. M. *Science* **2001**, *294*, 571.

(74) Karstens, T.; Kobs, K. *J. Phys, Chem* **1980**, *84*, 1871.

(75) Anderson, N. A.; Lian, T. *Annual Review of Physical Chemistry* **2005**, *56*, 491.

(76) Macklin, J. J.; Trautman, J. K.; Harris, T. D.; Brus, L. E. *Science* **1996**, *272*, 255.

(77) Newton, M. D. *Chem. Rev.* **1991**, *91*, 767.

(78) Grabowski, Z. R.; Rotkiewicz, K. *Chem. Rev.* **2003**, *103*, 3899.

(79) Magde, D.; Rojas, G. E.; Seybold, P. G. *Photochem. and Photobiol.* **1999**, *70*, 737.

(80) Lukosz, W.; Kunz, R. E. *Optics Communications* **1977**, *20*, 195.

(81) English, D. S.; Harbron, E. J.; Barbara, P. F. *J. Chem. Phys.* **2001**, *114*, 10479.

(82) Xie, X. S.; Trautman, J. K. *Annual Review of Physical Chemistry* **1998**, *49*, 441.

(83) *Single Molecule Spectroscopy: Nobel Conference Lectures*; Rigler, R.; Orrit, M.; Basche, T., Eds.; Springer: Berlin; New York, 1998.

(84) *Single-Molecule Optical Detection, Imaging and Spectroscopy.*; Basche, T.; Moerner, W. E.; Orrit, M.; Wild, U. P., Eds.; VCH: Weinheim, 1997.

(85) Marcus, R. A. *J. Chem. Phys.* **1965**, *43*, 679.

(86) Gao, Y. Q.; Georgievskii, Y.; Marcus, R. A. *J. Chem. Phys.* **2000**, *112*, 3358.

(87) Gao, Y. Q.; Marcus, R. A. *J. Chem. Phys.* **2000**, *113*, 6351.

(88) Gosavi, S.; Marcus, R. A. *J. Phys. Chem. B* **2000**, *104*, 2067.

(89) Pan, D.; Hu, D.; Lu, H. P. *J. Phys. Chem. B* **2005**, *109*, 16390.

(90) She, C.; Anderson, N. A.; Guo, J.; Liu, F.; Goh, W.; Chen, D.-T.; Mohler, D. L.; Tian, Z.-Q.; Hupp, J.; Lian, T. *J. Phys. Chem. B.* **2005**, *109*, 19345.

(91) Boschloo, G.; Fitzmaurice, D. *Journal of Physical Chemistry B* **1999**, *103*, 3093.

(92) Kresse, G.; Hafner, J. *Phys. Rev. B* **1993**, *47*, 558.

(93) Kresse, G.; Furthmuller, J. *Phys. Rev. B* **1996**, *54*, 11169.

(94) Kresse, G.; J. Furthmuller. *Computational Materials Science* **1996**, *6*, 15.

(95) Phillips, J. C.; Braun, R.; Wang, W.; Gumbart, J.; Tajkhorshid, E.; Villa, E.; Chipot, C.; Skeel, R. D.; Kale, L.; Schulten, K. *J. Comput. Chem.* **2005**, *26*, 1781.

(96) Cornell, W. D.; Cieplak, P.; Bayly, C. I.; Gould, I. R.; Merz, K. M.; Ferguson, D. M.; Spellmeyer, D. C.; Fox, T.; Caldwell, J. W.; P. A. Kollman. *J. Am. Chem. Soc.* **1995**, *117*, 5179.

(97) Bandura, A. V.; Sofo, J. O.; Kubicki, J. D. *J. Phys. Chem. B* **2006**, *110*, 8368.

(98) Li, J. R.; Nilsing, M.; Kondov, I.; Wang, H. B.; Persson, P.; Lunell, S.; Thoss, M. *J. Phys. Chem. C* **2008**, *112*, 12326.

(99) Macklin, J. J.; Trautman, J. K.; Harris, T. D.; Brus, L. E. *science* **1996**, *272*, 255.

(100) Lide, D. R.; Ed.;. *Handbook of Chemistry and Physics, 77th ed.*, *CRC Press: Boca Raton, FL, 1996; p 4-130-4-136.*

Chapter 4. Interfacial Electron Transfer Dynamics from Single QDs to Adsorbed F27 Molecules

4.1 Introduction

For the purpose of designing next-generation energy conversion devices, many efforts in the last decade have focused on designing ordered assemblies of nanostructures, metal semiconductor nanoparticles and carbon nanotubes.[1-5] Among these nanomaterials, semiconductor quantum dots (QDs), such as CdSe and CdS with their tunable band edges, can transfer electrons to various metal oxides such as TiO_2 and SnO_2 as well as molecular adsorbates, and hence offer new opportunities to harvest light energy in the entire visible region of solar light.[6-9] Understanding the interfacial electron transfer (ET) dynamics from QDs to metal oxides and molecular adsorbates is therefore essential in order to improve the efficiency of QD-based light energy conversion devices. Recent reports of multiple exciton generation (MEG) in some QDs may provide a potential way to improve the efficiency of QD-based solar cells,[8,10-13] and therefore have intensified the interest in QD exciton dissociation through interfacial ET. The reported observations of ultrafast ET dynamics from QDs to their adsorbates suggest the possibility of multiple exciton dissociation by interfacial ET which is fast enough to compete with the exciton-exciton annihilation process.[14-23] To gain further insight into the dynamics of charge transfer from QDs, the ET on the single QD level has also been investigated. [24-27]

Single QDs exhibit unique optical properties which are not observable in ensemble-averaged measurements. Fluorescence intermittency (known as “blinking) of single QDs has been extensively investigated in the past decade. [28-49] This fluctuation of fluorescence

intensity is positively correlated with the lifetime: the high fluorescence intensity states (on state) have long exciton lifetimes and the low intensity states (off state) have short exciton lifetimes, suggesting a fluctuation of the nonradiative decay rate. The formation of the off state is attributed to the photoinduced charging of QDs by charge transfer to trap states in the QDs and the surrounding matrix,[28-31,35,39,48,49] when the fast Auger relaxation pathway quenches the fluorescence of the QDs. The transition from the off state to the on state is due to the charge recombination process, which returns the QD to its neutral state. The probabilities of the QD staying in the on and off states obey a power-law dependence with an exponent of ~1.5. [29,36,45,49] However, It has also been reported that some QDs only follow the power-law blinking dynamics on a short time scale but show exponential decays on longer time scales. Although the nature of the traps states and the microscopic origin of these fluctuating transition rates remains unclear, models assuming diffusion-controlled electron transfer[29,42-45] and fluctuating tunneling barriers for electron transfer to and from trap states[35,48] have been shown to account for the power-law on- and off- time distribution functions. A recent report on the excitation power-dependent blinking dynamics also indicated that the truncated power-law blinking dynamics were due to the multi-exciton generation in single QDs which enhanced the probability of charging the QDs.[38]

The blinking dynamics of single QDs trigger an interesting question: how will this blinking dynamics affect and be affected by the interfacial ET dynamics from QDs? The answer can only be elucidated by the single QDs studies. So far, there are only a few published reports of single QD ET.[24-27] In their pioneer work, both Lian's and Majima's groups observed intermittent ET dynamics from single QDs to their molecular adsorbates.

The origin of the intermittent ET activity is still not clear. One suggested possibility is the fluctuation of ET rates.[24,25] The short and long lifetimes correlate with fast and slow ET rates, respectively.

In an effort to understand the interfacial ET dynamics as well as the relationship between blinking and ET activities, this chapter discusses the results of our investigation on ET dynamics from QDs to their adsorbed Fluorescien 27 (F27) dye molecules. This system was studied on both ensemble-averaged and single QD levels by transient absorption, ensemble and single-molecule time-resolved fluorescence spectroscopy.

4.2 Results and Discussion

4.2.1 Ensemble-Averaged ET Dynamics

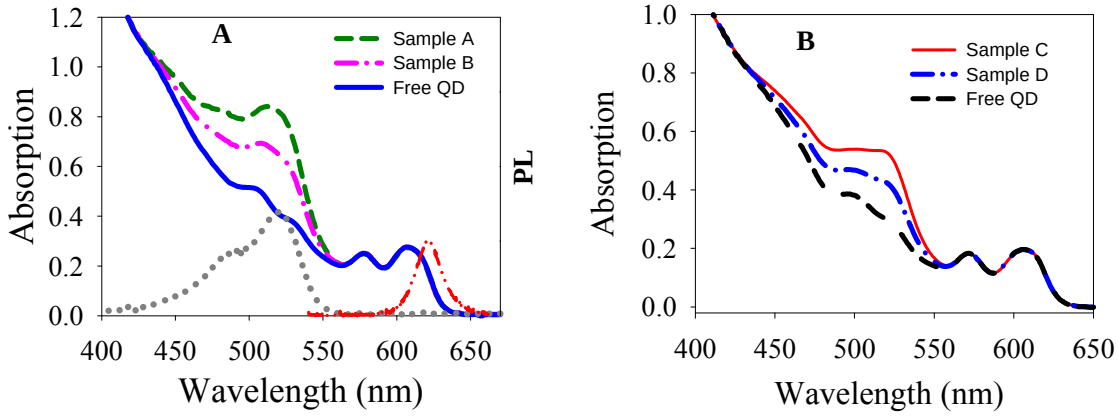

Figure 4.1 UV-vis absorption spectra of samples A and B (in panel A) and C and D (in panel B). The absorption spectrum of F27 and the photo luminescent spectrum of QD-F27 complex at high ratio excited at 400 nm are also plotted (red dashed lines) in panel A.

In this study, we choose core/multi-shell ($CdSe/CdS_{3ML}ZnCdS_{2ML}ZnS_{2ML}$) QDs whose lowest energy exciton absorption band is at 605 nm. The core/shell QD was

chosen because it has much higher quantum yield and is more stable in air compared to core QD, which can facilitate the single QD studies. To study the ensemble-averaged ET dynamics through transient absorption (TA) and fluorescence (FL) decay measurements, tree samples were prepared in heptane solution: free QDs (without F27) and QD-F27 complexes (Sample A, B, C and D) with different F27-to-QD ratios, whose UV-vis absorption spectra are as shown in Figure 4.1. Sample A and B are for ns transient absorption measurement and C and D are for fs transient absorption measurement. The exact ratios of the samples were not resolved because of the unknown extinction coefficient of the QDs. However, the F27-to-QD ratio of sample B is about twice that of sample A according to their absorption spectra. The excitation wavelengths for both ensemble and single QDs measurements were at 400 nm which selectively excited QDs, and the detected photons were from QDs only (see Figure 4.1).

Shown Figure 4.2 are the transient absorption spectra of free QD and QD-F27 complexes at different ratios at different delay times on ps (left panels) and ns (right panels) time scales. These spectra show an initial bleach and subsequent recovery of the exciton bands. The exciton bleach recover kinetics probed at around 605 nm show similar recovery on ps time scale (see Figure 4.3 A) for all samples but faster recover with higher F27-to-QD ratios on ns time scale (see Figure 4.3 B), suggesting the quenching of QD excitons by F27 which occurs on ns time scale. Additionally, the bleach of ground state F27 followed by a recovery process in the region of 450~540 nm is also clearly observed for the QD-F27 complexes. The absorption spectrum of F27 is overlapped with that of QD in this region, and the amplitudes of the F27 signals are much smaller than that of QD. Therefore, to clearly show the F27 signal, we have subtracted out the QD signal to

produce transient spectra that contain the contribution of the F27 signal only, as shown in Figure 4.4 A and B. We have scaled the free QD signal such that its bleach amplitude matches that of QD-F27 at 605 nm (where the signal is caused by QD exciton bleach only) and subtracted this scaled QD signal from Figure 4.2 E.

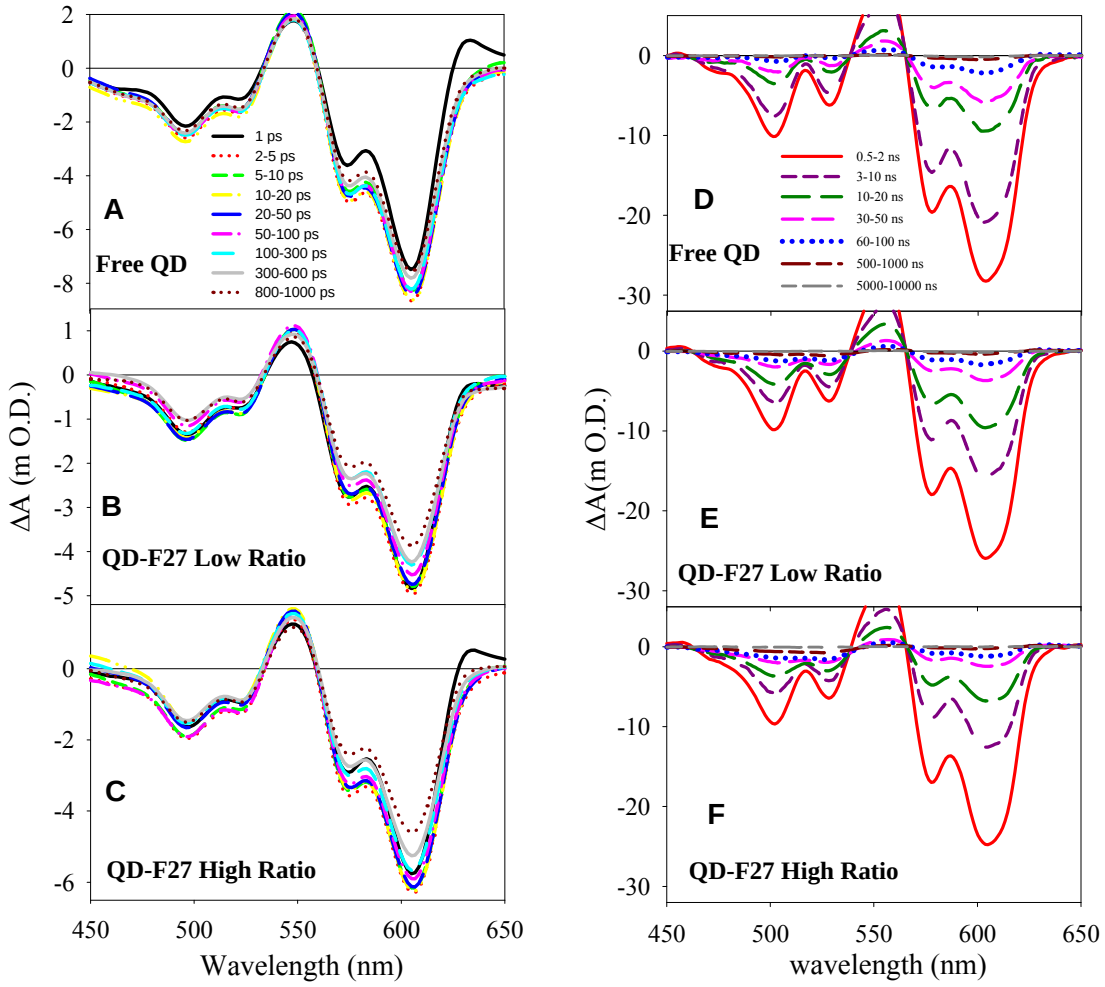

Figure 4.2. (Left panels) Transient absorption spectra on picoseconds time scale at indicated delay times following 400 nm excitation of (A) QDs and QDs-F27 complexes at low (B, sample C) and high (C, sample D) F27-to-QD ratios. (Right panels) Transient absorption spectra on ns time scale at indicated delay times following 400 nm excitation

of (D) QDs and QDs-F27 complexes at low (B, sample A) and high (C, sample B) F27-to-QD ratios.

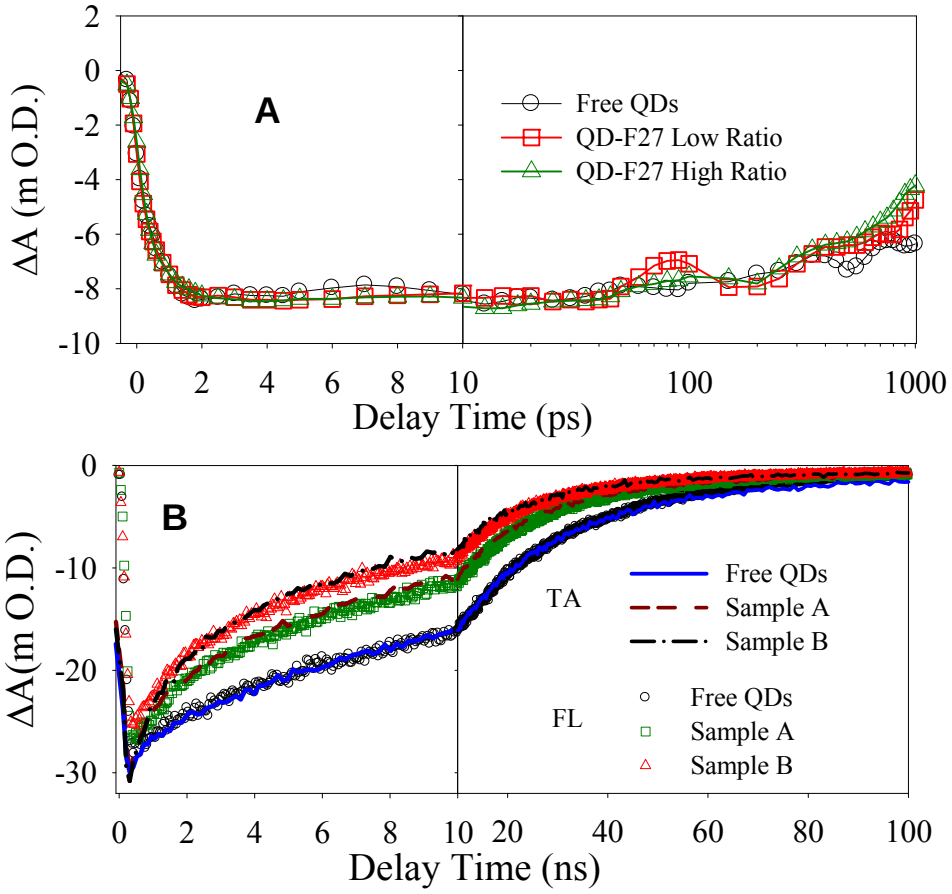

Figure 4.3. Transient absorption (TA) kinetics at ~ 605 nm (averaged from 601 to 610 nm) of free QD and QD-F27 complexes at different F27-to-QD ratios on picoseconds (in panel A, samples C and D) and ns time scale (in panel B, samples A and B). Also plotted in panel B are the ensemble-averaged fluorescence (FL) decays of free QDs and QD-F27 complexes. The FL kinetics have been inverted and normalized for better comparison with the TA kinetics.

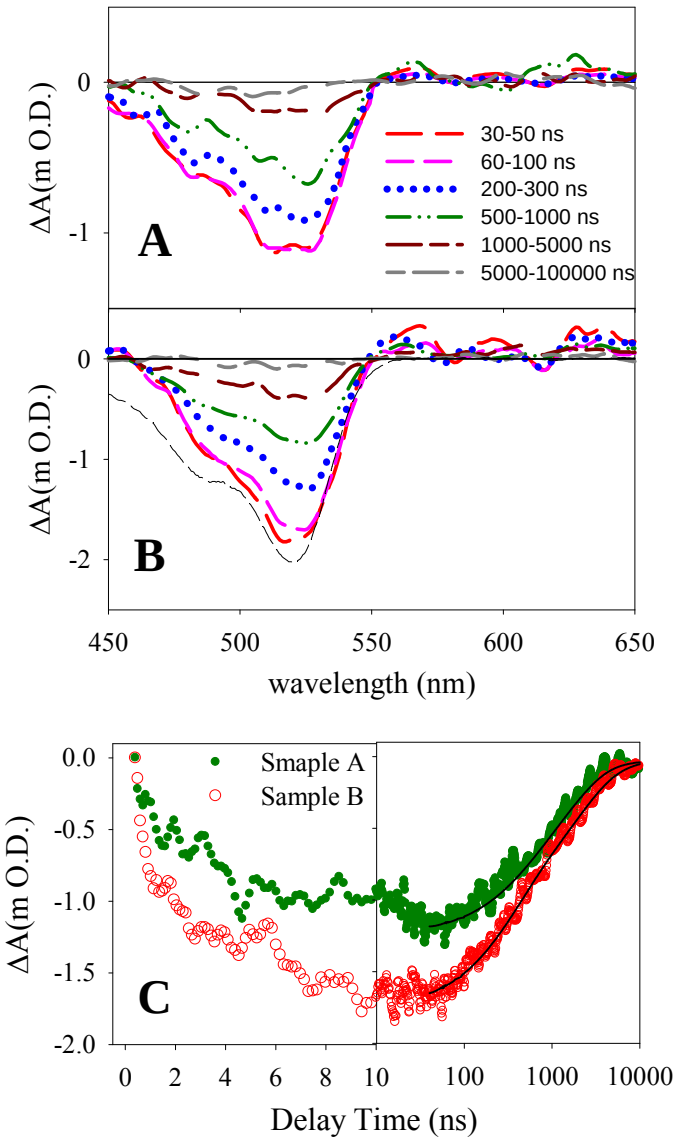

Figure 4.4. Transient spectra of F27 in sample A (A) and sample B (B) at indicated delay times obtained by subtracting the QDs signals (see text for details). The dashed black line is the ground state absorption spectrum of F27. (B) The kinetics of F27 bleach on ns time scale at ~525 nm (averaged from 521~530 nm) for sample A (green solid circles) and sample B (red open circles) and their corresponding bi-exponential fits (solid black lines) from 40 ns to 10 μs

The CdSe/$CdS_{3ML}ZnCdS_{2ML}ZnS_{2ML}$ QDs used in this study have a first exciton peak at 605 nm. The energetic of the electron and hole levels have not been directly measured, and they are estimated by the following procedures. These core/multi-shell structures were grown from CdSe cores with a first exciton peak at 574 nm. The radius of the CdSe core is estimated to be 1.8 nm by an empirical formula,[50] and 1.7 nm by a model that treats the electrons and holes as particles of effective masses of 0.13 and 0.45 m_0 (m_0 the free electron mass), respectively, confined in a finite spherical well.[51] From the calculated 1S electron, hole and exciton energy, the 1S exciton oxidation and reduction potentials in the CdSe core are determined to be -0.95 and +1.05 V (SCE), respectively.[14,52,53] Previous study of CdSe/CdS core/shell structures shows that the lowest energy conduction band electron is delocalized throughout the core and shell, whereas the valence band hole is localized in the core.[54,55] We assume in that quasi-type II core/multi-shell structure, the electron energy level is lowered while the hole level remains unaffected relative to the CdSe core. With these assumptions, the estimated 1S exciton oxidation and reduction potentials are -0.85 and +1.05 V (vs SCE), respectively, for the QDs used in this study.[27] The reduction and oxidation potentials of F27 are at -0.81 and +1.57 V (vs SCE) respectively[56]. The energetic diagram of the QD-F27 complex is show in Figure 4.5. Exciton quenching of QDs can be resulted by electron, hole and energy transfers from excited QDs to F27 molecules. According to the energetic diagram shown in Figure 4.5, QD exciton quenching by hole transfer to F27 is not energetically allowed and not observed in the transient absorption measurements, and energy transfer from QD to F27 is also excluded due to lack of spectral overlap of QD emission with F27 absorption. ET is the only pathway for the quenching of QD excitons.

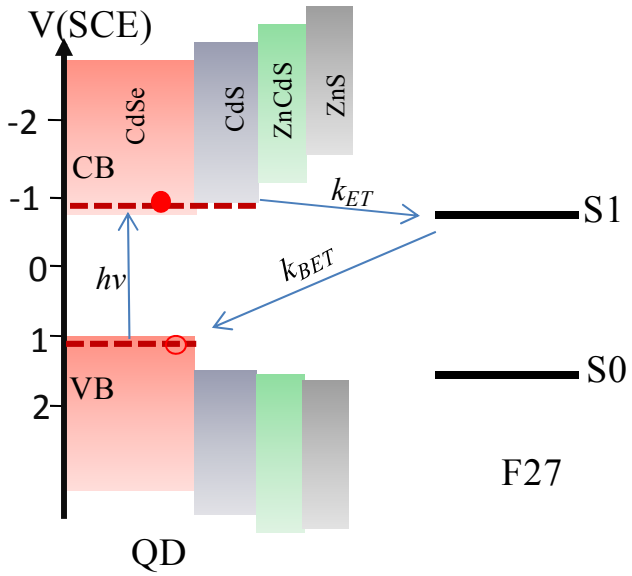

Figure 4.5. The energetic diagram of the QD-F27 complex.

The interfacial ET process leads to the formation of reduced F27 and oxidized QD, and the following charge recombination (back electron transfer: BET) process generates ground state QD and F27. The whole processe can be represented by following reaction scheme:

$$QD^{*}[1S(e),1S(h)] - F27 \xrightarrow{k_{ET}} QD^{+}[h] - F27^{-} \xrightarrow{k_{BET}} QD - F27 \quad \text{(Scheme 4.1)}$$

where QD*[1S(e), 1S(h)] represents excited state QD with an electron on 1S(e) level and a hole in 1S(h) level. This assignment of QD exciton quenching by ET to F27 is consistent with the observed transient absorption spectral features. First of all, the excitation of QD fills an electron in the 1S(e) level, resulting in the exciton bleach of QD. The ET from QD to F27 shortens the lifetime of the exciton and leads to the faster recovery kinetics of QD-F27 complex compared to free QD. Secondly, this ET process also generates reduced F27 and leads to the depletion of F27 ground state. Unfortunately, the reduced F27 has a spectral feature at ~390 nm[57] and is not observed in this study due

to the limited spectral range of the white light probe. The following BET process accounts for the recovery of F27 ground state.

The kinetics of the species in the QD-F27 complex in the ET reaction can be represented by following equations:

$$\frac{d}{dt}[QD*-F27] = -(k_{et} + k_0)[QD*-F27] \quad \text{(Eq. 4.1)}$$

$$\frac{d}{dt}[QD^+ - F27^-] = k_{et}[QD*-F27] \quad \text{(Eq. 4.2)}$$

$$\frac{d}{dt}[QD - F27] = k_0[QD*-F27] \quad \text{(Eq. 4.3)}$$

where k_0 is the intrinsic time constant of free QDs. The integration of Eq. 4.1 leads to

$$[QD*-F27](t) = N*(0)e^{-(k_0+k_{et})t} \quad \text{(Eq. 4.4)}$$

$N*(0) = [QD*\text{-}F27]$ is the initial concentration of excited QD. Inserting Eq. 4.4 to Eq 4.2 and 4.3 and integration over time generate

$$[F27^-](t) = [QD^+](t) = [QD^+ - F27^-](t) = N*(0)\frac{k_{et}}{k_{et} + k_0}[1 - e^{-(k_0+k_{et})t}] \quad \text{(Eq. 4.5)}$$

$$[QD](t) = [QD - F27](t) = [QD - F27](0) + N*(0)\frac{k_0}{k_{et} + k_0}[1 - e^{-(k_0+k_{et})t}] \quad \text{(Eq. 4.6)}$$

Here we assume $[F27^-](0) = 0$. According to the above equations, the QDs exciton bleach recovery and formation of reduced F27 have the same exponential kinetics but different amplitudes. This is consistent with the observed transient absorption kinetics, as shown in Figure 4.6. The F27 bleach kinetics for samples A and B agree well with their corresponding QD exciton bleach recovery kinetics in the first 10 ns, but deviate afterwards due to the BET process.

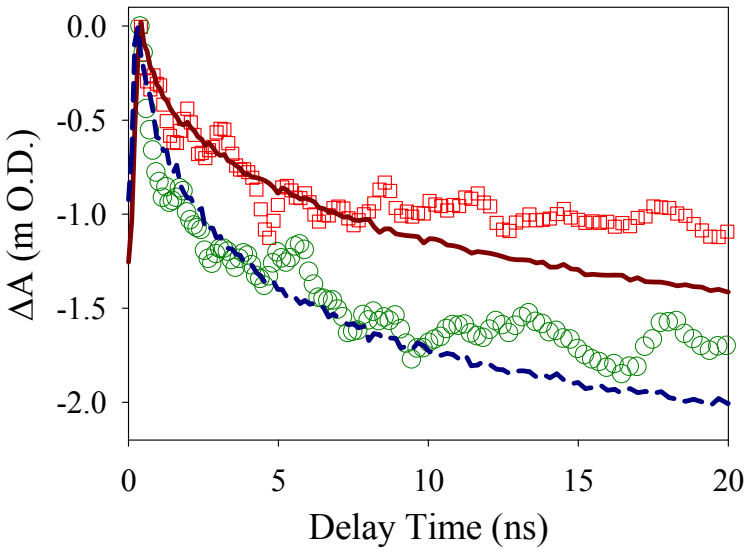

Figure 4.6. Comparison of transient absorption kinetics of QD-F27 complex at 605 nm (open symbols) and the kinetics of F27 bleach at 525 nm (lines) for sample A (red squares and solid line) and B (green circles and dashed line).

The ET rate can be modulated by varying the F27-to-QD ratios. As shown in Figure 4.3 B, the QD exciton bleach recovery kinetics of QD-F27 complexes are faster as the dye-to-QD ratio increases, indicating the faster ET dynamics for a higher ratio sample. The ensemble averaged fluorescence decays of the same free QDs and QD-F27 complexes (sample A and B) were also measured in heptane solution and compared with the transient absorption kinetics at 605 nm, as shown in Figure 4.3 B. The comparison shows well agreement between fluorescence decays and the exciton ground state transient absorption kinetics, indicating that the quenching of florescence is due to ET and the fluorescence lifetimes are measuring the ET dynamics. Comparison of the bleach recovery of free QD vs QD-F27 complexes allows an estimation of the ensemble-averaged ET time. As will be further discussed later, ET in this system occurs on a few to 10s of nanosecond timescale. It has been reported that in related QD-Dye complexes,

such as CdS-RhB[15], CdSe-ReBipyridyl,[14] CdSe-Methylene blue[23] and CdSe-RhB,[58] ultrafast ET dynamics up to a few ps were observed. The considerably slower ET rate in our studied system can be attributed to the presence of ZnS shells which reduce the electronic coupling strength between the QD and adsorbate, and the using of larger size QDs which gives a smaller driving force for ET.

The BET process can be monitored by the F27 bleach recovery kinetics at 525 nm, as shown in Figure 4.4 C. The recovery of F27 bleach is non-single-exponential, containing a small but non-negligible component that is slower than the 10 μs observation window of this transient absorption study. To estimate the BET rate, the kinetics of F27 in Figure 4.4 C after 40 ns are fit by bi-exponential functions. The time constants and amplitudes (in parenthesis) are 148 ns (23%) and 1667 ns (77%) for sample A, and 325 ns (47%) and 1847 ns (53%) for sample B. The amplitude weighted average BET time constants are 1320 and 1128 ns for sample A and B, respectively.

4.2.2 Single QD ET Dynamics

A sample of QD-F27 complex at single molecule concentration (~10^{-11} M) can be obtained by diluting from its original concentration (~10^{-7} M). However, it is found that the ensemble-averaged fluorescence decay of a QD-F27 complex becomes slower as the sample is diluted over 1000 times as shown in Figure 4.7, indicating a decrease of F27-to-QD ratio. This is due to the dissociation of F27 from QDs to maintain the equilibrium of the amount of F27 molecules in the solvent and on the QD surfaces as the solution is diluted. Since the concentration is down to ~10^{-11} M, it is difficult to quantitatively resolve the ratio by UV-vis spectroscopy after dilution.

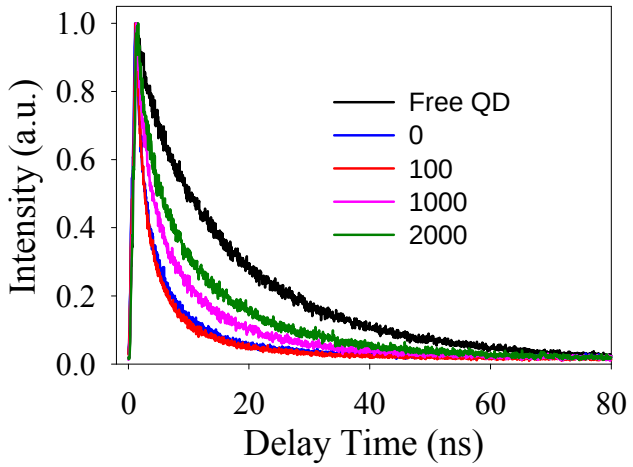

Figure 4.7. Ensemble-averaged fluorescence decays in heptane of free QDs and QD-F27 complex at different times of dilutions.

In this study, the QD-F27 complex was obtained directly at single molecule concentration, and the amount of F27 was controlled by the length of mixing time. Three samples (in heptane) were prepared. Sample **1** is free QDs without F27. Sample **2** and **3** are QD-F27 complexes which were obtained by mixing QD with F27 for ~6 and ~12 hours, respectively. Since the mixture time increases, the F27-to-QD ratio of Sample **3** is higher than that of Sample **2**. The samples are scattered on a glass cover slip. The emission between 540 nm to 675 nm from a single QD is detected, and collected photons were labeled by their arrival time (relative to the start of the experiments) and decay time (relative to the excitation pulse). The number of photons binned over a 50 ms window of arrival time was calculated to construct trajectories of fluorescence intensity (in units of counts per second or Hz) as a function of (arrival) time. Delay time histograms of detected photons within a 1 s window were constructed and fit by single exponential decays to determine their fluorescence lifetimes, and with step size of 1 s, lifetime

trajectories were constructed. Three typical fluorescence intensity and lifetime trajectories from each sample are shown in Figure 4.8 a, b and c, respectively.

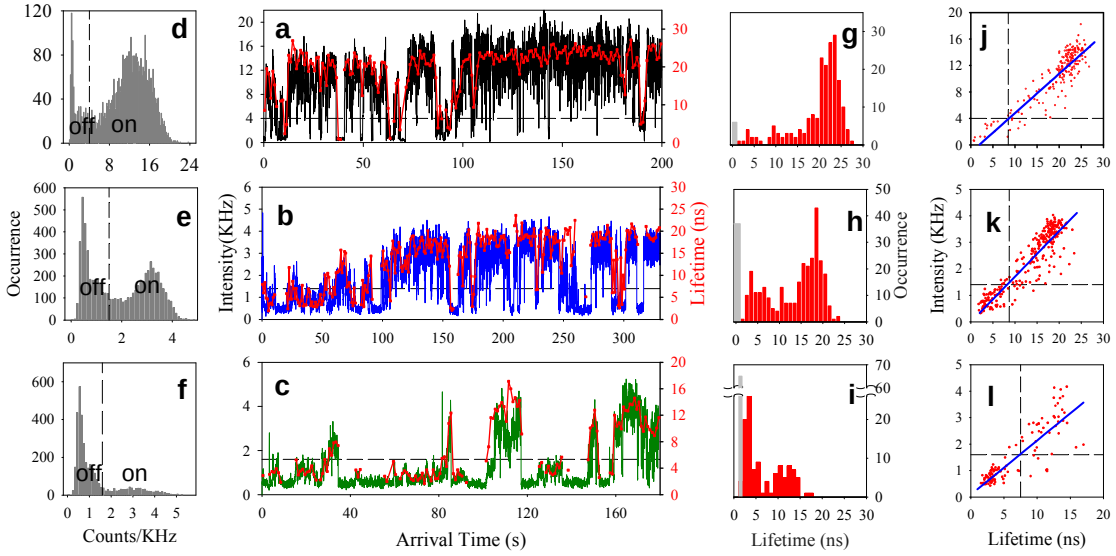

Figure 4.8. Typical fluorescence intensity (black) and lifetime (red) trajectories of QD from Sample **1** (a) and QD-F27 complexes from Sample **2** (b) and **3** (c). The corresponding fluorescence intensity histograms for trajectories a, b and c are in panel d, e and f, respectively. The dashed lines indicate the thresholds separating the on and off state. The corresponding lifetime histograms for trajectories in panel a, b and c are in panel g, h and i, respectively. The black bars in lifetime histograms indicate the occurrence of low-fluorescence intensity points along the trajectories, for which the lifetime have been assumed to be < 0.5 ns. The fluorescence intensity as a function of lifetime for QDs in a, b and c is plotted in panel j, k and l, respectively, and fit by a linear function (blue lines). The dashed lines indicate the intensity thresholds and their corresponding lifetime thresholds.

The histograms of fluorescence intensity of the QD and QD-F27 shown in panels a b and c in Figure 4.8 are plotted in panel d, e and f, respectively. The intensity distribution

of free QD without F27 shows two peaks at ~12 kHz and 0.54 kHz (background level). The high-intensity peak has been assigned to the QD's on state and low-intensity peak to the off-state.[29-37,39,41-49,59-63] However, the observed fluorescence intensity trajectories of QD-F27 complexes are different with those of free QDs. As shown in the panel e and f in Figure 4.8, as F27-to-QD ratio increases, the off-state becomes more and more dominant in the intensity histogram. There has been tow ways to determine the threshold. One is using the value of the average background plus its three times standard deviation. The other one is using the cut off point of on and off state in the intensity histogram. We used the latter method. Specifically, to determine the threshold intensity, the distribution was fit by a sum of two Gaussian functions. The point where these two Gaussians cross was taken as the threshold intensity, which for QDs shown in Figure 4.8 a, b and c are at 4.0, 1.4 and 1.6 kHz, respectively. Any point in the trajectory with intensity above (below) the threshold level was assigned to on (off) state. The same analysis was applied to all studied QDs and QD-F27 complexes to determine their individual threshold values and occurrence of on and off states.

The probability densities *P(t)* of a QD at on or off states for a duration time of *t* are defined as[36]

$$P_i(t) = \frac{N_i(t)}{N_{i,total}} \times \frac{1}{\Delta t_{avg}} \quad (i = \text{on or off}) \qquad \text{(Eq. 4.7)}$$

where *N(t)* is the number of on or off events of duration time of *t*, N_{total} the total number of on or off events, and Δt_{avg} the average time between nearest neighbor events as shown in Figure 4.9 A:

$$\Delta t_{avg} = \frac{(\Delta t_n + \Delta t_{n+1})}{2} \qquad \text{(Eq. 4.8)}$$

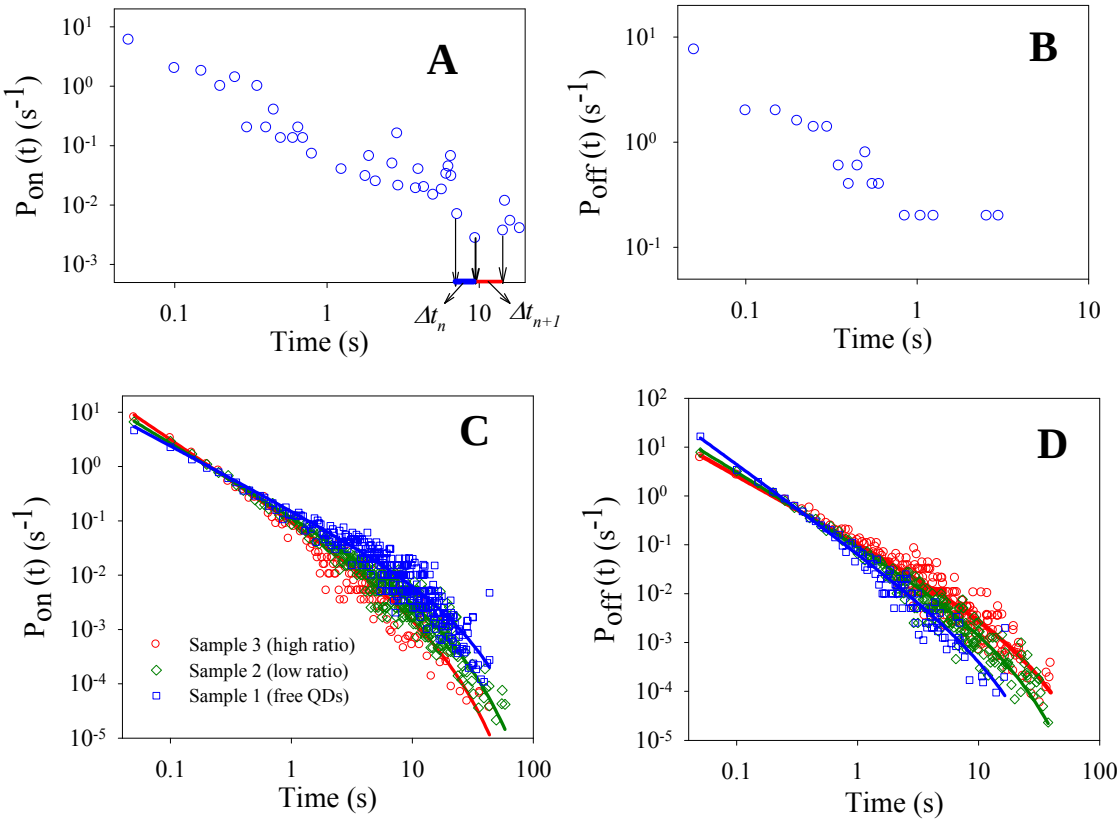

Figure 4.9. Probability density of (A) on states and (B) off states of the single QD shown in Figure 4.8 a. Probability density of (C) on states ($P_{on}(t)$) and (D) off states ($P_{off}(t)$) constructed from 45 free QDs from sample **1** (blue squares), 47 QD-F27 complexes from Sample **2** (green diamonds) and 42 QD-F27 complexes from Sample **3** (red circles). The solid lines are the best fits to Eq. 4.9 (see text).

$P_{on}(t)$ and *$P_{off}(t)$* distributions of the single QD in Figure 4.8 A are shown in Figure 4.9 A and B, respectively. Shown in Figure 4.9 C and D are the *$P_{on}(t)$* and *$P_{off}(t)$* distributions constructed from all studied QDs. Both *$P_{on}(t)$* and *$P_{off}(t)$* of single QDs from sample **1**, **2** and **3** show power law distributions at short time but exponential decays at long time, similar to those reported by other groups.[25,29,64,65] These *P(t)* distributions can be fit by a truncated power law function:[41,43-45,64]

$$P_i(t) = B_i t^{-\beta_i} \exp(-\Gamma_i t) \quad (i = \text{on or off}) \qquad \text{(Eq. 4.9)}$$

where B is the amplitude, β the power law exponent, and Γ the saturation rate. The fitting parameters are listed in Table 4.1. There are noticeable differences between free QDs and QD-F27 complexes. Compare to free QDs, QD-F27 complexes have larger β_{on} and Γ_{on} and smaller β_{off} and Γ_{off}, suggesting reduced probability densities of long on events and increased probability densities of long off events. Furthermore, as the F27-to-QD ratio increases, β_{on} and Γ_{on} is further increased and β_{off} and Γ_{off} is further decreased, suggesting that the QDs with more F27 molecules tend to have more long off and short on events.

Table 4.1. Fitting parameters of $P_{on}(t)$ and $P_{off}(t)$ for all single QDs from sample **1, 2** and **3**.The errors indicate one standard deviation.

Sample #	β_{on}	$1/\Gamma_{on}$ (s)	β_{off}	$1/\Gamma_{off}$ (s)
1	1.20 ± 0.05	20 ± 3	1.80 ± 0.1	10 ± 3
2	1.35 ± 0.02	17 ± 2	1.51 ± 0.06	13 ± 2
3	1.50 ± 0.07	13 ± 2	1.38 ± 0.06	20 ± 4

Consistent with the observations reported in the literatures,[24,33,39,47] the studied single free QD and QD-F27 complexes have shown the positive correlation between fluorescence intensity and lifetime, as shown in the panels j, k and l in Figure 4.8. The lifetime histograms of trajectories in panels a, b and c in Figure 4.8 are compared in panels g, h and i, respectively. The lifetimes at background levels were not accurately determined due to limited number of photons and were assumed to be < 0.5 ns, on the basis of positive correlation. Since the lifetime trajectory is positively correlated with the

fluorescence intensity, every fluorescence intensity threshold of a single QD has a corresponding lifetime threshold, as shown the dashed lines in panels j, k and l in Figure 4.8. This lifetime threshold separates a single QD lifetime distribution into on and off states. Take the QDs in panel a, b and c in Figure 4 as examples, the lifetime thresholds for on and off states are determined to be 8.5, 8.3 and 7.4 ns, respectively. The lifetime distributions of QD-F27 complexes from Sample **2** and **3** are significantly different from those of free QDs from Sample **1**. For free QD in panel a in Figure 4.8, the on state lifetimes are centered at ~23 ns, and the off state lifetimes are centered at ~0.5 ns with a small amplitude. For the QD-F27 complex from Sample **2** shown in panel b in Figure 4.8, the lifetime distribution also exhibits roughly two peaks: at ~19 ns for the on state and ~0.5 ns for the off state. Compared to the QD on glass, its on state lifetimes are shifted to shorter lifetime positions and the amplitude of off-state becomes much larger. As the dye-to-QD ratio increases, for the QD-F27 complex from Sample **3** shown in panel c in Figure 4.8, the on state is further shortened to ~13 ns, and the off state centered at ~0.5 ns becomes much more dominant in the lifetime distribution.

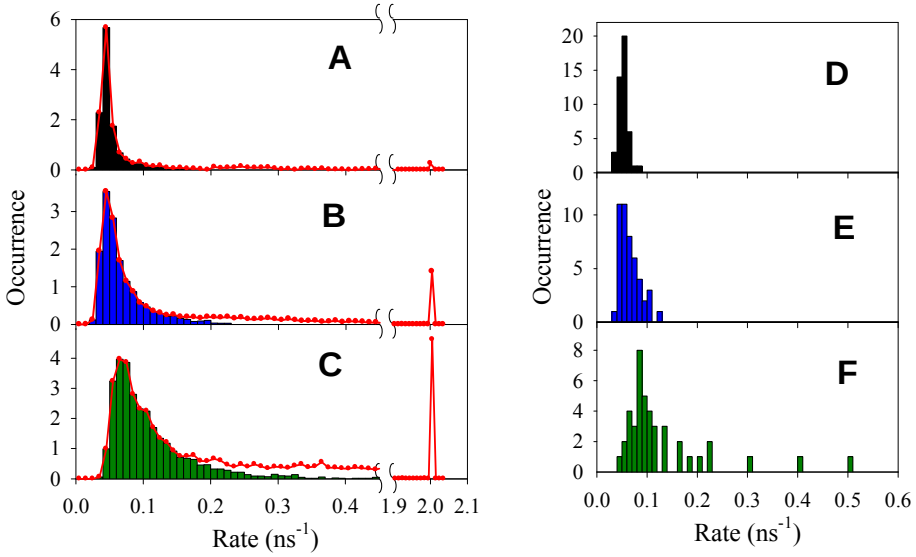

Figure 4.10. Total decay rate (left panels) and average decay rate calculated from on state lifetimes (right panels) histograms of (A and D) 45 QDs from sample **1**, (B and E) 47 QD-F27 complexes from sample **2** and (C and F) 42 QD-F27 complexes from sample **3**. The on state decay rate histograms are plotted as bars and the decay rate histograms including both on and off states are plotted as red solid lines. The peaks at 2 ns^{-1} indicates the occurrences of low fluorescence intensity (background) points whose lifetimes (rate) are assumed to be <0.5 ns (> 2 ns^{-1}).

The total decay rate (1/lifetime) histograms constructed by the summation of rate histograms of all studied single QDs and QD-F27 complexes from sample **1** (45 QDs), **2** (47 QD-F27 complexes) and **3** (42 QD-F27 complexes) are shown in panels A, B and C in Figure 4.10, respectively. The peaks at 2 ns^{-1} (1/500 ps) indicates the occurrence of low fluorescence intensity (background) points whose lifetimes are assumed to be < 500 ps. For comparison, the total on state decay rate histograms are also plotted in the same figure. The disagreement between these two kinds of histograms when the rate is higher than ~0.2 ns^{-1} is due to the presence of off state. It is clear that as the F27-to-QD ratio increases, the on state rate distributions shift to higher rate positions and become broader, and the disagreement between the rate histograms with and without off state is larger, indicating the increased amplitude of the off state.

The differences in the blinking statistics and the total decay rate histograms between QDs and QD-F27 complexes are attributed to the presence of interfacial ET from QD to F27. The increase (decrease) of relative contributions of off (on) states with F27-to-QD ratio is consistent with the trends of the on and off state probability densities shown in Figure 4.9. These results suggest a correlation between the single QD blinking and

interfacial ET dynamics in QD-F27 complexes. The decay rate of free QD is $k_0=k_r+k_{nr}$, where k_r and k_{nr} are the radiative and nonradiative decay rates, respectively. The free QDs fluorescence decay rate distribution defined as $I(k_0)$ in Figure 4.10 A indicates the variation of k_0 among different QDs at different times. For QD-F27 complexes, the fluorescence decay rate is $k=k_0+k_{ET}$, where k_{ET} is the interfacial ET rate, and the on state and total decay rate histograms of QD-F27 shown in Figure 4.10 B and C are defined as $H(k)$ and $H'(k)$, respectively. The broadening of the rate distributions of the QD-F27 complexes from each sample is due to the variation of k_{ET} among different QD-F27 at different times. For samples 1, 2 and 3, we also plotted the average on state rate histograms, as shown in Figure 10 D, E and F, respectively. The widths of these histograms are similar with those of their corresponding total rate histograms. This suggests that the broadening of rate distributions of QD-F27 is mainly due to the variation of ET rate among different QDs, which is mainly caused by the distribution of number of F27 molecules on each QD.

The measured distributions of decay rates of QD-F27 complexes ($H(k)$) are dependent on both the distributions of the interfacial ET rates ($F(k)$) and the intrinsic decay rates of QDs ($I(k_0)$):

$$H(k) = \int_0^\infty I(k_0)F(k-k_0)dk_0 \qquad \text{(Eq. 4.10)}$$

Thus the ET rate distribution can be obtained from the measured $H(k)$ and $I(k_0)$ according to Eq. 4.10. From the measured total ($H'(k)$) and on state ($H(k)$) decay rate distributions, and using the on state decay rate distribution of free QDs ($I(k_0)$), ET rate distributions $F'(k_{ET})$ and $F(k_{ET})$ for samples 2 and 3 can be obtained, as shown in Figures 4.11 B and

C. $F'(k_{ET})$ is the same as the $F(k_{ET})$ until the rate is higher than ~ 0.1 ns^{-1}. These differences reflect the contributions of off states to the total decay rate distributions.

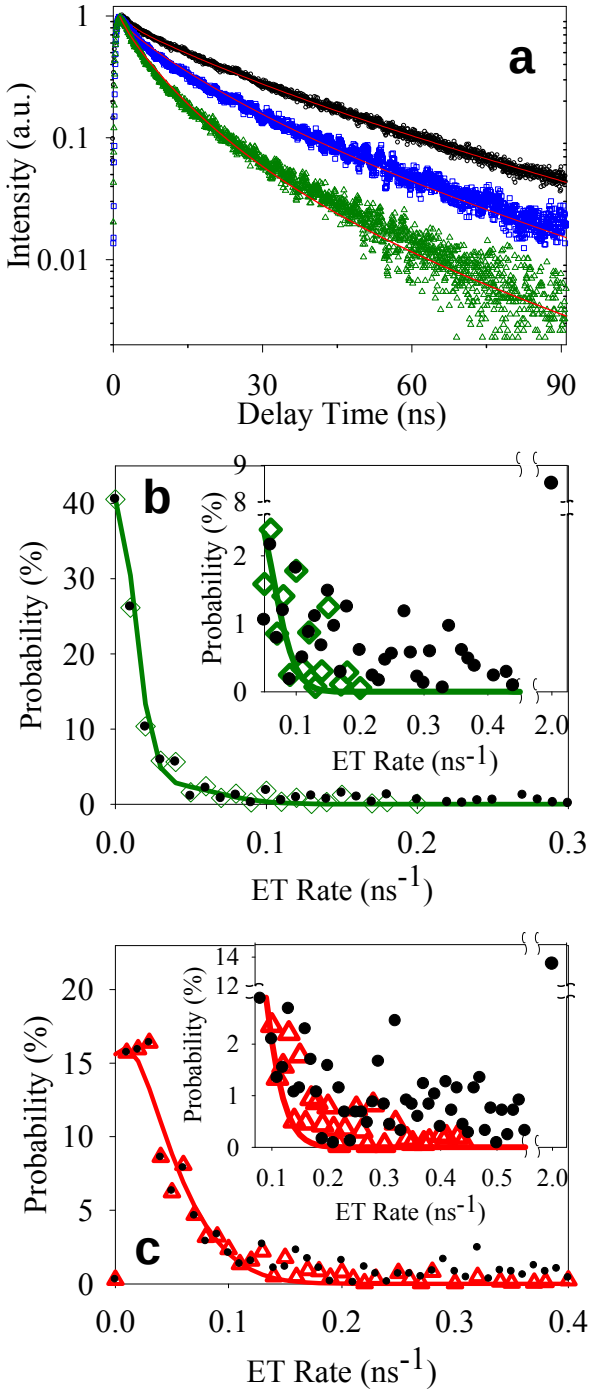

Figure 4.11. (A) Ensemble-averaged fluorescence decays of free QDs (black circle) and QD-F27 complexes from sample A' (blue square) and sample B' (green triangle) obtained under the same experimental conditions (on glass cover slip and dried in air) as single QD measurements. Solid lines are fits to these data according to Eq. 4.15 Distributions of ET rates in single QD-F27 complexes from sample 2 (B) and 3 (C). On state (green open diamonds in panel B and red open triangles in panel C) and total ET rate (black solid circles) distributions are obtained from on state (*H(k))* and total (*H'(k)*) rate distributions. Solid lines are fits of the distributions by Eq. 4.14. The insets show the expanded view of the distributions at higher rates. The best fits to A, B, and C yield k_1 = 0.03 ns^{-1} and w=0.06 ns^{-1}.

4.2.3. Correlation between Single QD Emission and Fluorescence Intensity (Lifetime)

The correlation between the blinking and ET dynamics of the single QD-F27 complexes indicates an intermittent ET dynamics. Similar ET dynamics between QD and adsorbed molecules have been reported in literatures.[24,25] It was suggested that for a QD-Dye ET system its off state can be due to fast ET process which can significantly quench the fluorescence of the single QDs, and the on state corresponds to the state when the ET is slow or not undergoing at all. It is speculated that the change of charge density and distribution in and around the QD can affect the ET rate by changing the energy level of conduction band, which leads to the change of the strength of electronic coupling and ET driving force. If this argument is true, the changing of the QD conduction band energy can probably be monitored by measuring its emission spectrum. Previous report has proved that the spectral diffusion shifts of single QDs were caused by the changes of

local electric field around the QDs, and such fluctuation of local electric field was attributed to the trapped electrons or holes on and around QDs.[66] This is evident in the correlation between blinking and fluctuation of emission spectrum of a QD.[40,66-68] We then simultaneously detected the fluorescence intensities, lifetimes, and spectra of single QDs and QD-F27 complexes. The results are shown in Figure 4.12. Figure 4.12 A shows a 3D image of spectrum trajectory of a single QD on glass. Two typical trajectories of fluorescence intensity and emission peak position for a single QD and QD-F27 complex are shown in the insets in Figure 4.12 B and C, respectively. To discover the correlation between fluorescence intensity and emission spectrum, the cross correction between these tow trajectories is calculated:

$$C(\tau) = \int_{-\infty}^{+\infty} \left(P(t) - \overline{P}\right) \otimes \left(L(t+\tau) - \overline{L}\right) d\tau \qquad \text{(Eq. 4.11)}$$

where *P(t)* and *L(t)* are the emission peak position and intensity trajectories, respectively; $\overline{P}$ and $\overline{L}$ are their corresponding average values; τ is the lag time between two functions. For both QDs and QD-F27 complexes, minimum cross correlation functions are found at τ=0, suggesting the fluorescence intensity and emission spectrum are anti-correlated. Two typical cross correlation functions are shown in Figure 4.12 B and C for single QD and QD-F27, respectively. The anti-correlations are verified by their corresponding fluorescence intensity and emission peak position trajectories (see the insets in Figure 4.12 B and C), showing red shifts of emission at low intensity levels. Since lifetime is positively correlated with fluorescence intensity, we can assume the anti-correlation between the lifetime and emission spectrum. However, no significant difference is found from the spectrum dynamics between QD and QD-F27. The histograms of emission peak positions constructed by 20 single QDs and 20 single QD-

F27 complexes shown in Figure 4.12 D and E are also found to be similar with each other. Under our experimental conditions, we are unable to resolve any correlations between QD emission spectrum and interfacial ET dynamics.

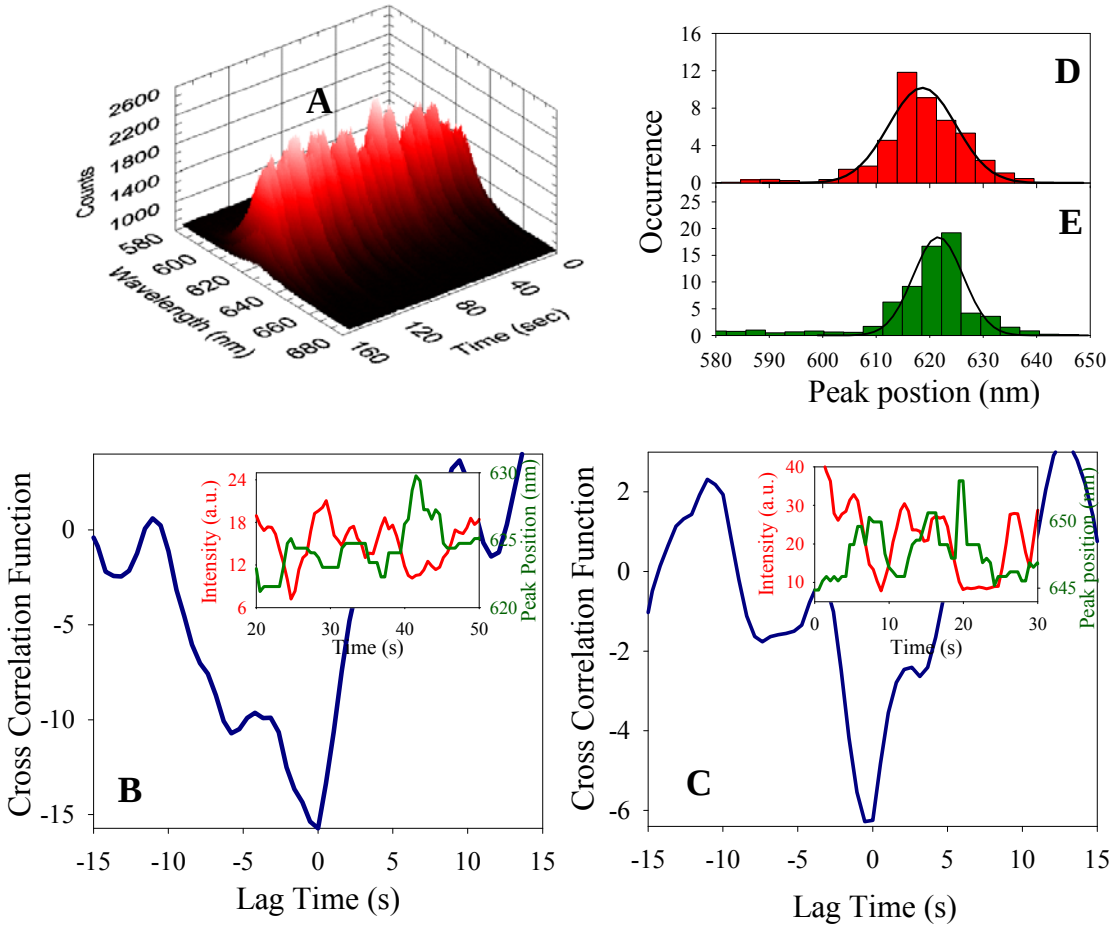

Figure 4.12. A 3D image of spectrum trajectory of a single QD on glass (A), and the cross correlation functions calculated from the fluorescence intensity and emission peak position trajectories of free single QD (B) and QD-F27 (C). Their corresponding intensity (red) and peak position (green) trajectories are in the insets. Also plotted are the histograms of emission peak positions constructed by peak position trajectories of 20 single QDs (D) and 20 single QD-F27 complexes (E). This experiment was conducted by splitting the collected fluorescence into two parts using a 50/50 beam splitter. One part

was detected by an APD and the other part was detected by monochromator (SP300i) coupled CCD (charged coupled device, Andor Newton). To obtain enough photons for emission spectrum, the laser power was increase to ~2 μW. The bin time for the emission spectrum is 0.5 s.

4.2.4 Comparison of Ensemble and Single QDs ET dynamics

The total ET rate distributions ($F'(k_{ET})$) of QD-F27 complexes from sample 2 and 3 contain fast components (> 0.5 ns^{-1}) that are not observed in the ensemble-averaged fluorescence decays and transient absorption data shown in Figure 4.3. The data in Figure 4.3 were obtained with samples in heptane solution whereas the single QDs were measured on glass cover slips in the absence of solvent. To ensure that the solvent environment was not the cause of the observed difference in these data, we have also measured the ensemble-averaged fluorescence decays of QD-F27 complexes under the same conditions as the single QD measurements. Shown in Figure 4.11 A are the ensemble-averaged fluorescence decays of free QDs and QD-F27 complexes from sample A' and B' (~10 times diluted from sample A and B) scattered on glass cover slip measured in air. The concentrations of the samples are ~10^6 higher than single QD measurements. During the measurements the samples were scanned at a speed of 0.1 μm/s to avoid photoinduced charging of the QDs. These decays are qualitatively similar to those in Figure 4.3 B, also indicating a lack of any fast components that are > 0.5 ns^{-1}.

To explain disagreement between ensemble and single QDs measurements and to gain insight into the heterogeneous distribution of ET rates, we propose the following model to describe both the single and ensemble-averaged ET rates. Our previous studies

about the electron or hole transfer dynamics between QDs and adsorbed molecules indicated that there is a distribution of the number of molecules on QDs.[58,69] If the adsorption process is random, which means that the probability of adsorbing a molecule is independent of the number of molecules already adsorbed, then the number of adsorbed molecules should obey a Poisson distribution: [58,69,70]

$$P_n = \frac{m^n}{n!} e^{-m} \qquad \text{(Eq. 4.12)}$$

where P_n is the probability of QDs with n adsorbed molecules and m is the average number of adsorbates per QD. We assume that for QDs with n adsorbates, there is a Gaussian distribution of ET rates with a width of w and center of nk_1:

$$G(k_{ET}) = \sqrt{\frac{2}{\pi w^2}} \times e^{-2\frac{(k_{ET}-nk_1)^2}{w^2}} \qquad \text{(Eq. 4.13)}$$

where k_1 is the rate constant of the 1:1 QD-F27 complex. We have assumed that the ET rate constant is linearly proportional to the number of adsorbates n and the width is same for QD-F27 complexes of different ratios. The combination of Eq.4.12 and 4.13 leads to a distribution of ET rate $F(k_{ET})$ of QD-F27 complexes with an average adsorbate number of m:

$$F(k_{ET}) = \sum_{n=1}^{\infty} \frac{m^n e^{-m}}{n!} \sqrt{\frac{2}{\pi w^2}} e^{-2\frac{(k_{ET}-nk_1)^2}{w^2}} + e^{-m}\delta(k_{ET}) \qquad \text{(Eq. 4.14)}$$

For an ensemble of QD-F27 complexes, the concentration of excited QD at delay time t is

$$\left[N_t^*\right] = \left[N_0^*\right] \sum_i A_i \left[\int_0^{\infty} F(k_{ET}) e^{-(k_{ET}+k_{0i})t} dk_{ET}\right] \qquad \text{(Eq. 4.15)}$$

where $[N_0^*]$ is the initial concentration of excited QDs and k_{0i} and A_i is the intrinsic decay time constant and amplitude, respectively, of the i^{th} component of the multi-

exponential decay kinetics of excited free QDs .The ensemble fluorescence decay of free QDs is fit by a multi-exponential function, as show in Figure 4.11 A. The fitting parameters (in the unit of ns^{-1} for rate constants) are

$$\sum_i A_i e^{k_{0i}t} = 0.13e^{-0.53t} + 0.45e^{-0.063t} + 0.42e^{-0.026t}$$

The ensemble fluorescence decays of QD-F27 complexes from sample A' and B' and the single QD ET rate distributions $F(k_{ET})$ from sample 2 and 3 are fit by Eq. 4.15 and 4.14, respectively. These fits are using the same k_1 and w values, but different m values to account for different average F27-to-QD ratio m for each sample. As shown in Figure 4.11, the traces are well fit by the functions, yielding the average F27-to-QD ratios of 0.7, 2.6, 0.3 and 0.9 for samples A', B', 2 and 3, respectively, and an average ET rate k_1 of 0.03 ns^{-1} and a width w of 0.06 ns^{-1}. However, the ET rate distributions $F'(k_{ET})$, which includes contributions from both on and off states, are not able to be fit by Eq. 4.14 when the k_{ET} is >~0.1 ns^{-1}, as shown in the insets in Figure 4.11 B and C. The discrepancies are due to the presence of the off state.

The off states of free QDs have been attributed to photo induced positively charging of QDs by transferring electrons to the trap states in and around QDs. The optical excitation of the positively charged QDs generates a positive trion (an exciton plus a hole), which can undergo fast nonradiative Auger relaxation. It has been reported that the Auger relaxation time for CdSe QDs with radius of 2.3 nm is ~45 ps.[71] If we assume a similar relaxation time in our CdSe core multi-layer QDs (core radius of 1.8 nm), the lifetimes of the off states in QD-F27 complexes appear to be dominated by the Auger relaxation time. Furthermore, for QD-F27 complexes, if the fluctuation of fluorescence intensity and lifetime is caused by fluctuation of ET rate and the fluctuation in lifetime is

a direct measure of ET rate variation, then the on and off states correspond to ET rates fluctuating from >2 ns^{-1} to ~0 ns^{-1}, and QDs spend significant amount of time to stay on their off state. However, such a fast ET rates were not observed from transient absorption and ensemble-averaged fluorescence measurements, from which the ET process was found to occur only on ns time scale. Based on above discussions, we speculate that the positively charging effect is still persist in QD-F27 complexes and the off state is not caused by ET process, but controlled by fast Auger relaxation process in charged QD.

4.2.5 Single QD Blinking and Interfacial ET Model

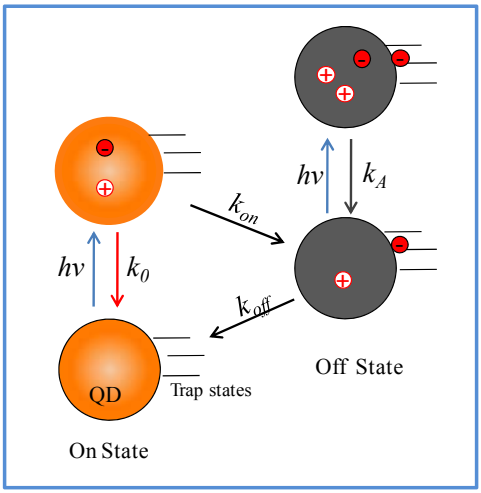

Figure 4.13. A model for on and off states in single free QDs.

The blinking model of single free QDs is presented in Figure 4.13. The on state corresponds to the neutral state of QD, and the QD exciton relaxes by emitting photons. The off state is positively charged state of QD which is formed by Auger ionization by transferring electrons to the trap states in and around QD. The excitation of charged QDs

generates positive trion whose exciton relaxes by fast nonradiative Auger process. The recombination of trapped electron with the hole in QD turns the QD back to its neutral state. The transition between neutral and charged states produce the blinking phenomena observed in the QD measurement.

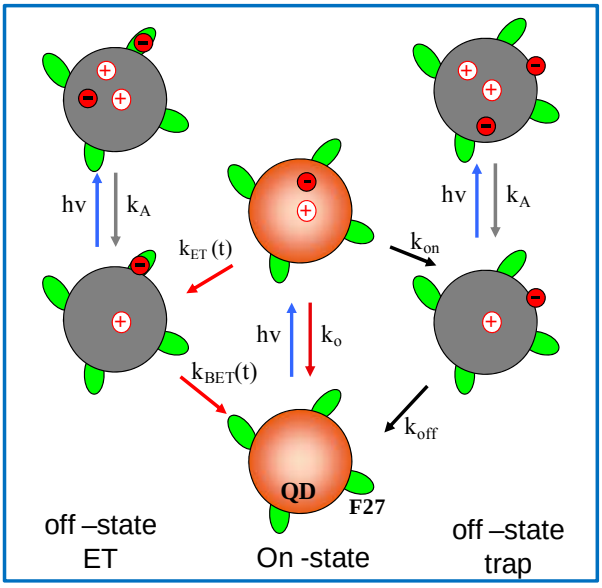

Figure 4.14. A model for on and off states in single QD-F27 complexes. ET from QDs to F27 provides an additional pathway for forming off states, leading to correlated single QD interfacial ET and blinking dynamics.

The ET and blinking model for QD-F27 complexes is described in Figure 4.14, showing a correlated interfacial ET and blinking dynamics of a single QD-F27 complex. The positive charging effect is still persisting in single QD-F27 complexes, and the observed intermittent ET dynamics are caused by the blinking of the QDs. The present of ET to the adsorbed F27 molecule offers additional pathway to produce positively charged QD (off state). The lifetime of this off state is determined by the charge recombination rate (k_{BET}) between the reduced adsorbate and the QD. The QD-F27 complex at on state is likely undergoing a reaction circle of interfacial ET followed by fast BET. Although

the average BET rate resolved by transient absorption measurement is about ~ 1 μs, this process is not completed by 10 μs, as shown in Figure 4.4 B. It is also possible that the charge-separated state can have finite probability on the 50-ms to 10-s timescale that was probed in the single QD studies. Thus, the interfacial ET process accounts for the observed more short on events and long off events for a QD-F27 complex compared to free QD. The effect of ET activity on blinking dynamics is enhanced as the density of electron acceptor (F27-to-QD ratio) increases. With the increase of ET rates, the probability of creating an off state increases, leading to higher contribution of off states in samples with higher F27-to-QD ratios, as shown in Figures 4.9 and 4.10.

4.3 Summary

This chapter discussed the studies of the ET dynamics from single CdSe core multi-layer shell QDs to adsorbed F27 molecules. The interfacial ET from QD to F27 was directly probed by transient absorption measurements of QDs and QD-F27 complexes. The QD exciton recover kinetics was faster in the presence of F27. The ET dynamics were ratio dependent. As the dye-to-QD ratio increased, the ET rate becomes faster. The bleach and bleach recovery kinetics of F27 molecules were also observed, and the charge recombination processes from reduced F27 to QD mainly occurred on ~1 μs time scale but not finished by 10 μs. The comparison between transient absorption kinetics and ensemble-averaged fluorescence decays of free QDs and QD-F27 complexes with different dye-to-QD ratios has shown well agreement, suggesting that the ET rate can be monitored by fluorescence lifetimes. The fluorescence intensities and lifetimes of single free QDs and QD-F27 complexes at different ratios were measured as a function of time. QD-F27 complexes showed intermittent ET dynamics which were highly related to the

blinking dynamics. Compared to free QDs, the presence of ET in the QD-F27 complexes led to larger fluorescence decay rate (shorter fluorescence lifetime) as well as shorter on state and longer off state blinking events with 0.05~100 second duration. As the ET rate increased (dye-to-QD ratio increased), the fluorescence decay rates were further increased and on (off) state events were further shortened (lengthened). Comparison of single and ensemble measurements showed that both ensemble-averaged fluorescence decays and the distribution of on state ET rates can be well-described by a model that assumes a Poisson distribution of the number adsorbed F27 on QDs, revealing an ET rate of 0.03 ns^{-1} in the 1:1 QD-F27 complex. The fluorescence decay rate of the off state was much faster than the ET rate, and was believed to be controlled by Auger relaxation in the charged QDs. The interfacial ET provided an additional pathway for generating off states in the QD-F27 complexes, affecting the single QD blinking dynamics. With increasing ET rates, the probability for generating off states increases, which led to correlated single QD interfacial ET and blinking dynamics in QD-acceptor complexes. Because blinking is a general phenomenon of single QDs, we believe that the correlated interfacial ET and blinking and the resulting intermittent ET activity are general phenomena of an electron donor-acceptor complex involving a single QD.

References

(1) Kamat, P. V. *Journal of Physical Chemistry B* 2002, *106*, 7729.

(2) Adams, D. M.; Brus, L.; Chidsey, C. E. D.; Creager, S.; Creutz, C.; Kagan, C. R.; Kamat, P. V.; Lieberman, M.; Lindsay, S.; Marcus, R. A.; Metzger, R. M.;

Michel-Beyerle, M. E.; Miller, J. R.; Newton, M. D.; Rolison, D. R.; Sankey, O.; Schanze, K. S.; Yardley, J.; Zhu, X. *Journal of Physical Chemistry B* 2003, *107*, 6668.

(3) Thomas, K. G.; Kamat, P. V. *Acc. Chem. Res. FIELD Full Journal Title:Accounts of Chemical Research* 2003, *36*, 888.

(4) Shipway, A. N.; Katz, E.; Willner, I. *Chem. Phys. Chem.* 2000, *1*, 18.

(5) Alstrum-Acevedo, J. H.; Brennaman, M. K.; Meyer, T. J. *Inorg. Chem.* 2005, *44*, 6802.

(6) Hodes, G. *Isr. J. Chem.* 1993, *33*, 95.

(7) Sasha, G.; Gary, H. *J. Phys. Chem. A* 1994, *98*, 5338.

(8) Nozik, A. J. *Physica E: Low-Dimensional Systems & Nanostructures (Amsterdam, Netherlands)* 2002, *14*, 115.

(9) Wang, Z. L. *J. Phys. Chem. A* 2000, *104*, 1153.

(10) Schaller, R. D.; Klimov, V. I. *Phys. Rev. Lett.* 2004, *92*, 186601.

(11) Ellingson, R. J.; Beard, M. C.; Johnson, J. C.; Yu, P.; Micic, O. I.; Nozik, A. J.; Shabaev, A.; Efros, A. L. *Nano Letters* 2005, *5*, 865.

(12) Klimov, V. I. *Annual Review of Physical Chemistry* 2007, *58*, 635.

(13) Klimov, V. I. *Applied Physics Letters* 2006, *89*, 123118/1.

(14) Huang, J.; Stockwell, D.; Huang, Z.; Mohler, D. L.; Lian, T. *J. Am. Chem. Soc.* 2008, *130*, 5632.

(15) Boulesbaa, A.; Issac, A.; Stockwell, D.; Huang, Z.; Huang, J.; Guo, J.; Lian, T. *J. Am. Chem, Soc.* 2007, *129*, 15132.

(16) Rossetti, R.; Beck, S. M.; Brus, L. E. *J. Am. Chem. Soc.* 1984, *106*, 980.

(17) Rossetti, R.; Brus, L. E. *J. Phys. Chem.* 1986, *90*, 558.

(18) Ramsden, J. J.; Gratzel, M. *Chem. Phys. Lett.* 1986, *132*, 269.

(19) Henglein, A. *Pure & Appl. Chem.* 1984, *56*, 1215.

(20) Logunov, S.; Green, T.; Marguet, S.; El-Sayed, M. A. *J. Phys. Chem. A* 1998, *102*, 5652.

(21) Burda, C.; Green, T. C.; Link, S.; El-Sayed, M. A. *J. Phys. Chem. B* 1999, *103*, 1783.

(22) Matylitsky, V. V.; Dworak, L.; Breus, V. V.; Basche, T.; Wachtveitl, J. *J Am Chem Soc* 2009, *131*, 2424.

(23) Huang, J.; Huang, Z.; Yang, Y.; Zhu, H.; Lian, T. *J. Am. Chem. Soc.* 2010, *132*, 4858.

(24) Issac, A.; Jin, S.; Lian, T. *J. Am. Chem. Soc.* 2008, *130*, 11280.

(25) Cui, S.-C.; Tachikawa, T.; Fujitsuka, M.; Majima, T. *J. Phys. Chem. C* 2008, *112*, 19625.

(26) Jin, S.; Lian, T. *Nano Letters* 2009, *9*, 2448.

(27) Jin, S.; Song, N.; Lian, T. *ACS Nano* 2010, *4*, 1545.

(28) Efros, A. L.; Rosen, M. *Physical Review Letters* 1997, *78*, 1110.

(29) Shimizu, K. T.; Neuhauser, R. G.; Leatherdale, C. A.; Empedocles, S. A.; Woo, W. K.; Bawendi, M. G. *Physical Review B: Condensed Matter and Materials Physics* 2001, *63*, 205316/1.

(30) Krauss, T. D.; O'Brien, S.; Brus, L. E. *Journal of Physical Chemistry B* 2001, *105*, 1725.

(31) Nirmal, M.; Dabbousi, B. O.; Bawendi, M. G.; Macklin, J. J.; Trautman, J. K.; Harris, T. D.; Brus, L. E. *Nature* 1996, *383*, 802.

(32) Empedocles, S.; Bawendi, M. *Acc. Chem. Res.* 1999, *32*, 389.

(33) Fisher, B. R.; Eisler, H.-J.; Stott, N. E.; Bawendi, M. G. *J. Phys. Chem. B* 2004, *108*, 143.

(34) Chung, I.; Bawendi, M. G. *Phys. Rev. B:* 2004, *70*, 165304/1.

(35) Kuno, M.; Fromm, D. P.; Johnson, S. T.; Gallagher, A.; Nesbitt, D. J. *Phys. Rev. B:* 2003, *67*, 125304/1.

(36) Kuno, M.; Fromm, D. P.; Hamann, H. F.; Gallagher, A.; Nesbitt, D. J. *J. Chem. Phys.* 2001, *115*, 1028.

(37) Kuno, M.; Fromm, D. P.; Gallagher, A.; Nesbitt, D. J.; Micic, O. I.; Nozik, A. J. *Nano Letters* 2001, *1*, 557.

(38) Peterson, J. J.; Nesbitt, D. J. *Nano Lett.* 2009, *9*, 338.

(39) Zhang, K.; Chang, H.; Fu, A.; Alivisatos, A. P.; Yang, H. *Nano Letters* 2006, *6*, 843.

(40) Montiel, D.; Yang, H. *J. Phys. Chem. A* 2008, *112*, 9352.

(41) Pelton, M.; Smith, G.; Scherer, N. F.; Marcus, R. A. *Proc. Natl. Acad. Sci. U. S. A.* 2007, *104*, 14249.

(42) Tang, J.; Marcus, R. A. *J. Chem. Phys.* 2006, *125*, 044703/1.

(43) Tang, J.; Marcus, R. A. *J. Chem. Phys.* 2005, *123*, 054704/1.

(44) Tang, J.; Marcus, R. A. *Phys. Rev. Lett.* 2005, *95*, 107401/1.

(45) Tang, J.; Marcus, R. A. *J. Chem. Phys.* 2005, *123*, 204511/1.

(46) Issac, A.; von Borczyskowski, C.; Cichos, F. *Phys.l Rev. B* 2005, *71*, 161302/1.

(47) Schlegel, G.; Bohnenberger, J.; Potapova, I.; Mews, A. *Phys. Rev. Lett.*. 2002, *88*, 137401.

(48) Verberk, R.; van Oijen, A. M.; Orrit, M. *Physical Review B: Condensed Matter and Materials Physics* 2002, *66*, 233202/1.

(49) Shimizu, K. T.; Woo, W. K.; Fisher, B. R.; Eisler, H. J.; Bawendi, M. G. *Physical Review Letters* 2002, *89*, 117401/1.

(50) Yu, W. W.; Qu, L.; Guo, W.; Peng, X. *Chem. Mater.* 2003, *15*, 2854.

(51) Haus, J. W.; Zhou, H. S.; Honma, I.; Komiyama, H. *Physical Review B* 1993, *47*, 1359.

(52) Brus, L. *J. Chem. Phys.* 1983, *79*, 5566.

(53) Brus, L. E. *J. Chem. Phys.* 1984, *80*, 4403.

(54) Garcia-Santamaria, F.; Chen, Y.; Vela, J.; Schaller, R. D.; Hollingsworth, J. A.; Klimov, V. I. *Nano Letters* 2009, *9*, 3482.

(55) Pandey, A.; Guyot-Sionnest, P. *Journal of Chemical Physics* 2007, *127*, 104710/1.

(56) Rao, P. *S.*; *Hayon, E. Journal of the American Chemical Society* 1974, *96*, 1287.

(57) Ponyaev, A. I.; Martynova, V. P.; El'tsov, A. V. *Russian Journal of General Chemistry* 2001, *71*, 1744.

(58) Boulesbaa, A.; Huang, Z.; Wu, D.; Lian, T. *Journal of Physical Chemistry C* 2010, *114*, 962.

(59) Kuno, M.; Fromm, D. P.; Hamann, H. F.; Gallagher, A.; Nesbitt, D. J. *J. Chem. Phys.* 2000, *112*, 3117.

(60) Chen, Y.; Vela, J.; Htoon, H.; Casson, J. L.; Werder, D. J.; Bussian, D. A.; Klimov, V. I.; Hollingsworth, J. A. *J. Am. Chem. Soc.* 2008, *130*, 5026.

(61) Fomenko, V.; Nesbitt, D. J. *Nano Lett.* 2008, *8*, 287.

(62) Mahler, B.; Spinicelli, P.; Buil, S.; Quelin, X.; Hermier, J.-P.; Dubertret, B. *Nature Materials* 2008, *7*, 659.

(63) Hohng, S.; Ha, T. *Journal of the American Chemical Society* 2004, *126*, 1324.

(64) Wang, S.; Querner, C.; Emmons, T.; Drndic, M.; Crouch, C. H. *J. Phys. Chem. B* 2006, *110*, 23221.

(65) Mandal, A.; Nakayama, J.; Tamai, N.; Biju, V.; Isikawa, M. *J. Phys. Chem. B* 2007, *111*, 12765.

(66) Empedocles, S. A.; Bawendi, M. G. *Science* 1997, *278*, 2114.

(67) Empedocles, S. A.; Bawendi, M. G. *Journal of Physical Chemistry B* 1999, *103*, 1826.

(68) Neuhauser, R. G.; Shimizu, K. T.; Woo, W. K.; Empedocles, S. A.; Bawendi, M. G. *Physical Review Letters* 2000, *85*, 3301.

(69) Huang, J.; Huang, Z.; Jin, S.; Lian, T. *J. Phys. Chem. C* 2008, *112*, 19734.

(70) Pons, T.; Medintz, I. L.; Wang, X.; English, D. S.; Mattoussi, H. *J. Am. Chem. Soc.* 2006, *128*, 15324.

(71) Klimov, V. I.; Mikhailovsky, A. A.; McBranch, D. W.; Leatherdale, C. A.; Bawendi, M. G. *Science* 2000, *287*, 1011.

Chapter 5. Interfacial Electron Transfer Dynamics from Single QDs to TiO_2 Nanoparticle and Rutile Single Crystals

5.1 Interfacial Electron Transfer from Single QDs to TiO_2 Nanoparticles

5.1.1 Introduction

Complementary to dye-sensitized solar cells (DSSC), quantum dot (QD) solar cells have also been considered as a promising low-cost alternative to conventional silicon-based cells in recent years.[1-5] One advantage of using QDs as a sensitizer is their tunable band gap, which offers the opportunity to improve light harvesting.[6-9] Furthermore, QDs provide the possibility of improving the efficiency of QD-based light conversion devices by generating multiexcitons with the absorption of one photon.[10-16] Several types of QD-based solar cells, using a combination of QDs such as CdSe and CdS with various semiconductor oxides such as TiO_2 and SnO_2 nanoparticles or nanorods, have been developed in recent years.[17-21] However, their power-conversion efficiencies are typically $\leq$ 2%, significantly lower than DSSCs, whose power-conversion efficiencies are up to 11%.[22-24] Studies on QD interfacial electron transfer (ET) and charge recombination dynamics are hence essential in order to improve the efficiencies of QD-based light conversion devices.

The ET dynamics from QDs to semiconductor oxides and their dependence on factors such as the QD size, pH of environmental solutions, and the variation of nanostructures of electron acceptors have been studied using ensemble-averaged transient absorption and

time-resolved fluorescence spectroscopy.[18,25,26] However, few reports exist on the ET dynamics from single QDs to semiconductor oxides.

The optical properties of single QDs have been extensively studied. The most well-known phenomenon is the fluorescence intermittency (known as blinking) of single QDs.[27-50] As discussed in Chapter 4, this blinking is due the photoinduced charging of QDs through the transfer of electrons to the trap states. The high fluorescence intensity (on) states have long exciton lifetimes and are from neutral QDs, whereas the low intensity (off) states have short exciton lifetimes and are from positively charged QDs. Our studies on the interfacial ET from single QDs to adsorbed organic dye molecules indicate that the blinking activities of QDs still persist in the donor-acceptor ET system. The results also revealed intermittent ET transfer dynamics which are modulated by the single QD blinking activity. The fluorescence decay rate of the off state of the QD-dye complex is much faster than the ET rate, and is believed to be controlled by Auger relaxation in the charged QDs. Interfacial ET provides an additional pathway for generating off states in the QD-F27 complexes, thus affecting the single QD blinking dynamics. Because blinking is a general phenomenon of single QDs, ET from QDs on semiconductor oxides could follow the same ET model.

To gain further insight into the ET dynamics from QDs to semiconductor oxides, the interfacial ET dynamics from single QDs to TiO_2 nanoparticles have been investigated by single particle fluorescence spectroscopy and compared to ensemble-averaged fluorescence decays. The results are discussed in the following section.

5.1.2 Results and discussion

The water soluble QDs used in this study were obtained from Ocean NanoTech, LLC, USA. They consist of a CdSe core, a multilayer shell of $CdS_{2ML}ZnCdS_{1ML}ZnS_{1ML}$ and capping ligands with carboxylic acid functional groups. The lowest energy exciton absorption and emission peaks of these QDs are at 580 nm and 605 nm, respectively, as shown in Figure 5.1 A. The single QD water solution was spin coated on the TiO_2 nanoparticle thin film and then the sample was washed by water to remove the weakly adsorbed QDs. The QDs were adsorbed on TiO_2 nanoparticles through their carboxylic acid functional groups. Figure 5.1 B shows a raster scanned image of single QDs sensitized on a TiO_2 nanoparticle thin film, showing well-separated single QDs.

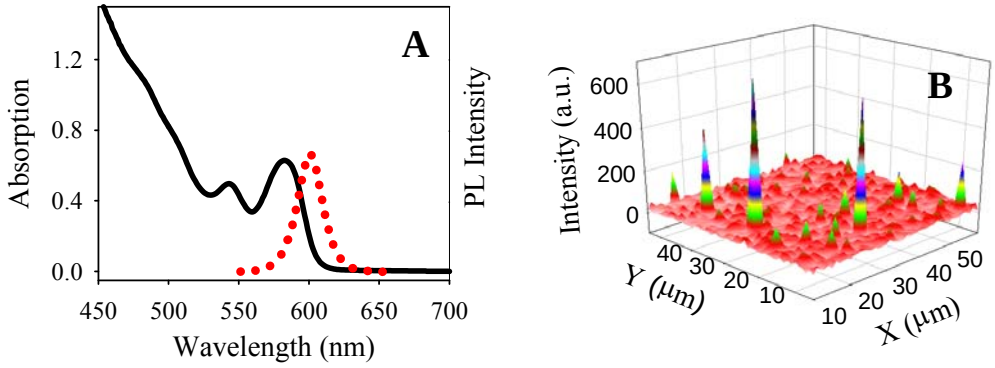

Figure 5.1. (A) UV-VIS absorption (black solid line) and fluorescence (red dot line) spectra of the QDs in water. (B) A raster scanned fluorescence image of single QDs on a TiO_2 nanoparticle thin film.

5.1.2.1 Single QD Dynamics

In the single QDs measurement, 49 single QDs on glass cover slip and 45 single QDs on TiO_2 nanoparticle thin film were studied. A few typical fluorescence intensity and lifetime trajectories of single QDs on glass and TiO_2 are shown in Figure 5.2. The intensity trajectories were constructed by the number of photons binned over 10 ms

(shown in the unit of KHz), and delay time histograms of detected photons within a 0.5s window were constructed and fit by single exponential decays to construct the fluorescence lifetime trajectories.

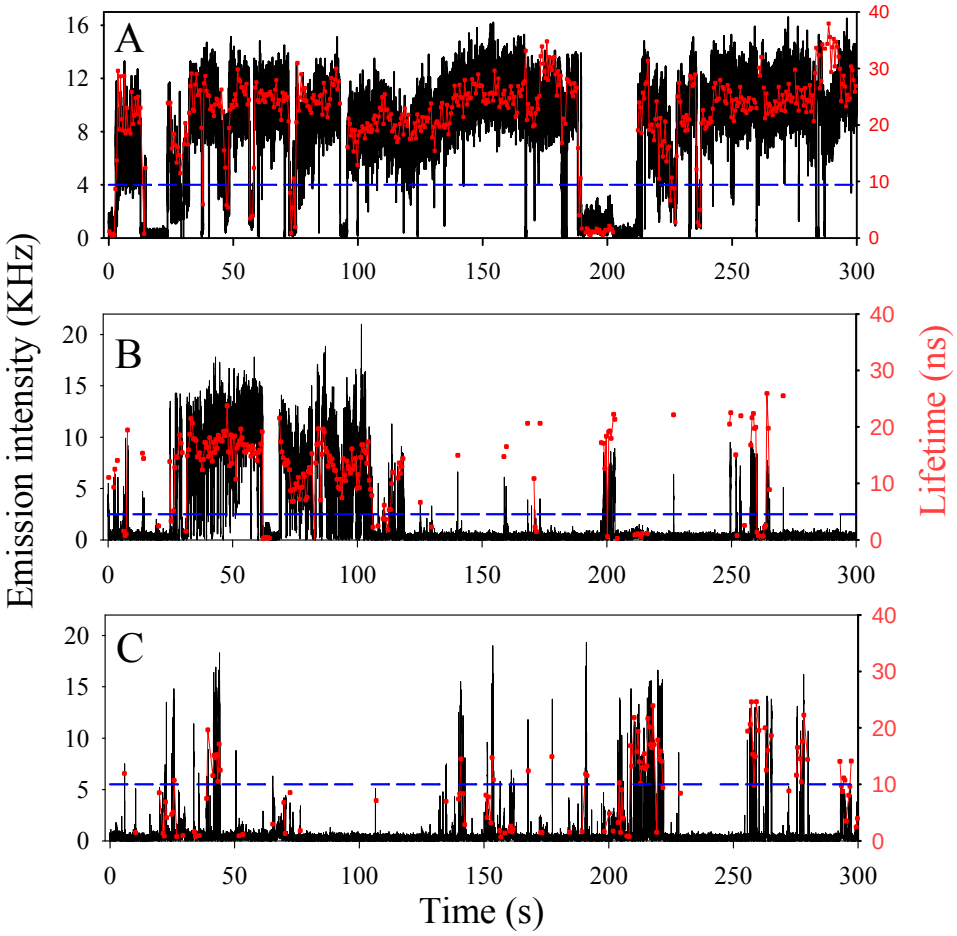

Figure 5.2. Typical fluorescence intensity (black) and lifetime trajectories (red) of single QDs on glass (A) and TiO2 nanoparticle thin film (B and C). The dashed lines are the thresholds separating the on and off states.

Blinking Dynamics. We first discuss the blinking dynamics of the single QDs. The histograms of fluorescence intensity of the QDs shown in Figures 5.2 A, B and C are plotted in Figure 5.3 A, B and C, respectively. The intensity distribution of QD on glass

(Figure 5.3A) shows two peaks at ~0.25 KHz (background level) and ~10.5 KHz. Similar fluorescence intensity distributions have been observed for all QDs examined on glass. The high intensity peak is referred as on state and low intensity peak as off state.[27-48,50,51] The observed fluorescence intensity trajectories of QDs on TiO_2 films are different from those on glass. As shown in Figure 5.3 B and C, the intensity histograms for QDs on TiO_2 can also be roughly characterized by two peaks of on and off states. However, it is dominated by the contribution of off states, indicating the QDs on TiO2 spend much more time remaining on the off sate than QDs on glass, as evident by the trajectories in Figure 5.2.

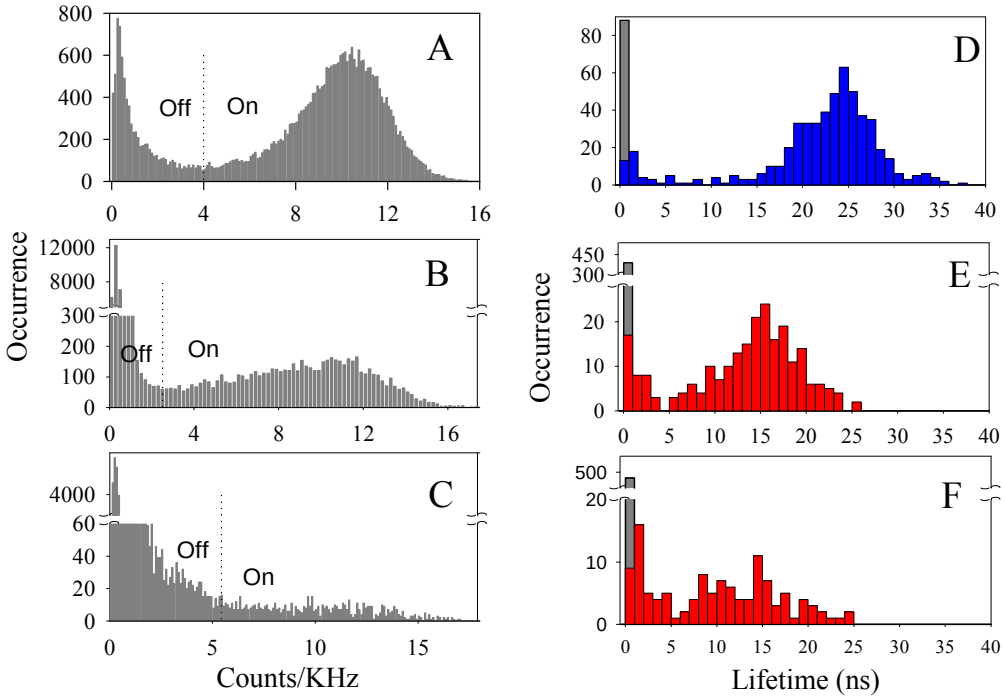

Figure 5.3. The fluorescence intensity (left panels) and lifetime (right panels) histograms of the single QDs shown in Figure 5.2 A (A and D), B (B and E) and C (C and F). The dashed lines in panels A, B and C indicate the threshold separating the on and off states.

Black bars in panels D, E and F indicate the occurrence of low fluorescence intensity points along the trajectories, for which the lifetimes have been assumed to be < 0.5 ns.

To quantitatively resolve the blinking dynamics of the single QDs, a threshold separating the on and off state is determined by fitting the intensity histograms by sum of two Gaussian functions. The point where these two Gaussians cross is taken as the threshold intensity, which for QDs shown in Figure 5.3 A, B and C are at fluorescence intensities of 4.0, 2.5 and 5.2 KHz, respectively. Any point in the trajectory with intensity above (below) the threshold level was assigned to on (off) state. The thresholds of on and off states are determined in the same way for all studied single QDs. The probability densities *P(t)* of a QD at on or off states for a duration time of *t* are defined as:[35]

$$P_i(t) = \frac{N_i(t)}{N_{i,total}} \times \frac{1}{\Delta t_{avg.}} \quad (i = \text{on or off}) \qquad \text{(Eq. 5.1)}$$

where $N(t)$ is the number of "on" or "off" events of duration time of t, N_{total} the total number of on or off events, and Δt_{avg} the average time between nearest neighbor events (see Chapter 4 for detail). The probability densities $P_{on}(t)$ and $P_{off}(t)$ of the single QDs on glass in Figure 5.2 A and on TiO_2 in Figure 5.2 B are shown in Figure 5.4 A and B, respectively. For these two particular QDs, the QD on TiO_2, compared to the QD on glass, has lower probability density of long on event and higher probability density of long off event, consistent with the observation from their fluorescence intensity trajectories shown in Figure 5.2.

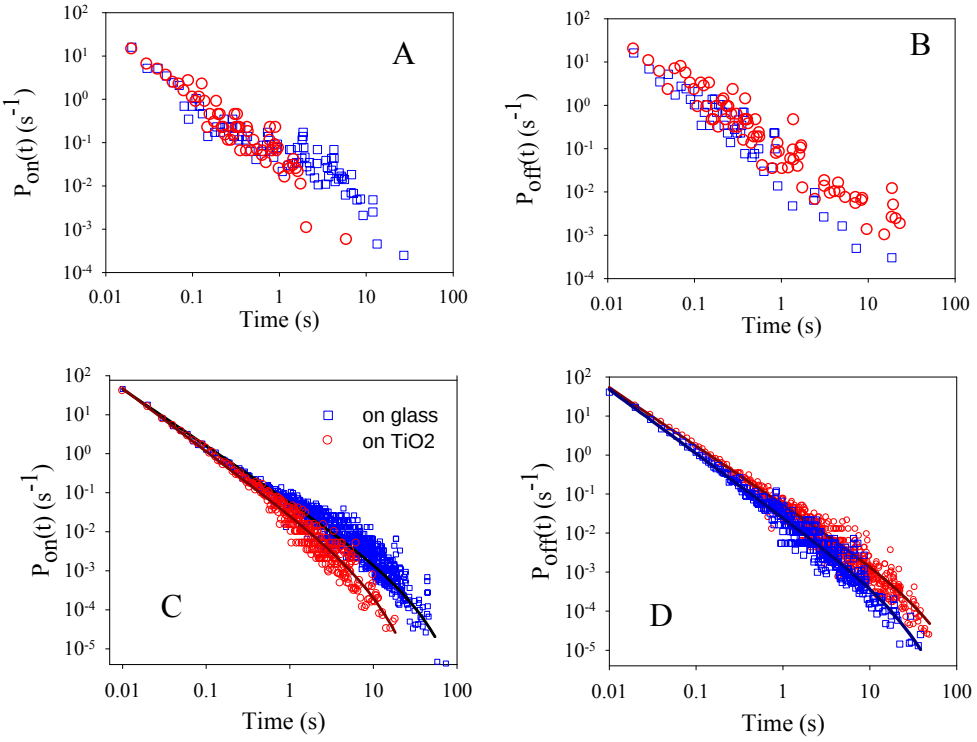

Figure 5.4. Probability density of (A) on-states ($P_{on}(t)$) and (B) off-states($P_{off}(t)$) of the single QDs on glass shown in Figure 5.2 A (blue open squares) and on TiO2 shown in Figure 5.2 B (red open circles). $P_{on}(t)$ and $P_{off}(t)$constructed from all studied 49 single QDs on glass and 45 single QDs on TiO_2 nanoparticles are shown in panels C and D, respectively. The solid lines are best fits to Eq. 5.2 (see text).

The total probability densities of on and off states constructed from all studied 49 QDs on glass and 45 QDs on TiO_2 are shown in Figure 5.4 C and D. They show power law distributions at short time but exponential decays at long time tails, similar to those of QD-F27 complexes discussed in Chapter 4 and the reported results by other groups.[27,52-54] These $P(t)$ distributions are fit by a truncated power law:[38,40-42,53]

$$P_i(t) = B_i t^{-m_i} \exp(-\Gamma_i t) \quad (i\text{= on or off}) \qquad \text{(Eq. 5.2)}$$

where B is the amplitude, m the power law exponent and Γ the saturation rate. The fitting parameters are listed in Table 5.1. The total blinking dynamics are qualitative consistent with those of single QDs shown in Figure 5.4 A and B. The power law exponents m_{on} and m_{off} are similar with reported values for CdSe QD.[27,38,51] However, there are noticeable differences between QDs on glass and on TiO_2. Compared to the QDs on glass, QDs on TiO_2 have larger m_{on} and Γ_{on}, indicating lower probability dentists of long on events, and smaller m_{off} and Γ_{off}, indicating increased probability densities of long off events.

Table 5.1. Fitting parameters of $P_{on}(t)$ and $P_{off}(t)$ for all single QDs on glass and TiO_2 nanoparticles. The error is one standard deviation.

	m_{on}	$1/\Gamma_{on}$ (s)	m_{off}	$1/\Gamma_{off}$ (s)
QDs on glass	1.45 ± 0.03	59 ± 7	1.64 ± 0.03	48 ± 8
QDs on TiO_2	1.61 ± 0.04	18 ± 2	1.50 ± 0.03	94 ± 19

Fluorescence Lifetimes. The positive correlation between fluorescence intensity and lifetime has been widely observed, and is due to the fluctuation of nonradiative decay rate. [32,37,44,55] Such positive correlation is also observed for QDs on glass and TiO_2 in this study, as shown the lifetime trajectories in Figure 5.2 A, B and C. Their corresponding lifetime histograms are shown in Figure 5.3 D, E and F, respectively. The lifetimes at the background level could not be accurately determined due to limited number of photons and are assumed to be < 0.5 ns on the basis of the positive correlation. For the typical QD on glass shown in Figure 5.2 A, its lifetime histogram (Figure 5.3 D) shows two peaks centered at ~23 ns and ~0.5 ns. The peak with higher lifetimes corresponds to the on state

and the peak with shorter lifetimes corresponds to the off state. However, for the typical QDs on TiO_2 shown in Figure 5.2 B and C, their on sate lifetimes are becomes shorter centered at ~15 ns and the off states centered at ~0.5 ns have much more contributions in the lifetime distributions (see Figure 5.3 E and F).

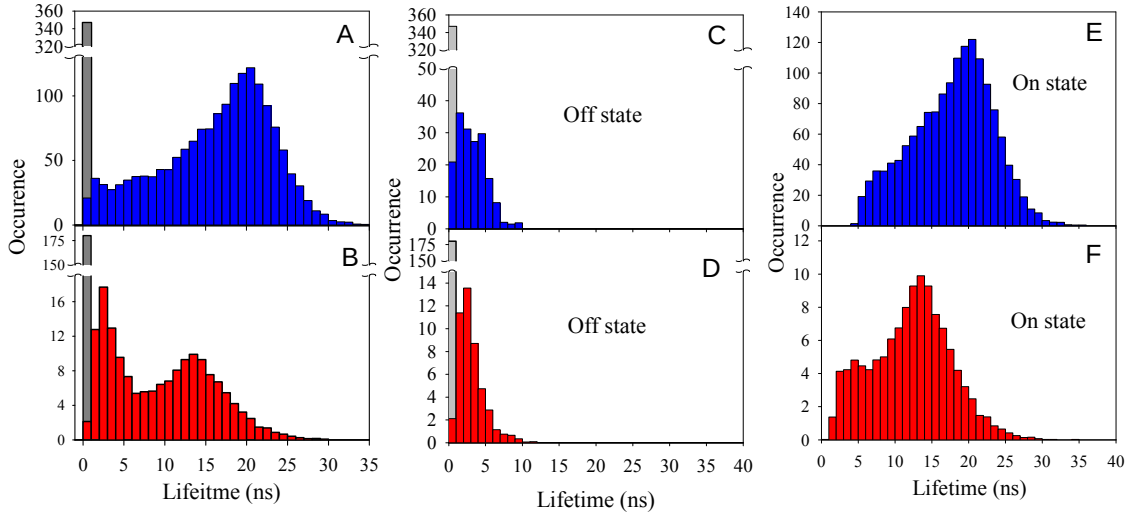

Figure 5.5. Total histograms of fluorescence lifetime distributions of (A) 49 QDs on a glass cover slip and (B) 45 QDs on TiO_2 nanoparticles. The total histograms with on and off states plotted separately are shown in panels C and E for QDs on glass and panels D and F for QDs on TiO_2. Black bars indicate the occurrence of low fluorescence intensity points along the trajectories, for which the lifetimes have been assumed to be < 0.5 ns.

Figure 5.5 A and B show the total fluorescence lifetime distribution constructed from the lifetime trajectories of 49 single QDs on glass cover slip and 45 single QDs on TiO_2 nanoparticles, respectively. To separate the on and off states in the total lifetime histograms, lifetime thresholds for on and off states of all studied QDs were determined by their corresponding intensity thresholds (see the detail in Chapter 4). The total lifetime histograms with on and off states plotted separately are shown in Figure 5.5 C and E for QDs on glass and Figure 5.5 D and F for QDs on TiO_2. The total distributions are

qualitative similar to those of single QDs. For QD on glass, the off state is centered at < 0.5 ns and the on state at 21 ns. For QDs on TiO_2, the off state lifetimes are still centered at ~0.5 ns, but the amplitude of off state becomes bigger. The peak position of the on state lifetime distribution is shifted to a shorter lifetime position (~14 ns) and its relative amplitude becomes much smaller.

The differences in blinking dynamics and lifetime distributions for QDs on glass and TiO_2 nanoparticles are attributed to the presence of ET from QD to TiO_2. The QDs used in this study is CdSe core multi-shell ($CdS_{2ML}ZnCdS_{1ML}ZnS_{1ML}$) QDs with the first exciton absorption peak at 580 nm. They were made from CdSe cores with a first exciton peak at 550 nm, whose 1S exciton oxidation and reduction potentials are determined to be -1.11 and + 1.05 V (SCE), respectively.[25,56,57] With assuming that the red shift of the absorption is due to the change of conduction band energy (see Chapter 4 for the detail), the estimated 1S exciton oxidation and reduction potentials are -1.01 and +1.05 V (vs SCE), respectively, for the core shell QDs used in this study. The conduction band edge position of TiO_2 at pH 2 to 7 is -0.5 to -0.8V (SCE),[58] suggesting that ET from QDs to TiO_2 nanoparticle is energetically allowed. The schematic diagram for the relevant energetics of QD and TiO_2 nanoparticle is shown in Figure 5.7 B. ET from CdSe QDs to TiO_2 nanoparticles has been observed by ultrafast transient absorption and time-resolved fluorescence studies,[59] and confirmed by photocurrent generation in CdSe sensitized TiO_2 nanocrystalline thin film solar cells.[18] Furthermore, the ET from similar CdSe core multishell QDs to the adsorbed F27 molecules has been directly observed by transient absorption measurements. The results were discussed in Chapter 4.

The presence of ET from QDs to TiO_2 shortens the on state lifetimes and increases the contribution of off state in the total lifetime distribution. Furthermore, the presence of ET decreases (increase) the probability of long on (off) event in the blinking dynamics for QDs on TiO_2. These observations are similar with those in QD-F27 complexes discussed in Chapter 4. The single QD studies of QD-F27 complexes indicated an intermittent ET transfer dynamics which is modulated by the blinking of the single QDs. Only the lifetimes in on state are measuring the ET dynamics, and the lifetimes in off states are believed to be controlled by Auger relaxation in the charged QDs. The interfacial ET provides an additional pathway for generating off states in the QD-F27 complexes, affecting the single QD blinking dynamics. It is not clear whether the QDs on TiO_2 nanoparticles follow the same ET model. To confirm the ET from QDs to TiO_2 and discover the ET dynamics in QD/TiO_2 system, the ensemble-averaged fluorescence decays of QDs on glass and TiO_2 are studied and compared with the results from single QDs measurements. The results are discussed below.

5.1.2.2 Comparison of Ensemble and Single QDs ET Dynamics

The blinking of single QDs on glass is believed to be due to the photoinduced charging of QDs by transferring electrons to the trap states in and around QDs. The off states are positively charged states of QDs whose fluorescence intensity and lifetime are decreased by the fast nonradiative Auger relaxation. Although the nature of the trap states and the microscopic origin of these fluctuating transition rates remains unclear, models assuming diffusion-controlled electron transfer[27,39-42] and fluctuating tunneling barriers for electron transfer to and from trap states[34,45] have been shown to account for the

power-law on and off time distribution functions. Previous studies have indicated that the photoinduced charging effect can still persist in the ensemble-averaged fluorescence measurements.[40] Figure 5.6 A shows the fluorescence intensity as a function of detection time of an ensemble of QDs on glass and TiO_2. The fluorescence intensity traces were obtained by continuously exciting the same QDs and recording the fluorescence intensity as a function of time. The intensity trace of QDs on glass stays on the constant level in the first 500 s, and then start to decrease afterwards and finally reaches equilibrium at 1900 s. The decrease of the intensity is due to the increased number of charged QDs under continuous photo excitation. The comparison of the fluorescence decays at time 0 and 1900 s are shown in Figure 5.6 B. A faster component is observed in the decay at later time, suggesting the presence of charged QDs whose lifetimes become shorter. For QDs on TiO_2, their fluorescence intensity decreases much faster than that on glass, indicating that the ET from QDs to TiO_2 accelerates the charging effect of the QDs by generating positively charged QDs through ET.

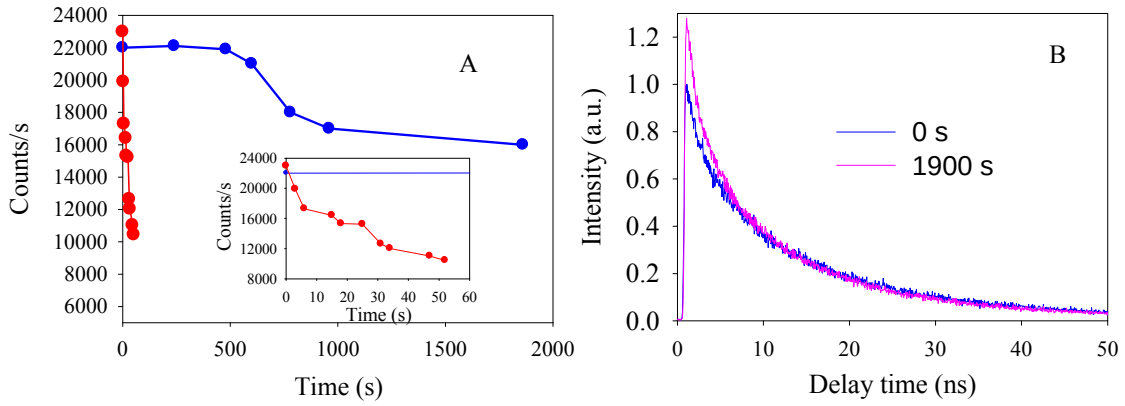

Figure 5.6. (A) Fluorescence intensity as a function of detection time of an ensemble of QDs on glass (blue) and TiO_2 (red). The inset shows the expanded view of the fluorescence intensity traces. The fluorescence decays of QDs on glass at t=0 and 1900 s

are shown in panel B. The laser power (~ 200 nw) is the same as in single QDs measurements.

The ensemble-averaged fluorescence decays of QDs on glass and TiO_2 nanoparticle thin films are shown in Figure 5.2 A. These samples are studied using the same set-up and under the same excitation power density as single QD studies. To avoid photoinduced charging of QDs, these samples are prepared by using a starting QD solution of ~1 μM, which is ~$1x10^5$ times higher than that in single QD measurement. Furthermore, they are raster scanned at a speed of ~100 nm/s to avoid repetitive illumination of the same QDs. The fluorescence intensity is nearly constant throughout the examined sample region of ~10 μm^2. The emission intensity on TiO_2 is roughly 240 times higher than the average on state emission intensity of single QDs on TiO_2, suggesting that there are ~240 QDs within the laser focus. The corresponding particle density of 4800 QDs/μm^2 is ~$2.5x10^5$ times higher than the single particle sample and is consistent with the difference in the starting concentrations of QDs used in preparing these samples. Analysis of QDs on glass revealed that the emission intensity of the high concentration sample is ~280 higher than the single QD on-state, suggesting a number density similar to those on TiO_2.

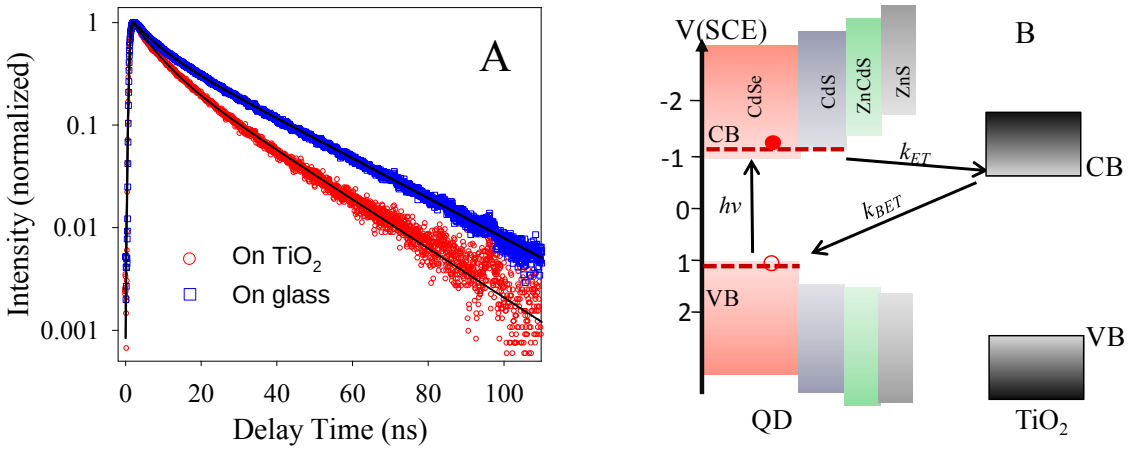

Figure 5.7. (A) Ensemble-averaged fluorescence decays of QDs on glass and TiO_2 nanoparticle thin film. Solid lines are the best bi-exponential fits. (B) The schematic diagram for the relevant energetics of ET between QD and TiO_2 nanoparticle.

As shown in Figure 5.7, the QDs on TiO_2 have faster ensemble-averaged fluorescence decay than on glass, confirming the quenching of QD excitons by ET from QDs to TiO_2. These decay curves can be well fit by bi-exponential functions:

$$S(t) = A_1 e^{-\tau_1} + A_2 e^{-\tau_2} \qquad \text{(Eq. 5.3)}$$

$$\tau_{ave.} = \frac{A_1\tau_1 + A_2\tau_2}{A_1 + A_2} \qquad \text{(Eq. 5.4)}$$

The fitting parameters are listed in Table 5.2. The amplitude weighted average lifetimes are 16.5 ns on glass and 10.7 ns on TiO_2 according to Eq. 5.4. Assuming that the difference in fluorescence decay rates can be attributed to ET from QD to TiO_2, an average ET rate can be estimated to be 3.2×10^7 s^{-1}. ET rate from CdSe core (capped by mercaptopropionic acid) on TiO_2 nanoparticles was reported to be 6.3×10^7 and 6.7×10^8 s^{-1} for QDs with first exciton peak at 605 nm and 570nm, respectively.[18] The observed

slower ET rate from our CdSe/ZnS QD (first exciton peak at 585 nm) may be attributed to the presence of the multi-shells and different surface ligands.

Table 5.2. Fitting parameters of ensemble-averaged fluorescence decays of QDs on glass and TiO2 according to Eq. 5.3. The amplitude weighted lifetime is calculated based on Eq. (5.4). The errors indicate one standard deviation.

	A_1	τ_1 (ns)	A_2	τ_2 (ns)	$\tau_{ave.}$ (ns)
on glass	0.37±0.004	6.4±0.07	0.63±0.004	22.4±0.08	16.5±0.1
on TiO_2	0.56 ±0.007	5.0±0.07	0.44±0.007	18.0±0.17	10.7±0.2

The previous studies on the interfacial ET from single QDs suggested an intermittent ET dynamics to explain the observed fluctuation of fluorescence intensity and lifetime.[52,55] There are two possible origins of the intermittent ET dynamics. In the first case, the fluctuating lifetime may be caused by a corresponding fluctuation of ET rates. As a result, states with short and long lifetimes have fast and slow ET rates, respectively.[52,55] In the second scenario, as we have discussed in Chapter 4 on the studies of QD-F27 complexes, the lifetime of the off states is dominated by the Auger relaxation process in charged QDs, similar to single QDs on glass. In these off states, exciton quenching by ET is not competitive with Auger relaxation and QDs become ET inactive. We then discuss the results in two cases:

1) The off states of QDs on TiO_2 are caused by fast ET rates. The fluctuation of lifetimes of the QDs suggests the fluctuation of ET rates from < 500 ps to tens of ns time scale. The lifetime distributions in Figure 5.5 indicates that QDs on TiO_2 spend most of

their times on the fast ET state. However, the ensemble-averaged fluorescence decay data shown in Figure 5.7 suggest that ET time is on the 10s of ns time scale in this system, much slower than the sub-nanosecond lifetime of the off states for QDs on glass and TiO_2. The discrepancy between the ensemble and single QDs measurements are not able to be explained in this case.

2) The ET rate is slow and the off states of QDs are controlled by the Auger process, and the fluctuations of QD lifetime and intensity are controlled by the QD blinking dynamics. In this case, the ET in the off state can not compete with the fast Auger relaxation process. In the on state, ET from QDs to TiO_2 shortens lifetimes. The blinking of QDs leads to intermittent ET activities. To support this assignment, the sum of single QDs fluorescence decays is compared with the ensemble-averaged fluorescence decay for QDs on TiO_2. As having mentioned above, the photoinduced charging effect has been minimized in the ensemble-averaged measurements by rapidly scanning the sample. If the short lifetime peak (off state) in the lifetime distribution of single QDs on TiO_2 can be attributed to Auger relaxation in charged QDs, it should not be present in ensemble-averaged measurements under conditions of negligible particle charging. As shown in Figure 5.8 A, a comparison of the ensemble-averaged fluorescence decay with the sum of single QD decays reveals that they differ at the early delay time (<3ns) but agree at later decay times. The sum of single QDs decays can be considered as the ensemble-averaged decay of the same bunch of QDs under continuous excitation. The difference shown Figure in 5.8 A is similar with that in Figure 5.6 B, where the fast component is due to the presence of charged QDs. Therefore, the faster component in the sum of single QD decays is attributed to the charged states (off states) of QDs on TiO_2. Furthermore, we

constructed a fluorescence decay curve using only on states in the lifetime histograms of single QDs. As shown in Figure 5.8 A, this average single QD on state decay curve is in good agreement with the ensemble-averaged fluorescence decay. A similar comparison for QD on glass, shown in Figure 5.8 B, also reveals the difference of ensemble-averaged and the sum of single QD decays at early delay time and the agreement at later delay time. The difference in this case is much smaller, which is consistent with the relatively smaller off state amplitude in the lifetime histogram for single QDs on glass, as shown in Figure 5.5. Again the ensemble-averaged decay can be reasonably reproduced by the sum of single QD on state decays.

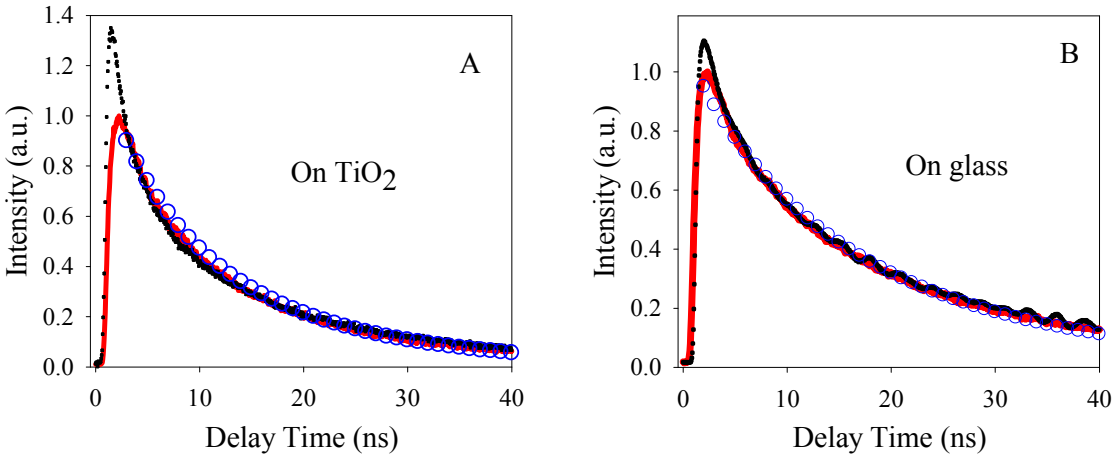

Figure 5.8. Comparison of ensemble averaged fluorescence decay (red solid line) with the sum of single QD decays (black dotted line) and the sum of single QD on state decays (blue open circles) for QDs on a TiO_2 nanoparticle thin film (A) and glass cover slip (B).

5.1.2.3 ET Rate Distribution on TiO_2

The comparison between ensemble and single QD measurements indicated that the QDs on TiO_2 flow the same ET model as in the QD-F27 complexes. The on state

lifetimes of QDs on TiO_2 are measuring the ET rates. We then plot the on state rate (1/lifetime) distributions of QDs on glass and TiO_2, as shown in Figure 5.9 A and B. The rate distribution of QDs on glass is defined as $I(k_0)$, where k_0 is the intrinsic decay constant of QDs and equals to the sum of radiative decay constant (k_r) and nonradiative decay constant (k_{nr}). The distribution indicates the variation of k_0 between different QDs at different times. The rates distribution of QDs on TiO_2 is define as $H(k)$, which is dependent on both the distributions of the interfacial ET rates ($F(k_{ET})$) and the intrinsic decay rates of QDs ($I(k_0)$):

$$H(k) = \int_0^\infty I(k')F(k_{ET} - k')dk' \qquad \text{(Eq. 5.5)}$$

Thus the ET rate distribution $F(k_{ET})$ can be obtained from the measured $H(k)$ and $I(k_0)$ according to Eq. 5.5. The ET rate distribution of QDs on TiO_2 is shown in Figure 5.9 C and D. The wide distribution of ET rates contains contributions from both static and dynamic heterogeneities of the ET process. The average ET rate is calculated to be 3.9×10^7 s^{-1}, similar with that from ensemble-averaged measurements.

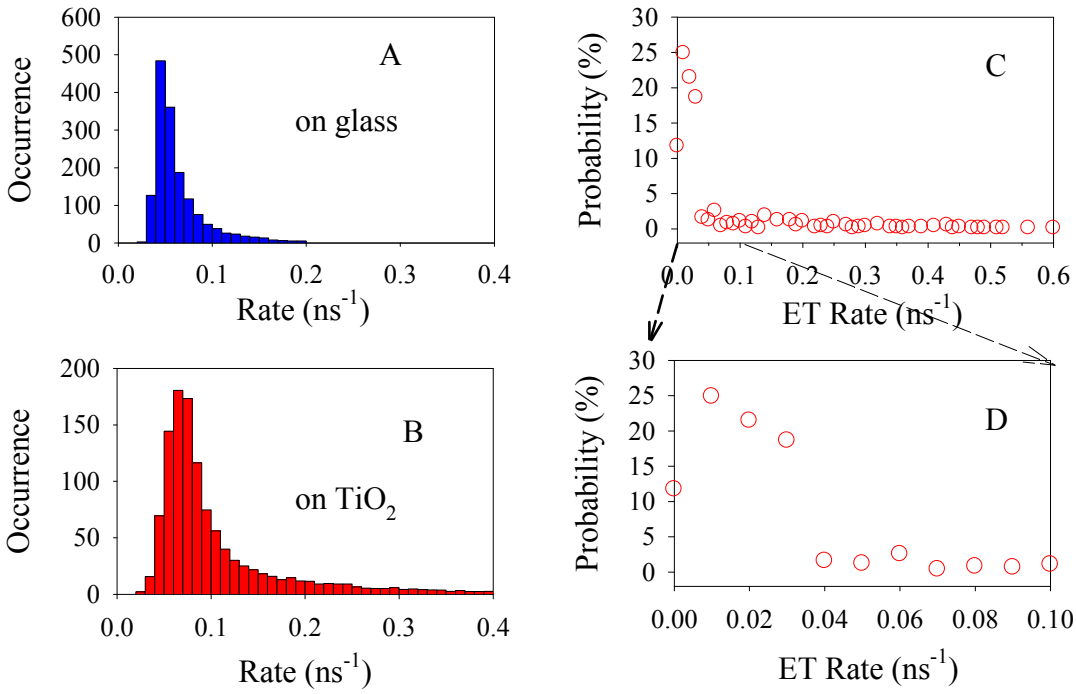

Figure 5.9. On state fluorescence decay rate (1/lifetime) histograms of single QDs on glass (A) and TiO_2 (B). (C) ET rate distributions of single QDs on TiO2 obtained according to Eq. 5.5. Its expanded view is shown in panel D.

5.1.2.4 Single QDs ET Model on TiO_2

The interfacial ET dynamics from single CdSe core multi-shell QDs to TiO_2 nanoparticles is then summarized in this section. As shown in Figure 5.10, the QDs on TiO_2 nanoparticles also exhibit intermittent ET dynamics that controlled by the blinking of QDs. The lifetimes of the off states of QDs on TiO_2 are controlled by the fast Auger relaxation in positive charged QDs. The QDs at on states are likely undergoing reaction circles of interfacial ET followed by fast BET. The on state lifetimes are measuring the ET dynamics.

The ET activity of QDs on TiO_2 also affects its blinking dynamics. ET from QDs to TiO_2 provides additional pathway to generate positively charged QDs, and hence shortens the on event in the blinking activity. The lifetime of charged QDs generated by ET is determined by the charge recombination process of the electrons in TiO_2 particles and holes in QDs. Previous studies have shown that charge recombination from TiO_2 nanoparticles to molecular sensitizers exhibited stretched exponential kinetics,[60] due to a distribution of trap state energies for electrons in TiO_2.[61,62] Furthermore, a non-single exponential charge recombination process which is not completed by 10 μs has been directly observed by transient absorption measurement in the studies of QD-F27 ET system. Therefore, it is likely that the back ET kinetics from TiO_2 nanoparticles to QDs is also highly non-exponential, increasing the probability densities of off states on the 10 ms to 100 s timescale, as shown in Figure 5.4.

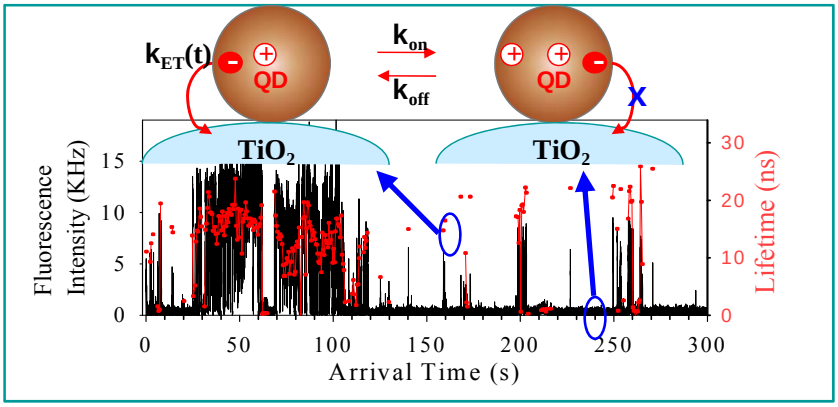

Figure 5.10. The interfacial ET model from single QDs to TiO_2 nanoparticles.

5.1.3 Summary

In summary, the interfacial ET dynamics from single CdSe core multi-shell ($CdS_{2ML}ZnCdS_{1ML}ZnS_{1ML}$) QDs to TiO_2 nanoparticles have been studied on both single

particle and ensemble levels by time-resolved fluorescence spectroscopy. The single QDs on TiO_2 have shown intermittent ET dynamics modulated by the blinking of QDs. Comparisons of sum of single QD decays with ensemble-averaged fluorescence decays suggested that the lifetime of the off state was controlled by Auger relaxation, and the shortened lifetime of the on state could be attributed to ET to TiO_2 nanoparticles. Compared to QDs on glass, the presence the ET on TiO_2 led to shorter fluorescence lifetimes, and offered an additional pathway to generate charged QDs, resulting in smaller long on event and larger long off event probability densities in the blinking dynamics. The QDs on TiO_2 exhibited a broad distribution of ET rates, indicating the static and dynamics heterogeneities of the ET process. The average ET rate from single QDs to TiO_2 was estimated to be 3.9×10^7 s^{-1}, which is consistent with that from ensemble-averaged measurements.

5.2 Electron Transfer Dynamics of Single Quantum Dots on The (110 and 001) Surfaces of Rutile TiO_2 Single Crystals

5.2.1 Introduction

Understanding interfacial electron transfer (ET) dynamics to and from quantum dots (QDs) to semiconductor nanomaterials is essential for the improvement of QD-based solar cells.[20,63] Previous studies of interfacial ET from dye molecules and QDs to semiconductor nanoparticles such as TiO_2 have revealed highly heterogeneous ET dynamics on both the ensemble average[20,64] and single molecule (particle) levels.[65-67] For QDs on oxide nanoparticles, the heterogeneity can be caused by distributions of a number

of properties of the oxide (exposed surfaces, defects, adsorption sites) and QDs (size, shape, and charge) as well as their interactions. These complexities hinder a detailed understanding of the important factors that control the ET rate. It is therefore desirable to investigate these IET processes in well characterized model systems.

The TiO_2 surface has received considerable attention for many years due to its role in many applications ranging from solar cell devices[2,24] and sensors,[68,69] to photocatalysis for water splitting[70] and waste water treatment.[71] Studies on the surface of TiO_2 have shown rutile single crystals to be more attractive because of their stable and well-characterized surface structure. TiO_2 rutile single crystals have different types of surfaces according to the cutting directions. Previous studies have revealed different catalytic abilities for different surfaces.[72,73] It is therefore interesting to know whether these different surfaces may have different effects on the ET dynamics. Studies addressing this question can provide essential information necessary for a detailed understanding of the important factors that control the interfacial ET rate. Unfortunately, ET dynamics on rutile single crystals cannot be studied by ensemble-averaged transient absorption measurements.

In this section, we will discuss the preliminary results of our investigation of the ET from single QDs on the (110) and (001) surfaces of rutile TiO_2 single crystals as model systems for TiO_2 nanoparticles. We show that the average lifetimes of QDs on single crystals are shortened compared to those on glass due to ET. The QDs on the (110) and (001) surfaces have different ET rates. The distribution of lifetimes on the (110) single crystal is much narrower than that on TiO_2 nanoparticles, suggesting that the distribution of ET rates in the latter system is dominated by site heterogeneities of TiO_2 nanoparticles.

5.2.2 Results and Discussion

QDs used in this study are the same as those in the study of QD-TiO_2 nanoparticle system. A rutile TiO_2 single crystal cut in the (110) direction (10×10 mm in area and 1.0 mm thick) was purchased from MTI Corporation. Prior to preparing samples for IET studies, the single-crystal was first cleaned by Nochromix sulfuric acid solution, washed by water (Millipore, 18.2 MΩ·cm), and then illuminated by UV light for ~1 hour.[74]

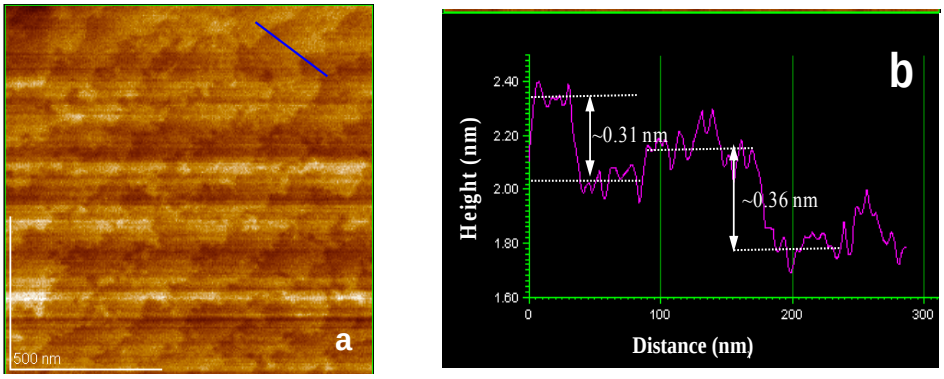

Figure 5.11. (a)Non-contact AMF image for (110)-cut surface of TiO_2 (rutile) single crystal. (b) The height trajectory as a function of distance along the blue line in panel a.

The adsorption of QDs on TiO_2 single crystal was studied by atomic force microscope (AFM). The non-contact AFM image of the TiO_2 (110) surface in Figure 5.12 a shows clear step edges with step heights of ~0.3-0.4 nm (Figure 5.12 b), consistent with previous reports.[75,76] To load the QDs, an aqueous QD solution of ~1 nM was spin coated onto the TiO_2 single crystal surface. The sample was then rinsed with water and dried in nitrogen. Figure 5.12 a shows typical AFM images of QDs on the TiO_2 (110) surface. In addition to step edges similar to those seen for bare surfaces, it shows well dispersed bright spots that are believed to be the single QDs. The heights of scans along the blue and red lines in Figure 5.12 a are potted in Figure 5.12 b, indicating the presence of a QD and step edge, respectively. The histogram of QD heights (Figure 5.12 c) shows

an average value of 5.0 ± 0.6 nm, consistent with consistent with the average diameter (5.7± 0.7 nm) determined by transmission electron microscopy (See Figure 2.8). The average width of bright spots is 60 ± 12 nm, which is limited by the lateral resolution of the AFM tip. Previous studies show that molecular adsorbates with carboxylic acid anchoring groups bind to surface Ti sites. [77,78] It is likely that these QDs are also bound to the TiO2 (110) surface Ti sites through their surface carboxylic groups.

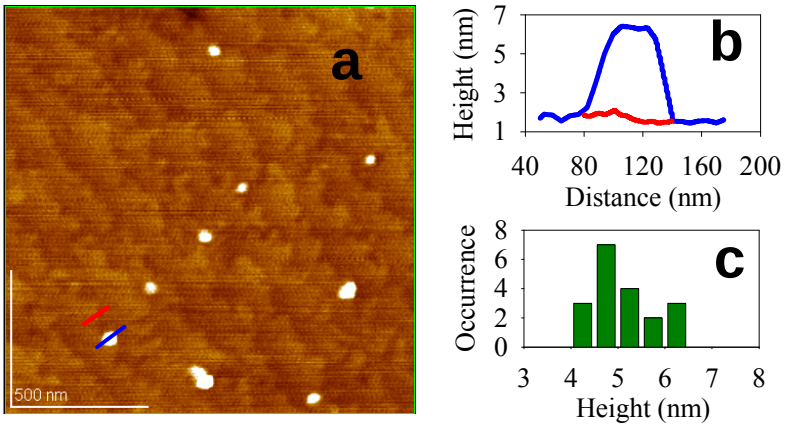

Figure 5.12. (a) AFM image of QDs on the (110) surface of a rutile TiO_2 single crystal. (b) Height vs position along the blue (blue) and red (red) lines in panel a. (c) Histogram of QD heights in panel a.

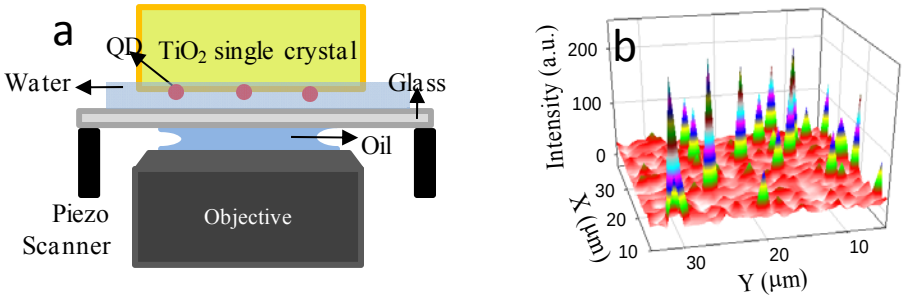

Figure 5.13. (a) Setup for the fluorescence detection of single QDs adsorbed on the surface of TiO_2 single crystals. (b) Fluorescence image of single QDs on the (110) surface of a rutile TiO_2 single crystal.

For fluorescence measurements, aqueous QD solutions of ~10 pM for single QD and ~1 μM for ensemble-averaged detections were spin coated on the surfaces of the substrates. The samples were then washed by water to remove weakly absorbed QDs. Because the thickness of the single crystal (1 mm) is larger than the working distance of the objective, the single crystal was put on top of a cover slip with the QD-coated surface facing the cover slip, as shown in Figure 5.13 a. For comparison, single QDs on glass and TiO_2 nanoparticle thin films were also studied in the same manner. The QDs were excited at 500 nm (~150 nW) and emissions between 540 - 675 nm were detected. Figure 5.13 b shows a raster scan fluorescence image of single QDs on the rutile (110) TiO_2 single crystal surface. The ensemble-averaged fluorescence decays on QDs on glass, 110 and 001 rutile single crystals are shown in Figure 5.14. The QDs on TiO_2 single crystals decays faster than those on glass, suggesting the quenching of QD excitons by ET. Furthermore, the fluorescence decay on 001 is faster than that on 110, indicating a faster ET rate for QDs on 001 single crystal.

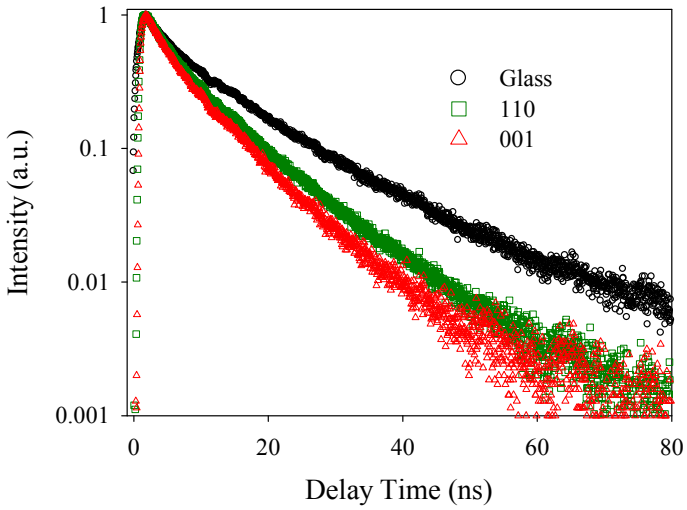

Figure 5.14. Ensemble-averaged fluorescence decays of QDs on glass (black circles), TiO_2 single crystal 110 (green squares) and 001 (red triangles).

52, 56, 60 and 15 single QDs on glass cover slip, TiO_2 nanoparticles, rutile 110 and rutile 001 TiO_2 single crystals were studied, respectively. Figures 5.15 a, b, c and d show typical fluorescence intensity and lifetime trajectories of single QDs each substrate. The corresponding lifetime histograms of these single QDs are shown in Figures 5.15 e, f, g and h, respectively. The lifetime trajectories were constructed from lifetimes calculated using photons within 1 s bin time and 1 s step size. These single QDs show correlated fluctuations in fluorescence intensity and lifetime, indicating a variation of nonradiative decay rates. This phenomenon has been extensively studied for QDs on glass and the low intensity states have been attributed to photoinduced charging of QDs, which increases the rate of Auger recombination.[28,29,79]

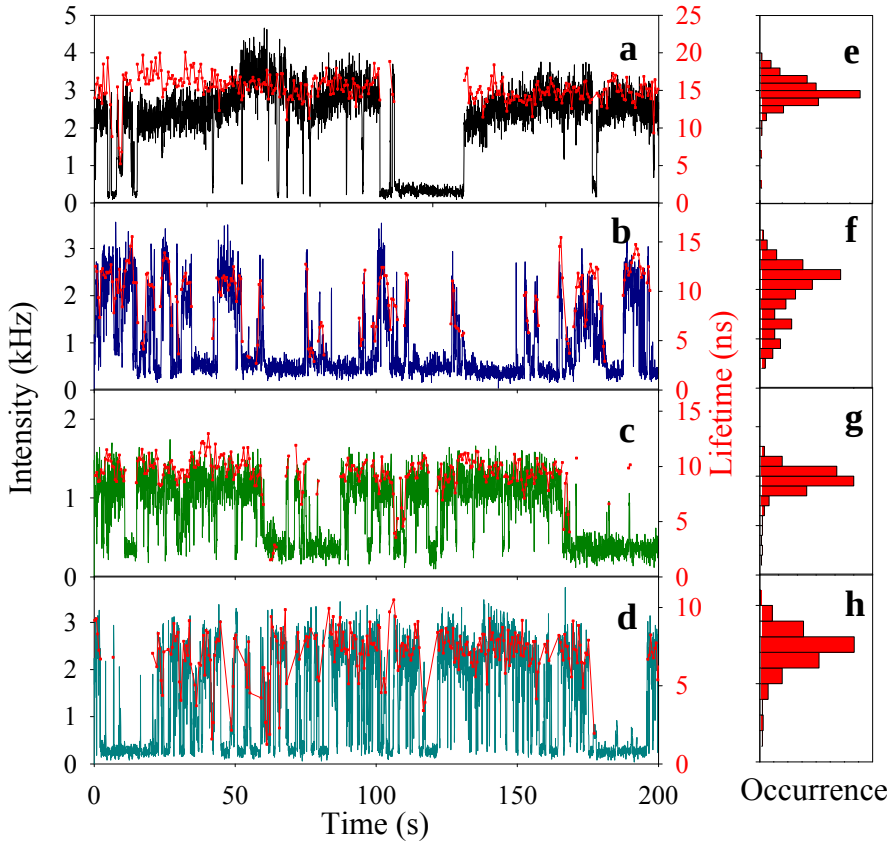

Figure 5.15. Typical fluorescence intensity (black, blue and green) and lifetime (red) trajectories are shown for single QD on (a) glass, (b) TiO_2 nanoparticles and (c) the (110) and (d) (001) rutile TiO_2 single crystals. The corresponding lifetime histograms of these single QDs are shown in (e), (f), (g) and (h), respectively. Lifetimes at background levels were not determined due to the limited number of photons.

The total rate (1/lifetime) histograms of single QDs on glass, TiO_2 nanoparticles, and rutile 110 and 001 TiO_2 single crystals are compared in Figures 5.15 a, b, c and d, respectively. They are the sum of rate histograms of single QDs and represent the ensemble rate distributions on these substrates. It should be noted that the QDs in this study are immersed in water and their rates are bigger than those exposed to air.[20,65] The distribution peaks of QDs on TiO_2 nanoparticles and single crystals are center at bigger rate positions than on glass. This can be attributed to the presence of interfacial ET from QDs to TiO_2.[20,65] The rate histogram of QDs on rutile 001 is distributed at bigger positions than on rutile 110. This trend is consistent with the ensemble-averaged fluorescence decays shown in Figure 5.14, suggesting faster ET rates of single QDs on rutile 001.

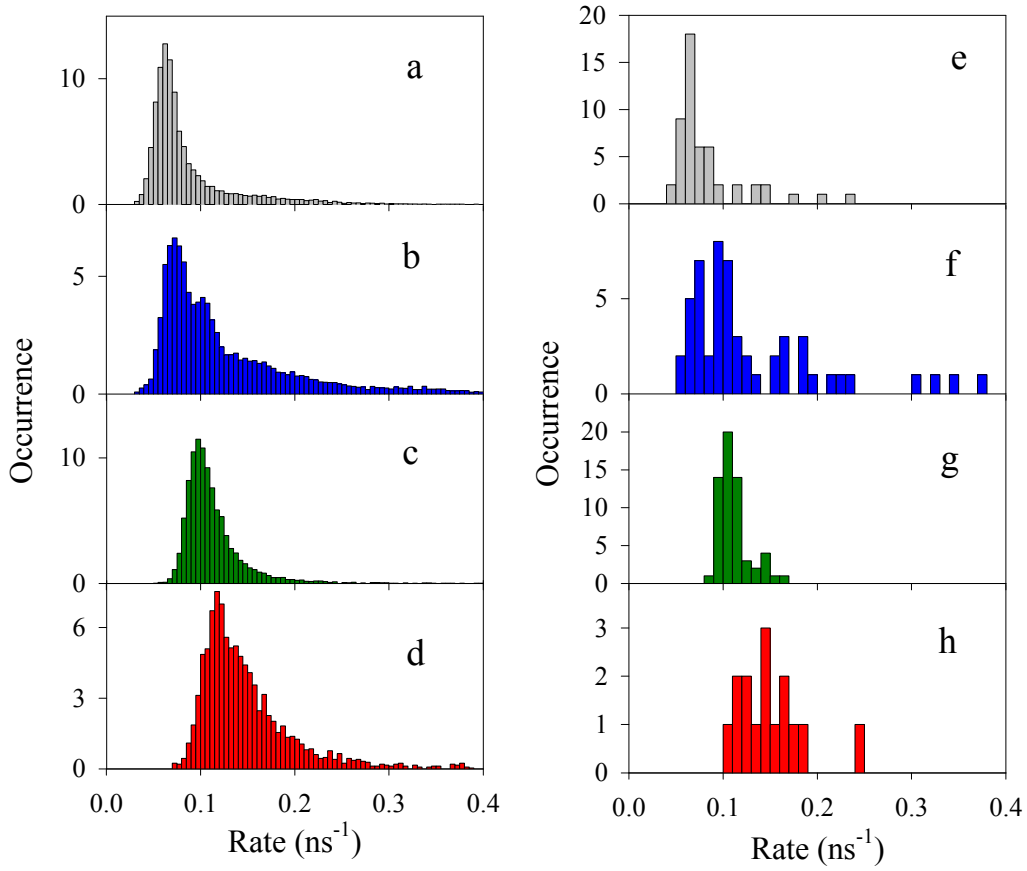

Figure 5.16. Total rate (left panels) and average rate (right panels) of single QDs on glass (a and e), TiO_2 nanoparticles (b and f) and rutile 110 (c and g) and 001 (d and h) of TiO_2 single crystals.

The total decay rate of QDs on glass is $k_0=k_r+k_{nr}$, where k_0, k_r and k_{nr} are the total, radiative and nonradiative decays rates, respectively. The observed distribution of fluorescence decay rates for QDs on glass, defined as $h(k_0)$, indicate a variation of k_0 among QDs. [28,29,79] For QDs on TiO_2, the decay rate is given by $k=k_0+k_{ET}$, where k_{ET} is the interfacial ET rate. Assuming the same distribution of k_0 on the TiO_2 nanoparticles, single crystal and glass, the observed distribution of decay rates on TiO_2, defined as $g(k)$, is:

$$g(k) = \int_0^\infty h(k')f(k_{ET} - k')dk' \qquad \text{(Eq. 5.6)}$$

where $f(k_{ET})$ is the ET rate distribution. Based on Eq. 5.6, we obtained the distributions of ET rates on these substrates, as shown in Figure 5.16.

The comparison of the ET distributions on different substrates shows following differences:

(1) These distributions indicated a substrate dependent ET dynamics on TiO_2. The ET rates of the QDs become bigger in the sequence of TiO_2 nanopartilce, rutile 110 and rutile 001. It is interesting to find that the ET rates are faster on rutile 001 than that on rutile 110.

(2) The width of the rate distributions on the rutile 110 single crystal is much narrower than that on TiO_2 nanoparticles. The broader ET rate distribution on the TiO_2 nanoparticles can be caused by both larger site and dynamic heterogeneities. The site heterogeneity is a measure of how the ET rate of single QDs varies in different sites and the dynamic heterogeneity reflects how the decay rate changes with time on these sites. To represent the site heterogeneity, we have calculated the average decay rate (averaged over the duration of the trajectory) for each QD. As shown in Figure 5.15 e-h, the distribution of the average decay rates on the TiO_2 nanoparticles is much broader than that on the rutile 110 single crystal, similar to the trend of the total decay rate histograms. It suggests that the larger heterogeneity on the TiO_2 nanoparticles is mainly caused by their site heterogeneity. At different adsorption sites, both the ET driving force and electronic coupling strength may vary, leading to a distribution of ET rates.

However, the ET rate distribution of QDs on rutile 001 is not as narrow as that on rutile 110. The QDs on rutile 001 tend to have a broader and bigger ET rate distribution

than on rutile 110. These differences are probably due to the different surface structures of these two types of single crystals. Further experiments are required to confirm these observations.

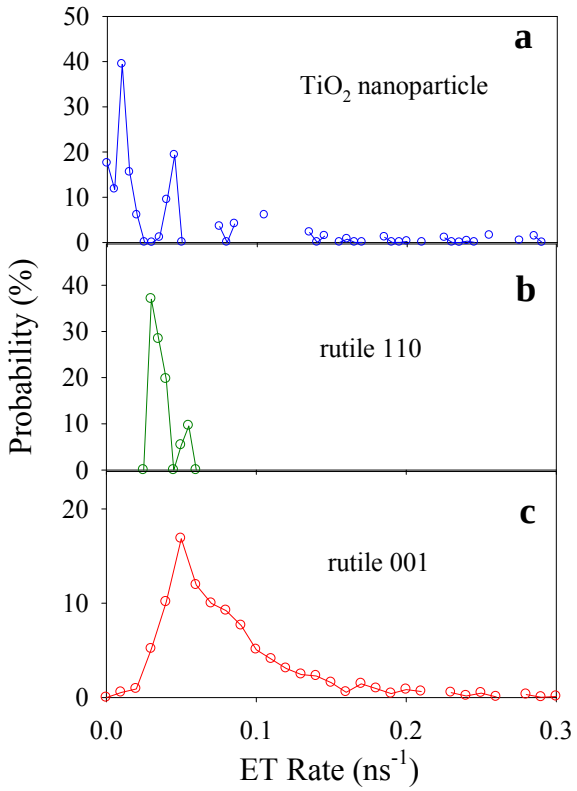

Figure 5.17. ET rate distributions of single QDs on TiO2 nanoparticles (a) and rutile 110 (b) and 001 (c) TiO_2 single crystals obtained according to Eq. 5.6.

5.2.3 Summary and Future Work

In summary, we have demonstrated for the first time the study of ET from single QDs to TiO_2 single crystals. Both ensemble-averaged and single QD measurements indicated faster ET rates on rutile 001 than on rutile 110. Compared to QDs on TiO_2 nanoparticles, QDs on the surface of rutile 110 TiO_2 single crystal have considerably narrower ET distribution, suggesting a less heterogeneous distribution of ET rates on the single crystal

surface. The different ET properties of QDs on rutile 110 and 001 are probably due to the difference in the surface structures of these two types of single crystals. However, further experiments are required to confirm the observations discussed above:

(1) Single QDs studies on different substrates will be repeated to confirm observed ET rates distributions.

(2) Ensemble-averaged fluorescence decays of QDs on different substrates will be repeated and compared with the results of single QD studies.

(3) Beside the studied substrates, ET dynamics on rutile 100 TiO_2 single crystal will also be studied.

References:

(1) Hodes, G. *J. Phys. Chem. C* 2008, *112*, 17778.

(2) Kamat, P. *J. Phys. Chem. C* 2008, *112*, 18737.

(3) Shalom, M.; Dor, S.; Ruhle, S.; Grinis, L.; Zaban, A. *J. Phys. Chem. C* 2009, *113*, 3895.

(4) de Mello Donega, C.; Hickey, S. G.; Wuister, S. F.; Vanmaekelbergh, D.; Meijerink, A. *J. Phys. Chem. B* 2003, *107*, 489.

(5) Niitsoo, O.; Sarkar, S. K.; Pejoux, C.; Ruhle, S.; Cahen, D.; Hodes, G. *J. Photochem. Photobiol. A* 2006, *181*, 306.

(6) Hodes, G. *Isr. J. Chem.* 1993, *33*, 95.

(7) Sasha, G.; Gary, H. *J. Phys. Chem. A* 1994, *98*, 5338.

(8) Nozik, A. J. *Physica E: Low-Dimensional Systems & Nanostructures (Amsterdam, Netherlands)* 2002, *14*, 115.

(9) Wang, Z. L. *J. Phys. Chem. A* 2000, *104*, 1153.

(10) Schaller, R. D.; Klimov, V. I. *Phys. Rev. Lett.* 2004, *92*, 186601.

(11) Ellingson, R. J.; Beard, M. C.; Johnson, J. C.; Yu, P.; Micic, O. I.; Nozik, A. J.; Shabaev, A.; Efros, A. L. *Nano Letters* 2005, *5*, 865.

(12) Luther, J. M.; Beard, M. C.; Song, Q.; Law, M.; Ellingson, R. J.; Nozik, A. J. *Nano Letters* 2007, *7*, 1779.

(13) Schaller, R. D.; Sykora, M.; Pietryga, J. M.; Klimov, V. I. *Nano Letters* 2006, *6*, 424.

(14) Trinh, M. T.; Houtepen, A. J.; Schins, J. M.; Hanrath, T.; Piris, J.; Knulst, W.; Goossens, A. P. L. M.; Siebbeles, L. D. A. *Nano Letters* 2008, *8*, 1713.

(15) Klimov, V. I. *Annual Review of Physical Chemistry* 2007, *58*, 635.

(16) Murphy, J. E.; Beard, M. C.; Norman, A. G.; Ahrenkiel, S. P.; Johnson, J. C.; Yu, P.; Micic, O. I.; Ellingson, R. J.; Nozik, A. J. *Journal of the American Chemical Society* 2006, *128*, 3241.

(17) Tachibana, Y.; Akiyama, H. Y.; Ohtsuka, Y.; Torimoto, T.; Kuwabata, S. *Chemistry Letters* 2007, *36*, 88.

(18) Kongkanand, A.; Tvrdy, K.; Takechi, K.; Kuno, M.; Kamat, P. V. *Journal of the American Chemical Society* 2008, *130*, 4007.

(19) Brown, P.; Kamat, P. V. *Journal of the American Chemical Society* 2008, *130*, 8890.

(20) Robel, I.; Subramanian, V.; Kuno, M.; Kamat, P. V. *J. Am. Chem. Soc.* 2006, *128*, 2385.

(21) Farrow, B.; Kamat, P. V. *Journal of the American Chemical Society* 2009, *131*, 11124.

(22) Cahen, D.; Hodes, G.; Graetzel, M.; Guillemoles, J. F.; Riess, I. *J. Phys. Chem.* 2000, *104*, 2053.

(23) Graetzel, M. *Nature* 2001, *414*, 338.

(24) Graetzel, M. *Nature (London, United Kingdom)* 2003, *421*, 586.

(25) Huang, J.; Stockwell, D.; Huang, Z.; Mohler, D. L.; Lian, T. *J. Am. Chem. Soc.* 2008, *130*, 5632.

(26) Chakrapani, V.; Tvrdy, K.; Kamat, P. V. *Journal of the American Chemical Society* 2010, *132*, 1228.

(27) Shimizu, K. T.; Neuhauser, R. G.; Leatherdale, C. A.; Empedocles, S. A.; Woo, W. K.; Bawendi, M. G. *Physical Review B: Condensed Matter and Materials Physics* 2001, *63*, 205316/1.

(28) Krauss, T. D.; O'Brien, S.; Brus, L. E. *Journal of Physical Chemistry B* 2001, *105*, 1725.

(29) Nirmal, M.; Dabbousi, B. O.; Bawendi, M. G.; Macklin, J. J.; Trautman, J. K.; Harris, T. D.; Brus, L. E. *Nature* 1996, *383*, 802.

(30) Empedocles, S.; Bawendi, M. *Acc. Chem. Res.* 1999, *32*, 389.

(31) Shimizu, K. T.; Woo, W. K.; Fisher, B. R.; Eisler, H. J.; Bawendi, M. G. *Physical Review Letters* 2002, *89*, 117401/1.

(32) Fisher, B. R.; Eisler, H.-J.; Stott, N. E.; Bawendi, M. G. *J. Phys. Chem. B* 2004, *108*, 143.

(33) Chung, I.; Bawendi, M. G. *Phys. Rev. B:* 2004, *70*, 165304/1.

(34) Kuno, M.; Fromm, D. P.; Johnson, S. T.; Gallagher, A.; Nesbitt, D. J. *Phys. Rev. B:* 2003, *67*, 125304/1.

(35) Kuno, M.; Fromm, D. P.; Hamann, H. F.; Gallagher, A.; Nesbitt, D. J. *J. Chem. Phys.* 2001, *115*, 1028.

(36) Kuno, M.; Fromm, D. P.; Gallagher, A.; Nesbitt, D. J.; Micic, O. I.; Nozik, A. J. *Nano Letters* 2001, *1*, 557.

(37) Zhang, K.; Chang, H.; Fu, A.; Alivisatos, A. P.; Yang, H. *Nano Letters* 2006, *6*, 843.

(38) Pelton, M.; Smith, G.; Scherer, N. F.; Marcus, R. A. *Proc. Natl. Acad. Sci. U. S. A.* 2007, *104*, 14249.

(39) Tang, J.; Marcus, R. A. *J. Chem. Phys.* 2006, *125*, 044703/1.

(40) Tang, J.; Marcus, R. A. *J. Chem. Phys.* 2005, *123*, 054704/1.

(41) Tang, J.; Marcus, R. A. *Phys. Rev. Lett.* 2005, *95*, 107401/1.

(42) Tang, J.; Marcus, R. A. *J. Chem. Phys.* 2005, *123*, 204511/1.

(43) Issac, A.; von Borczyskowski, C.; Cichos, F. *Phys.l Rev. B* 2005, *71*, 161302/1.

(44) Schlegel, G.; Bohnenberger, J.; Potapova, I.; Mews, A. *Phys. Rev. Lett.*. 2002, *88*, 137401.

(45) Verberk, R.; van Oijen, A. M.; Orrit, M. *Physical Review B: Condensed Matter and Materials Physics* 2002, *66*, 233202/1.

(46) Chen, Y.; Vela, J.; Htoon, H.; Casson, J. L.; Werder, D. J.; Bussian, D. A.; Klimov, V. I.; Hollingsworth, J. A. *J. Am. Chem. Soc.* 2008, *130*, 5026.

(47) Fomenko, V.; Nesbitt, D. J. *Nano Lett.* 2008, *8*, 287.

(48) Mahler, B.; Spinicelli, P.; Buil, S.; Quelin, X.; Hermier, J.-P.; Dubertret, B. *Nature Materials* 2008, *7*, 659.

(49) Peterson, J. J.; Nesbitt, D. J. *Nano Lett.* 2009, *9*, 338.

(50) Hohng, S.; Ha, T. *Journal of the American Chemical Society* 2004, *126*, 1324.

(51) Kuno, M.; Fromm, D. P.; Hamann, H. F.; Gallagher, A.; Nesbitt, D. J. *J. Chem. Phys.* 2000, *112*, 3117.

(52) Cui, S.-C.; Tachikawa, T.; Fujitsuka, M.; Majima, T. *J. Phys. Chem. C* 2008, *112*, 19625.

(53) Wang, S.; Querner, C.; Emmons, T.; Drndic, M.; Crouch, C. H. *J. Phys. Chem. B* 2006, *110*, 23221.

(54) Mandal, A.; Nakayama, J.; Tamai, N.; Biju, V.; Isikawa, M. *J. Phys. Chem. B* 2007, *111*, 12765.

(55) Issac, A.; Jin, S.; Lian, T. *J. Am. Chem. Soc.* 2008, *130*, 11280.

(56) Brus, L. *J. Chem. Phys.* 1983, *79*, 5566.

(57) Brus, L. E. *J. Chem. Phys.* 1984, *80*, 4403.

(58) Hagfeldt, A.; Gratzel, M. *Chem. Rev.* 1995, *95*, 49.

(59) Robel, I.; Kuno, M.; Kamat, P. V. *J. Am. Chem. Soc.* 2007, *129*, 4136.

(60) Haque, S. A.; Tachibana, Y.; Klug, D. R.; Durrant, J. R. *J. Phys. Chem. B* 1998, *102*, 1745.

(61) Nelson, J. *Phys. Rev. B* 1999, *59*, 15374.

(62) Barzykin, A. V.; Tachiya, M. *J. Phys. Chem. B* 2002, *106*, 4356.

(63) Huynh, W. U.; Dittmer, J. J.; Alivisatos, A. P. *Science* 2002, *295*, 2425.

(64) Anderson, N. A.; Lian, T. *Annual Review of Physical Chemistry* 2005, *56*, 491.

(65) Jin, S.; Lian, T. *Nano Letters* 2009, *9*, 2448.

(66) Lu, H. P.; Xie, X. S. *Journal of Physical Chemistry B* 1997, *101*, 2753.

(67) Biju, V.; Micic, M.; Hu, D.; Lu, H. P. *Journal of the American Chemical Society* 2004, *126*, 9374.

(68) Zakrzewska, K.; Radecka, M. *Thin Solid Films* 2007, *515*, 8332.

(69) Zhou, H.; Gan, X.; Wang, J.; Zhu, X. L.; Li, G. X. *Anal. Chem.* 2005, *77*, 6102.

(70) Shahed U. M. Khan; Al-Shahry, M.; Jr., W. B. I. *science* 2002, *297*, 2243.

(71) Carp, O.; Huisman, C. L.; Reller, A. *Prog. Solid St. Chem.* 2004, *32*, 33.

(72) Morris Hotsenpiller, P. A.; Bolt, J. D.; Farneth, W. E.; Lowekamp, J. B.; Rohrer, G. S. *J. Phys. Chem. B* 1998, *102*, 3216.

(73) Lowekamp, J. B.; Rohrer, G. S.; Morris Hotsenpiller, P. A.; Bolt, J. D.; Farneth, W. E. *J. Phys. Chem. B* 1998, *102*, 7323.

(74) Ushiroda, S.; Ruzycki, N.; Lu, Y.; Spitler, M. T.; Parkinson, B. A. *Journal of the American Chemical Society* 2005, *127*, 5158.

(75) Diebold, U.; Lehman, J.; Mahmoud, T.; Kuhn, M.; Leonardelli, G.; Hebenstreit, W.; Schmid, M.; Varga, P. *Surf. Sci.* 1998, *411*, 137.

(76) Nakamura, R.; Ohashi, N.; Imanishi, A.; Osawa, T.; Matsumoto, Y.; Koinuma, H.; Nakato, Y. *J. Phys. Chem. B* 2005, *109*, 1648.

(77) Diebold, U. *Surf. Sci. Rep.* 2003, *48*, 53.

(78) Sasahara, A.; Pang, C. L.; Onishi, H. *J. Phys. Chem. B* 2006, *110*, 4751.

(79) Efros, A. L.; Rosen, M. *Physical Review Letters* 1997, *78*, 1110.

Chapter 6. Exciton Quenching and Suppressed Blinking Dynamics of Single Quantum Dots on ITO

6.1 Introduction

Colloidal semiconductor nanocrystal quantum dots (QD) have become more attractive recently due to their many applications in developing QD-based devices, such as quantum dot light emitting devices (LED) [1,2] and solar cells.[3-5] The QD fluorescence and interfacial charge transfer properties are important factors that control the performance of these QD-based devices. Unlike molecular chromophores, previous studies have shown that single QDs exhibit strong fluorescence intermittence (known as "blinking"),[6-33] which is attributed to the photoinduced charging of QDs by charge transfer to trap states in QDs and the surrounding matrix. The blinking activity can affect or be affected by the environment as well as reactions involving the QDs. However, it still remains unclear how the fluorescence properties of single QDs are affected under a device environment.

The blinking of QDs can be affected by interfacial electron transfer (ET), and the correlation between blinking and interfacial ET has been recently investigated.[34-36] For QDs on TiO_2 nanoparticle thin films, the blinking of single QDs led to intermittent ET dynamics, while at the same time, the presence of ET enhanced the blinking acitivity.[35] A similar correlation has also been observed for QDs with adsorbed electron acceptors.[34,36]

QD blinking can also be affected by the environment. Since blinking has been consider an intrinsic limitation in many applications of QDs, there have been many

efforts to design novel QD structures and schemes for suppressing the blinking activity.[10,25-27,29,31-33,37] One strategy is to alter the environment and the surface coating materials of QDs. For example, a near complete suppression of QD blinking in *β*-mercaptoethanol (BME) solutions has been reported previously. The mechanism of the observed blinking suppression was suggested to be the elimination of charged QDs by electron transfer from the thiol moiety in the solution.

An important component of most QD-based devices is the indium tin oxide (ITO) thin film, used for its good electric conductivity and optical transparency. Studying the blinking dynamics of single QDs on ITO is essential to the understanding of fluorescence properties of QDs in a device environment. Since ITO is n-doped In_2O_3, two phenomena are expected for QDs adsorbed on it. First, photoinduced interfacial ET from QDs to ITO is energetically allowed because of the lower conduction band edge of ITO. Secondly, as an n-doped semiconductor, the Fermi level of ITO is near its conduction band edge and higher than that of a neutral QD. When these materials are in contact, the equilibrium of their Fermi levels will lead to the formation of negatively charged QDs. For example, a recent ensemble average measurement has shown that under external bias, QDs on ITO can be charged and their exciton lifetimes can be greatly reduced.[38]

How will the QD blinking activity be affected by ITO, on which both interfacial ET and charging can occur? To address this question, we have studied exciton quenching dynamics of single QDs adsorbed on ITO-coated cover slips and compared them with those on glass and In_2O_3 nanocrystalline thin films. We report in this chapter that for single QDs on ITO, the exciton lifetimes are significantly shortened and their blinking

activities are dramatically suppressed. The possible origins of the observed phenomena will be discussed.

6.2. Results

The ITO glass cover slips (15-30 ohms, 18×18 mm^2, ~10% doping) used in this study were purchased from SPI Supplies. The ITO films were first washed by 2-propanol, dried in air and rapidly scanned over a flame for a few seconds to remove any adsorbed organic materials before use. The flame treatment process did not change the resistance of ITO. The CdSe core multi-shell ($CdS_{3ML}ZnCdS_{2ML}ZnS_{2ML}$) QDs used in this study are the same as in chapter 2. Their lowest energy exciton absorption band is at 605 nm. As have mentioned in the introduction, for QDs on ITO both interfacial ET and charging of QDs can occur. To examine these two effects, the QDs on ITO are compared with those on glass and In_2O_3 which is the intrinsic semiconductor of ITO (Sn doped In_2O_3). Three samples were then prepared by spin coating QD heptane solutions on ITO, glass and In_2O_3 nanocrystalline thin film. The fluorescence intensity and lifetime trajectories were recorded for 47, 45, and 50 single QDs on ITO, glass, and In_2O_3, respectively. Intensity trajectories, i.e. count rates as a function time, were constructed by binning the detected photons within a 50 ms window. The delay time histograms constructed from photons within a 0.5 s bin time were fit by single exponential decay to obtain their lifetimes along the trajectories. Figure 6.1 shows typical fluorescence intensity and lifetime trajectories of single QDs on these substrates. The remaining trajectories for single QDs on ITO and In_2O_3 are shown in the Appendix 1 and 2, respectively. Compared with QDs on glass and In_2O_3, single QDs on ITO exhibit very different fluorescence and lifetime properties. The differences are discussed below.

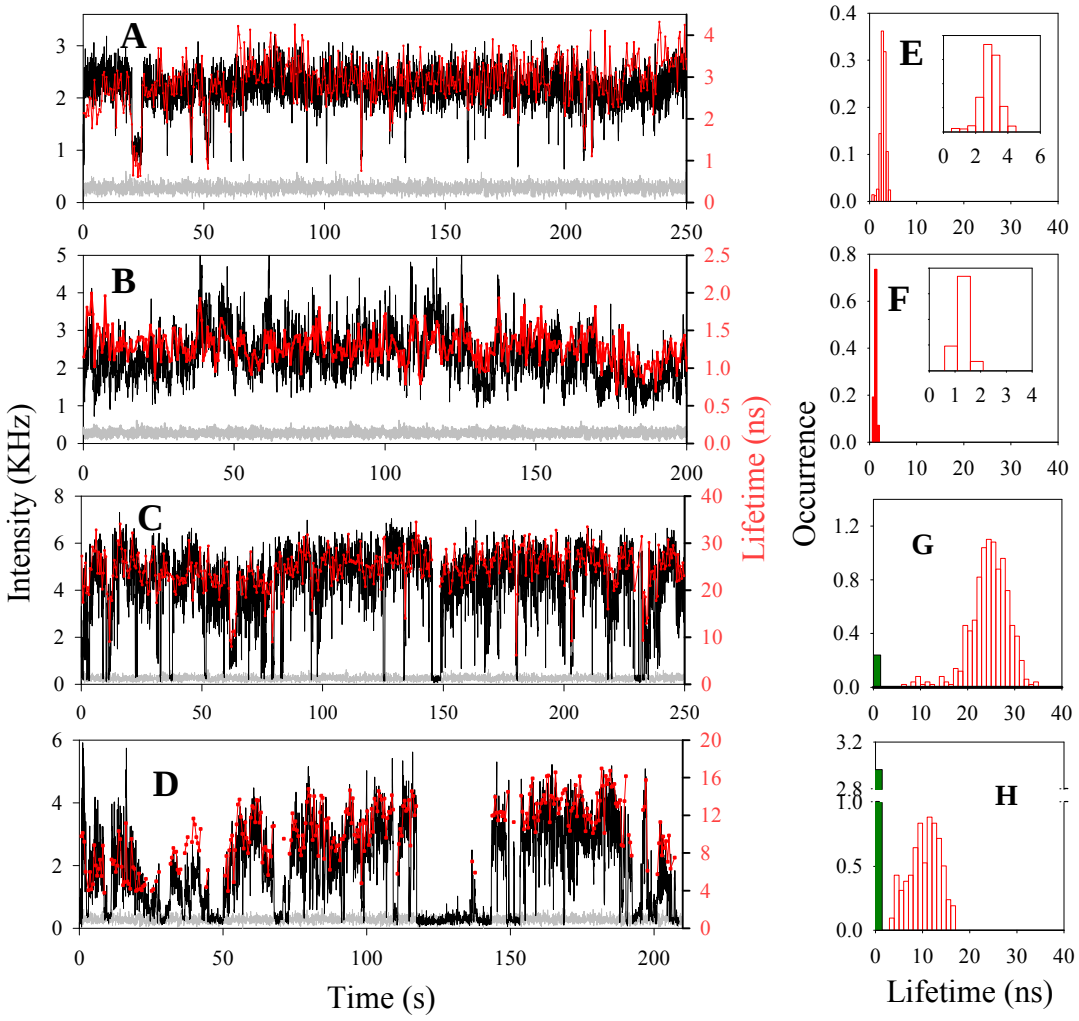

Figure 6.1. Typical fluorescence intensity (black) and lifetime (red) trajectories of single CdSe/CdZnS QDs on (A and B) ITO, (C) glass and (D) In_2O_3. The grey trajectories indicate the background levels. The lifetime histograms of the QDs in A, B, C and D are plotted in panel E, F, G and H, respectively. In panel E and F, the insets show the expanded view of the data at short lifetimes. Green bars in panel G and H indicate the occurrence of points with background intensity levels, for which the lifetime is assumed to be < 0.25 ns.

6.2.1 Suppressed Blinking Dynamics

The first interesting phenomenon observed from QDs on ITO is their significantly suppressed blinking activities. Fluorescence intermittence (blinking) is a common property of single QDs.[6-29,31] For example, single QDs on glass (Figure 6.1 C) and In_2O_3 (Figure 6.1 D) show strong fluorescence fluctuation between low intensity (background, off state) and high intensity (on state) levels. The off state is attributed to the formation of charged state QD with a hole in its valence band and an electron in trap state or electron acceptor such as TiO_2. However, for QDs on ITO, as shown in Figure 6.1 B and C, the occurrence of blinking events is significantly reduced and the duration of the off state is shortened.

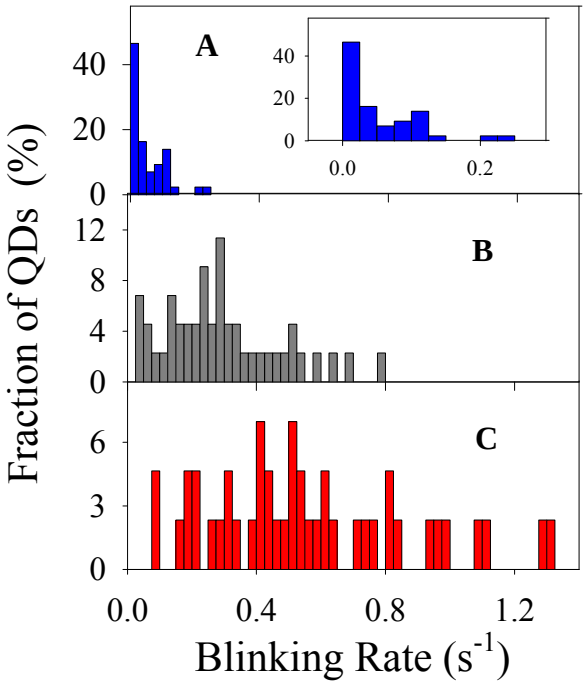

Figure 6.2. Histograms of blinking frequencies of 47 single QDs on ITO (A), 45 single QDs on glass (B) and 50 single QDs on In_2O_3 (C). In panel A, an expanded view of the data are shown in the inset.

To compare the blinking activities of single QDs on different substrates, we have calculated the blinking frequency (number of blinking events per second over 180 second long trajectories) for all measured single QDs. The threshold fluorescence intensity, I_{Th}, separating the on and off states is defined as:

$$I_{Th} = I_{ave.} + 3\sigma \qquad \text{(Eq. 6.1)}$$

where $I_{ave.}$ is the average fluorescence intensity of the background and σ is its standard deviation. A blinking event is defined as a transition between the on and off states. The histograms of blinking frequencies for single QDs on ITO, glass, and In_2O_3 are shown in Figure 6.2 A, B, and C, respectively. For QDs on glass, the blinking frequency is broadly distributed with an average value of 0.30 Hz. On In_2O_3, the single QDs blink more rapidly with an average frequency of 0.56 Hz. However, for QDs on ITO, the average blinking frequency is dramatically reduced to 0.05 Hz and 95% of QDs have a blinking frequency of less than 0.14 Hz.

Furthermore, we have calculated the on and off state probability densities *P(t)* of single QDs according to the following definition:[14]

$$P_i(t) = \frac{N_i(t)}{N_{i,total}} \times \frac{1}{\Delta t_{avg.}} \quad (i = \text{on or off}) \qquad \text{(Eq. 6.2)}$$

where N (t) is the number of on or off events of duration time of t, N_{total} is the total number of on or off events, and Δt_{avg} is the average time between nearest neighbor events (for detail see chapter 4) . As shown in Figure 6.3 A and B, $P_{on}(t)$ and $P_{off}(t)$ of single QDs on different substrates show a power law distribution at short time but exponential decay at long time tails, similar to those reported in the literatures.[6,35,36,39-41] These *P(t)* distributions can be fit by a truncated power law:[17,19-21,39]

$$P_i(t) = B_i t^{-m_i} \exp(-\Gamma_i t) \quad (i\text{= on or off}) \qquad \text{(Eq. 6.3)}$$

where B is the amplitude, m the power law exponent and Γ the saturation rate. The fitting parameters are listed in Table 6.1. Compared to glass, single QDs on ITO have a smaller Γ_{on} and larger Γ_{off}, suggesting increased probability densities of long on events and decreased probability densities of long off events. In fact, no off events with durations of longer than 3 s were observed for QDs on ITO. The blinking dynamics of QDs on ITO is consistent with the suppressed blinking activity observed in their fluorescence trajectories. In contrast, single QDs on In_2O_3 shows smaller probability of long on events and larger probability of long off events than those on glass. The blinking dynamics of QDs on In_2O_3 are similar with that of QDs on TiO_2 which has been discussed in Chapter 5, and is attributed to the presence of ET from QDs to In_2O_3.

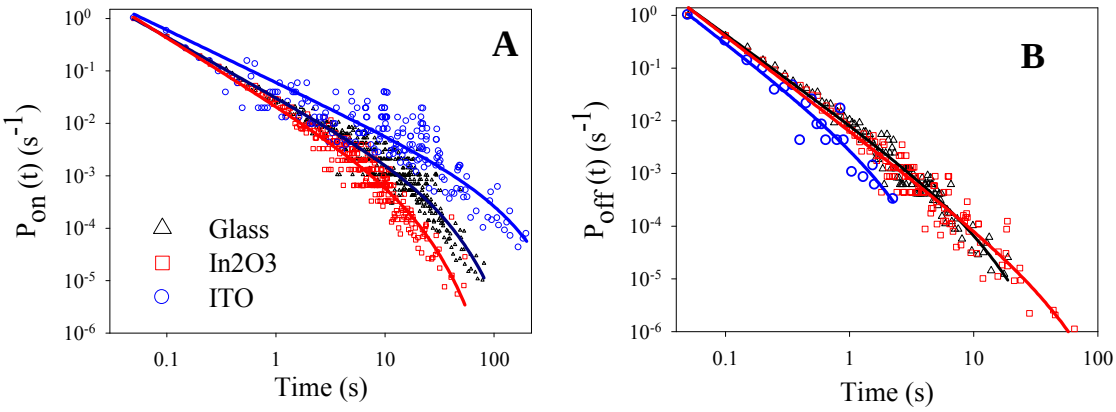

Figure 6.3. Normalized probability density of (A) on states ($P_{on}(t)$) and (B) off states($P_{off}(t)$) all single QDs on ITO (blue circle), glass (black triangle), and In_2O_3 (red square). The solid lines are best fits by Eq. 6.3.

Table 6.1. Fitting parameters of $P_{on}(t)$ and $P_{off}(t)$ for all single QDs on glass, In_2O_3 and ITO. Error indicates one standard deviation.

	m_{on}	$1/\Gamma_{on}$ (s)	m_{off}	$1/\Gamma_{off}$ (s)
QDs on ITO	0.90 ± 0.05	84 ± 18	1.82 ± 0.3	1.7 ± 0.7
QDs on glass	1.15 ± 0.04	28 ± 3	1.70 ± 0.06	10 ± 2
QDs on In_2O_3	1.30 ± 0.05	15 ± 1	1.80 ± 0.07	39 ± 14

6.2.2 Exciton Quenching Dynamics

The second important phenomenon observed from QDs on ITO is their significantly shortened lifetimes. Taking the QDs in Figure 6.1 A~D as examples, their lifetime histograms are plotted in Figure 6.1 E~H, respectively. The lifetimes at background level cannot be accurately determined due to low count rates and were assumed to be < 0.25 ns. The single QD on glass shown in Figure 6.1 C has a broad on state lifetime distribution centered at 23 ns (Figure 6.1 G). However, for the QDs on ITO (Figure 6.1 A and B), the lifetimes are much shorter (with distribution peaks at < 3 ns) and becomes much narrower than QDs on glass and In_2O_3. For these two typical QDs on ITO, there are no lifetime points from background levels because of their suppressed blinking activities.

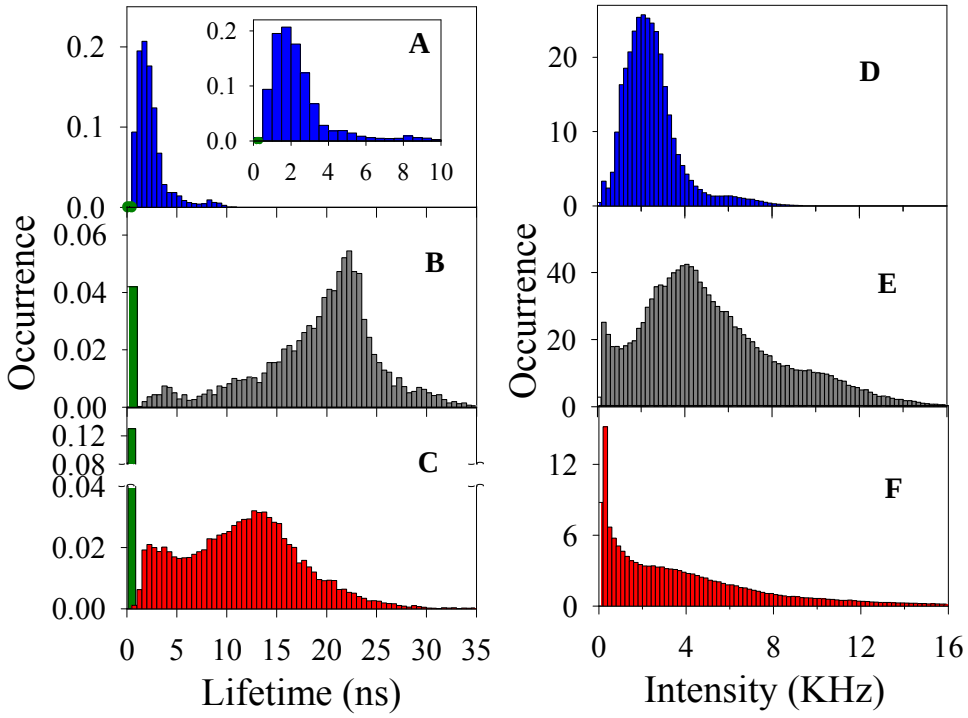

Figure 6.4. Comparison of lifetime and intensity distributions of single QDs on different substrates (47 on ITO, 45 on glass and 50 on In_2O_3). Left panels: the histograms of lifetime trajectories of all single QDs on (A) ITO, (B) glass and (C) In_2O_3. The green bars indicate the occurrence of low intensity points along the trajectories, for which the lifetimes have been assumed to be < 0.25 ns. Middle panels: the histograms of the fluorescence intensity of all studied singe QDs on (D) ITO, (E) glass, and (F) In_2O_3.

Figure 6.4 shows the total fluorescence lifetime and intensity distributions of all studied single QDs on ITO, glass and In_2O_3. The total distributions are constructed by adding up histograms of single QDs. The total lifetime distribution of QDs on glass are consistent with those discussed in chapter 4 and 5, showing an off state peak at shorter lifetime position (events with background fluorescence intensity level) and a broad on state peak centered at ~22 ns. For QDs on In_2O_3, the on state distribution is shifted to

shorter lifetimes with a peak at ~ 14 ns and the amplitude of the off state is increased. For QDs on ITO, their on state lifetime distribution is centered at ~2.5 ns and becomes much narrower. Furthermore, the amplitude of off states becomes negligible, indicating the suppression of blinking. Because of the correlated change of fluorescence intensity and lifetime, a corresponding trend is also observed in the total fluorescence intensity distributions on these substrates. The total intensity histogram of QDs on glass shows broad distribution and two peaks for the on and off states. The on state distribution is broad with peak at a count rate of ~4 KHz (4000 counts per second) and the off state peak is centered at ~400 Hz (background). For QD on In_2O_3, the amplitude of the off state peak becomes much larger and there is no apparent peak position in the on state intensity distribution. The intensity histogram of QDs on ITO shifts to lower intensity level with a peak centered at ~2 KHz. The distribution becomes much narrower, and there is negligible amplitude of off states, indicating again the suppression of blinking activities.

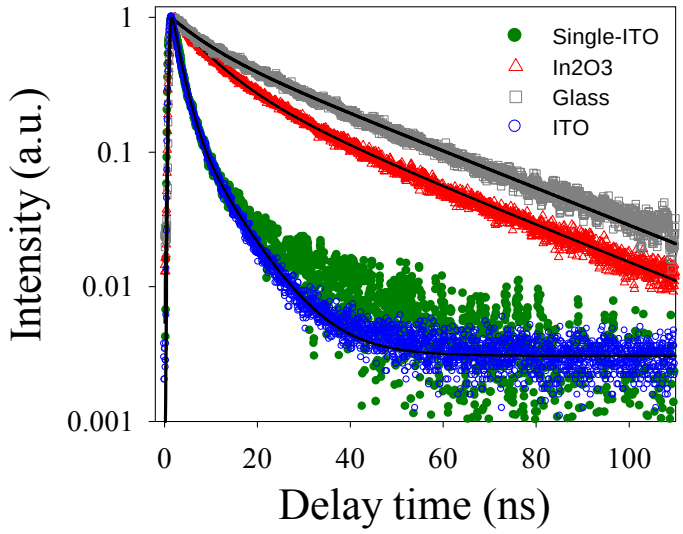

Figure 6.5. Ensemble averaged fluorescence decays of QDs on ITO (blue filled circles), glass (black squares), and In_2O_3 (red triangles). Solid lines are best bi-exponential fits.

The fluorescence decay of the sum of all single QDs on ITO (green open circles) is also shown

To confirm the observations of single QDs measurements, the ensemble-averaged fluorescence decays of QDs on glass, In_2O_3, and ITO are also measured. The ensemble measurements were conducted by using samples with QD coverage level of ~ 10^4 times higher than those in single QD measurements. To avoid repetitive illumination of the same QDs, the samples were raster scanned at a speed of ~100 nm/s during the measurement. As shown in Figure 6.5, ensemble-averaged fluorescence decays of QDs on these substrates follow the same trend of decay rates as observed in single QD measurements. For QDs on glass and In_2O_3, the sums of single QDs decays agree well with the ensemble-averaged decays at long delay times (> 5ns) but show faster components at early delay time, as shown in Figure 6.6. The difference is more pronounced on In_2O_3 than glass due to the presence of ET. Similar differences between the sum of single QDs and ensemble-averaged measurement was observed in our previous comparison of QDs on TiO_2 (see chapter 5).[35] Under single QD conditions, the repetitive illumination of QDs leads to the charging of QDs (off state) by transferring electron to trap states (or electron acceptors),[28] which results in a larger amplitude of fast decay components than the ensemble decay kinetics due to fast Auger relaxation in charged particles. In contrast, for QDs on ITO, the sum of single QD decays agrees well with the ensemble-averaged decay, consistent with the observed much smaller off state contribution in the single QD trajectories. These curves show a slight difference in long delay times, when the photon count is low. This difference is attributed to a higher noise

level in the single QD measurements. The comparison presented here confirms that the observed single QDs are representative of the whole ensembles on these substrates. The decay curves shown in Figure 6.5 can be well fit by bi-exponential functions. The fitting parameters are listed in Table 6.2. The amplitude weighted average time constants ($\tau_{ave.}$) are 22.9 ns on glass, 16.0 ns on In_2O_3 and 3.0 ns on ITO.

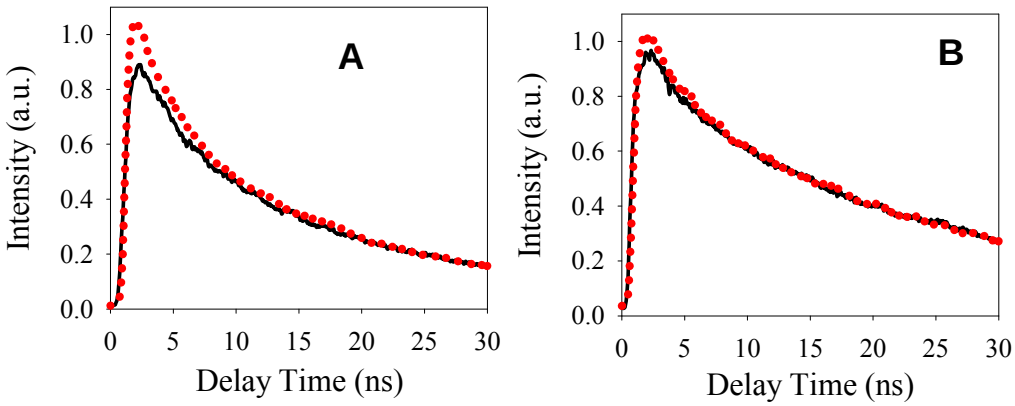

Figure 6.6. Comparison between ensemble-averaged fluorescence decays (black lines) and sum of single QDs decays (red dotted lines) of QDs on In_2O_3 (A) and glass (B).

Table 6.2. The fitting parameters of the ensemble-averaged fluorescence decays of QDs on ITO, glass and In2O3 shown in Figure 6.5. The error indicates one standard deviation.

	A_1	τ_1 (ns)	A_2	τ_2 (ns)	$\tau_{ave.}$ (ns)
on glass	0.36 ± 0.005	7.5 ± 0.15	0.64 ± 0.006	31.5 ± 0.18	22.9 ± 0.3
on In_2O_3	0.61 ± 0.007	7.6 ± 0.10	0.39 ± 0.008	29.1 ± 0.35	16.0 ± 0.4
on ITO	0.85 ± 0.004	2.0 ± 0.01	0.15 ± 0.004	8.7 ± 0.18	3.0 ± 0.2

6.3 Discussion

6.3.1 Charging of QDs on ITO

The QDs used in this study have a first exciton peak at 605 nm. They are the same as in the study of QD-F27 complex discussed in Chapter 4. The estimated valence and conduction band potentials are +1.03 V and -0.85 V (vs. SCE), respectively.[42-44] The conduction and valence band potentials of In_2O_3 at pH=7 are at -0.4 V and 2.1 V (vs. SCE), respectively.[45] The energy diagram of QD and In_2O_3 (ITO) are shown in Figure 6.7 A. The offset of conduction band edge positions in In_2O_3 and QD should enable photo-induced electron transfer from excited QDs to In_2O_3. ET from dye molecules (with excited state potentials similar to the QDs) to In_2O_3 nanocrystalline thin films has been observed previously.[46,47] Furthermore, ET from similar CdSe core multi-shell QDs to TiO_2 nanoparticles has also been reported and verified in CdSe/TiO_2 based solar cells.[4,48-51] For these reasons, we attribute the shorter lifetimes of QDs on In_2O_3 to ET from QD to In_2O_3. The observed blinking (Figure 6.3) and exciton quenching dynamics (Figure 6.4) of QDs on In_2O_3 are very similar as those of QDs on TiO_2, suggesting that QDs on In_2O_3 also follow intermittent ET dynamics modulated by blinking of QD. The presence of ET provides additional pathway to generate charged QDs and hence reduced the long on state probability. An average ET rate is estimated to be 1.9×10^7 s^{-1} for QDs on In_2O_3 by comparing the ensemble-averaged lifetimes on glass and In_2O_3. This ET rate is similar to those for the similar QDs on TiO_2.[35]

The conduction and valence band potentials for ITO are similar to those for In_2O_3.[45] However, their Fermi levels are different. The electron density is estimated to be

~2.2×10^{21}/cm^3 for a 10% doping ITO.[52] The Fermi level of the ITO film could then be calculated by[53]

$$E_f = E_i + kT\ln\left(\frac{N}{N_i}\right) \qquad \text{(Eq. 6.4)}$$

where E_f and E_i are the Fermi energy of the doped (ITO) and intrinsic (In_2O_3) semiconductor, N is the electron density of ITO, N_i is the conduction band electron density of the intrinsic semiconductor, k is the Boltzmann constant and T is the temperature. E_i is assumed to be at the middle of the band gap for In_2O_3. N_i can be calculated by[54]

$$N_i(T) = 2.5\left(\frac{m_c m_v}{m_0^{\,2}}\right)^{3/4}\left(\frac{T}{300K}\right)^{3/2}\exp\left(-\frac{E_g}{2kT}\right)10^{19}\,cm^{-3} \qquad \text{(Eq. 6.5)}$$

where E_g is the band gap energy of the semiconductor, m_c and m_v is the effective mass of the conduction band electron and valence band hole, respectively, and m_0 is the mass of electron. Taking E_g = 2.5 eV,[45] m_c = 0.3 m_0, m_v = 0.6 m_0 for In_2O_3,[55] N_i is calculated to be ~4.95×10^{-3} cm^{-3} at 298 K. Taking E_i = ~0.9 eV (vs. SCE), N = 2.2×10^{21} cm^{-3}, the Fermi level of ITO, E_f, is estimated to be ~100 meV higher than its conduction band edge. The energy levels of ITO are shown in Figure 6.7.

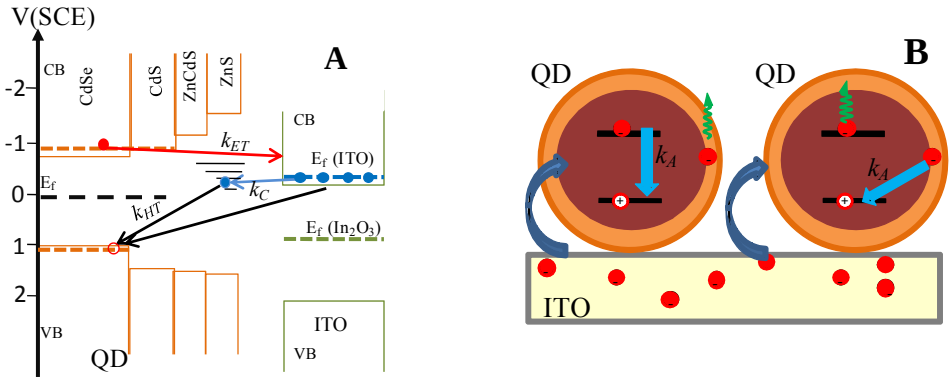

Figure 6.7. (A) A schematic diagram of relevant energy levels for possible electron transfer pathways between QDs and ITO and In_2O_3. k_{ET} indicates electron transfer from QD to ITO(or In_2O_3), k_{HT} indicates hole transfer processes on ITO, and k_c indicates charging of QDs on ITO. (B) Proposed Auger relaxation processes in a negatively charged QD on ITO.

According to the relevant energy levels of QDs and ITO in Figure 6.7 A, the interfacial ET from QDs to ITO is energetically allowed. A previous study of ET from adsorbed molecules to ATO (Sb doped SnO_2) has shown that the ET rate was independent of the doping levels and was similar to that in un-doped SnO_2.[56] Although the Fermi level in ITO is close to its conduction band edge, only states near the band edge are filled. Most conduction band states are unoccupied and the density of electron accepting states for ET from QDs should not be significantly smaller than QD/In_2O_3. For this reason, we assume that the ET rate from QDs to ITO is similar to that in QD/In_2O_3. However, the observed average lifetime for QDs on ITO is significantly faster than on In_2O_3, suggesting that the fast quenching of QD excitons cannot be attributed to ET from QDs to ITO. The n-doped ITO must provide additional quenching pathways that are not available on In_2O_3 or glass and correspond to the observed shortening lifetimes.

6.3.2 Fluorescence and Lifetime Dynamics in Charged QDs

We then examine the charging effect of QDs on ITO. Because of the higher Fermi level in ITO than QDs, when they come in contact, electrons in ITO will be transferred to QDs until their Fermi levels are equilibrated. As a result, QDs will become negatively charged. A recent study of CdSe/CdS core/shell QDs on ITO showed the formation of negatively charged QDs under negative bias voltage. [38] As the bias voltage increased, the Fermi level of ITO was higher, and the QDs became more negatively charged. Under our experimental conditions, there is no applied external bias, and the initial Fermi level of ITO is below the conduction band edge of the QDs. The electrons in the negatively charged QDs likely fill in the trap states below the conduction band edge.

We speculate that these trapped electrons can also provide two non-radiative pathways to quench the QD excitons:

(1) *Fast Auger relaxation.* As shown in Figure 6.7 B, the optical excitation of the negatively charged QDs on ITO produces negative trions (an exciton and an electron), whose lifetimes are shorter than single excitons in neutral QDs due to the presence of Auger relaxation pathway involving the additional electron. This assignment is supported by the previous studies of ensemble-averaged fluorescence decays of QDs on ITO under negative bias voltage. It was reported that fluorescence lifetimes of QDs decreased with increased negative bias and the trion lifetimes of 700~1500 ps were determined.[38] In our experimental condition (without bias voltage), the observed average lifetimes for QDs on ITO is about 3 ns, suggesting that these Auger relaxation processes is slightly slower than those reported for negative trions.[38]

(2) *Charge recombination.* The fast quenching of QD excitons on ITO can also caused by charge recombination (hole transfer k_{HT} in Figure 6.7 A) between the additional electron in trap state or electrons in ITO conduction band and the hole in QD valence band, as shown in Figure 6.7 B. For intrinsic semiconductors, the charge recombination process occurs after ET and the recombination time are normally on ns to μs time scale. However, for n-doped ITO the presence of the electrons in the ITO conduction band and the additional electrons in trap states of QD can facilitate the charge recombination process, shortening the lifetimes. The effect of Fermi level change on charge transfer and recombination has been investigated in dye/TiO_2 complexes by varying the external bias, indicating an enhanced charge recombination rate as the Fermi level of TiO_2 was increased.[57,58] Furthermore, previous studies about ET dynamics from sensitized dye molecules ($ReClPO_3$) to ATO have shown that the charge recombination rate was enhanced as the doping level increased.[56] We currently measure the exciton quenching dynamics of the same QDs on ATO with different doping levels. Preliminary results have shown that shorter lifetimes of QDs on ATO are not able to be attributed to the ET from QDs to ATO. Further insight into the origin of exciton quenching of QDs on n-doped substrate will be provide by using transient absorption spectroscopy.

It is believed that in the off-state, QDs are charged and its excitons are non-emissive due to fast Auger relaxation process involving the additional charge.[6-29,31] A direct measurement of QDs under optical illumination show that QDs become positively charged.[7] A recent study of the lifetime and emission of intensity of negative trions show that negatively charged QDs are optically bright and cannot account for the off state of

single QDs.[38] These studies suggest that in off states QDs are positively charged. For the QDs on ITO, the holes are short lived due to fast hole transfer processes to either the trapped electrons in the negatively charged QD or to ITO, inhibiting the formation of the off state. It should be noted that suppression of blinking has also been reported for QDs in a reducing solution environment, which also provides electron source to remove any long-lived holes in the QD.[26,29] Furthermore, in contact with the ITO, the charges of the QDs are likely maintained at a constant level because of Fermi level equilibration. For this reason, charging-induced non-radiative decays should remain constant, which may be the reason for the small variations of intensity and lifetime throughout the trajectories and among different QDs on ITO.

Suppression of blinking and reduction of lifetime have also been observed for single QDs on nanostructured metal substrates.[10,37,59] In those cases, the reduction of lifetime is accompanied by an increase of fluorescence intensity, suggesting an enhancement of radiative decay rates. This has been attributed to the enhanced electromagnetic field strength on roughened metal surfaces. The suppression of blinking of QDs may be caused by the shortening of ionized period through fast charge recombination process, and/or the enhancement of radiative decay rate which enables the observation of charged QDs. For single QDs on ITO, the shortenned fluorescence lifetime is accompanied by a decrease of fluorescence intensity. This result suggests that the main effect of ITO is an enhancement of nonradiative decay rate, consistent with the findings by an ensemble average study of negatively charged CdSe/CdS core/shell QDs.[38]

6.4 Summary

The exciton quenching dynamics of single CdSe core multi-shell QDs adsorbed on glass, In_2O_3 and ITO have been compared. A good agreement of the average fluorescence lifetimes determined by single QDs and ensemble-averaged measurements on these substrates was observed, suggesting that the single QDs studied were representative of the ensembles. Single QDs on In_2O_3 showed shorter fluorescence lifetimes and higher blinking frequencies than on glass. These differences can be attributed to the presence interfacial ET from QDs to In_2O_3, and are consistent with previous finding of single QDs on TiO_2. In comparison to glass and In_2O_3, single QDs on ITO showed suppressed blinking activity as well as reduced and more narrowly distributed fluorescence lifetimes and intensity. Due to the high doping level in ITO, the equilibration of the Fermi levels of QDs and ITO led to the formation of negatively charged QDs. We speculate that the Auger relaxation processes in these negatively charged QDs shorten their fluorescence lifetime and suppress their blinking activities. This study shows that the blinking of single QDs can be effectively suppressed on the surface of ITO. This phenomenon may also be observable for other QDs and on different n-doped semiconductors.

References:

(1) Colvin, V. L.; Schlamp, M. C.; Alivisatos, A. P. *Nature* 1994, *370*, 354.

(2) Coe, S.; Woo, W.-K.; Bawendi,M. G.; Bulović, V. *Nature* 2002, *420*, 800.

(3) Huynh, W. U.; Dittmer, J. J.; Alivisatos, A. P. *Science* 2002, *295*, 2425.

(4) Robel, I.; Subramanian, V.; Kuno, M.; Kamat, P. V. *J. Am. Chem. Soc.* 2006, *128*, 2385.

(5) Shalom, M.; Rűhle, S.; Hod, I.; Yahav, S.; Zaban, A. *J. Am. Chem. Soc.* 2009, *131*, 9876.

(6) Shimizu, K. T.; Neuhauser, R. G.; Leatherdale, C. A.; Empedocles, S. A.; Woo, W. K.; Bawendi, M. G. *Physical Review B: Condensed Matter and Materials Physics* 2001, *63*, 205316/1.

(7) Krauss, T. D.; O'Brien, S.; Brus, L. E. *Journal of Physical Chemistry B* 2001, *105*, 1725.

(8) Nirmal, M.; Dabbousi, B. O.; Bawendi, M. G.; Macklin, J. J.; Trautman, J. K.; Harris, T. D.; Brus, L. E. *Nature* 1996, *383*, 802.

(9) Empedocles, S.; Bawendi, M. *Acc. Chem. Res.* 1999, *32*, 389.

(10) Shimizu, K. T.; Woo, W. K.; Fisher, B. R.; Eisler, H. J.; Bawendi, M. G. *Physical Review Letters* 2002, *89*, 117401/1.

(11) Fisher, B. R.; Eisler, H.-J.; Stott, N. E.; Bawendi, M. G. *J. Phys. Chem. B* 2004, *108*, 143.

(12) Chung, I.; Bawendi, M. G. *Phys. Rev. B:* 2004, *70*, 165304/1.

(13) Kuno, M.; Fromm, D. P.; Johnson, S. T.; Gallagher, A.; Nesbitt, D. J. *Phys. Rev. B:* 2003, *67*, 125304/1.

(14) Kuno, M.; Fromm, D. P.; Hamann, H. F.; Gallagher, A.; Nesbitt, D. J. *J. Chem. Phys.* 2001, *115*, 1028.

(15) Kuno, M.; Fromm, D. P.; Gallagher, A.; Nesbitt, D. J.; Micic, O. I.; Nozik, A. J. *Nano Letters* 2001, *1*, 557.

(16) Zhang, K.; Chang, H.; Fu, A.; Alivisatos, A. P.; Yang, H. *Nano Letters* 2006, *6*, 843.

(17) Pelton, M.; Smith, G.; Scherer, N. F.; Marcus, R. A. *Proc. Natl. Acad. Sci. U. S. A.* 2007, *104*, 14249.

(18) Tang, J.; Marcus, R. A. *J. Chem. Phys.* 2006, *125*, 044703/1.

(19) Tang, J.; Marcus, R. A. *J. Chem. Phys.* 2005, *123*, 054704/1.

(20) Tang, J.; Marcus, R. A. *Phys. Rev. Lett.* 2005, *95*, 107401/1.

(21) Tang, J.; Marcus, R. A. *J. Chem. Phys.* 2005, *123*, 204511/1.

(22) Issac, A.; von Borczyskowski, C.; Cichos, F. *Phys.l Rev. B* 2005, *71*, 161302/1.

(23) Schlegel, G.; Bohnenberger, J.; Potapova, I.; Mews, A. *Phys. Rev. Lett.*. 2002, *88*, 137401.

(24) Verberk, R.; van Oijen, A. M.; Orrit, M. *Physical Review B: Condensed Matter and Materials Physics* 2002, *66*, 233202/1.

(25) Chen, Y.; Vela, J.; Htoon, H.; Casson, J. L.; Werder, D. J.; Bussian, D. A.; Klimov, V. I.; Hollingsworth, J. A. *J. Am. Chem. Soc.* 2008, *130*, 5026.

(26) Fomenko, V.; Nesbitt, D. J. *Nano Lett.* 2008, *8*, 287.

(27) Mahler, B.; Spinicelli, P.; Buil, S.; Quelin, X.; Hermier, J.-P.; Dubertret, B. *Nature Materials* 2008, *7*, 659.

(28) Peterson, J. J.; Nesbitt, D. J. *Nano Lett.* 2009, *9*, 338.

(29) Hohng, S.; Ha, T. *Journal of the American Chemical Society* 2004, *126*, 1324.

(30) Efros, A. L.; Rosen, M. *Physical Review Letters* 1997, *78*, 1110.

(31) Wang, X.; Ren, X.; Kahen, K.; Hahn, M. A.; Rajeswaran, M.; Maccagnano-Zacher, S.; Silcox, J.; Cragg, G. E.; Efros, A. L.; Krauss, T. D. *Nat.* 2009, *459*, 686.

(32) Odoi, M. Y.; Hammer, N. I.; Early, K. T.; McCarthy, K. D.; Tangirala, R.; Emrick, T.; Barnes, M. D. *Nano Letters* 2007, *7*, 2769.

(33) Hammer, N. I.; Early, K. T.; Sill, K.; Odoi, M. Y.; Emrick, T.; Barnes, M. D. *Journal of Physical Chemistry B* 2006, *110*, 14167.

(34) Issac, A.; Jin, S.; Lian, T. *J. Am. Chem. Soc.* 2008, *130*, 11280.

(35) Jin, S.; Lian, T. *Nano Lett.* 2009, *9*, 2448.

(36) Cui, S.-C.; Tachikawa, T.; Fujitsuka, M.; Majima, T. *J. Phys. Chem. C* 2008, *112*, 19625.

(37) Ray, K.; Badugu, R.; Lakowicz, J. R. *Journal of the American Chemical Society* 2006, *128*, 8998.

(38) Jha, P. P.; Guyot-Sionnest, P. *ACS Nano* 2009, *3*, 1011.

(39) Wang, S.; Querner, C.; Emmons, T.; Drndic, M.; Crouch, C. H. *J. Phys. Chem. B* 2006, *110*, 23221.

(40) Mandal, A.; Nakayama, J.; Tamai, N.; Biju, V.; Isikawa, M. *J. Phys. Chem. B* 2007, *111*, 12765.

(41) Durisic, N.; Wiseman, P. W.; GruÌˆtter, P.; Heyes, C. D. *ACS Nano* 2009, *3*, 1167.

(42) Huang, J.; Stockwell, D.; Huang, Z.; Mohler, D. L.; Lian, T. *J. Am. Chem. Soc.* 2008, *130*, 5632.

(43) Brus, L. *J. Chem. Phys.* 1983, *79*, 5566.

(44) Brus, L. E. *J. Chem. Phys.* 1984, *80*, 4403.

(45) Erbs, W.; Kiwi, J.; Gratzel, M. *Chemical Physics Letters* 1984, *110*, 648.

(46) Guo, J.; Stockwell, D.; Ai, X.; She, C.; Anderson, N. A.; Lian, T. *Journal of Physical Chemistry B* 2006, *110*, 5238.

(47) Huang, J.; Stockwell, D.; Boulesbaa, A.; Guo, J.; Lian, T. *J. Phys. Chem. C* 2008, *112*, 5203.

(48) Brown, P.; Kamat, P. V. *J. Am. Chem. Soc.* 2008, *130*, 8890.

(49) Farrow, B.; Kamat, P. V. *J. Am. Chem. Soc.* 2009, *131*, 11124.

(50) Kongkanand, A.; Tvrdy, K.; Takechi, K.; Kuno, M.; Kamat, P. V. *J. Am. Chem. Soc.* 2008, *130*, 4007.

(51) Robel, I.; Kuno, M.; Kamat, P. V. *J. Am. Chem. Soc.* 2007, *129*, 4136.

(52) Brewer, S. H.; Franzen, S. *Chem. Phys.* 2004, *300*, 285.

(53) Hunter, L. P. *Intorduction to Semiconductor Phenomena and Devices* 1996 Addison.

(54) Ashcroft, N. W.; Mermin, N. D. *Solid State Physics; Thomson Learning:* 1976.

(55) Hamberg, I.; Granqvist, C. G. *J. Appl. Phys.* 1986, *60*, R123.

(56) Guo, J.; She, C.; Lian, T. *J. Phys. Chem. B.* 2005, *109*, 7095.

(57) Haque, S. A.; Tachibana, Y.; Willis, R. L.; Moser, J. E.; Graetzel, M.; Klug, D. R.; Durrant, J. R. *J. Phys. Chem. B* 2000, *104*, 538.

(58) Haque, S. A.; Tachibana, Y.; Klug, D. R.; Durrant, J. R. *J. Phys. Chem. B* 1998, *102*, 1745.

(59) Ito, Y.; Matsuda, K.; Kanemitsu, Y. *Physical Review B* 2007, *75*, 033309.

Appendix 1. Samples of fluorescence intensity (blue) and lifetime (red) trajectories of single QDs on ITO. Gray lines indicate the background level.

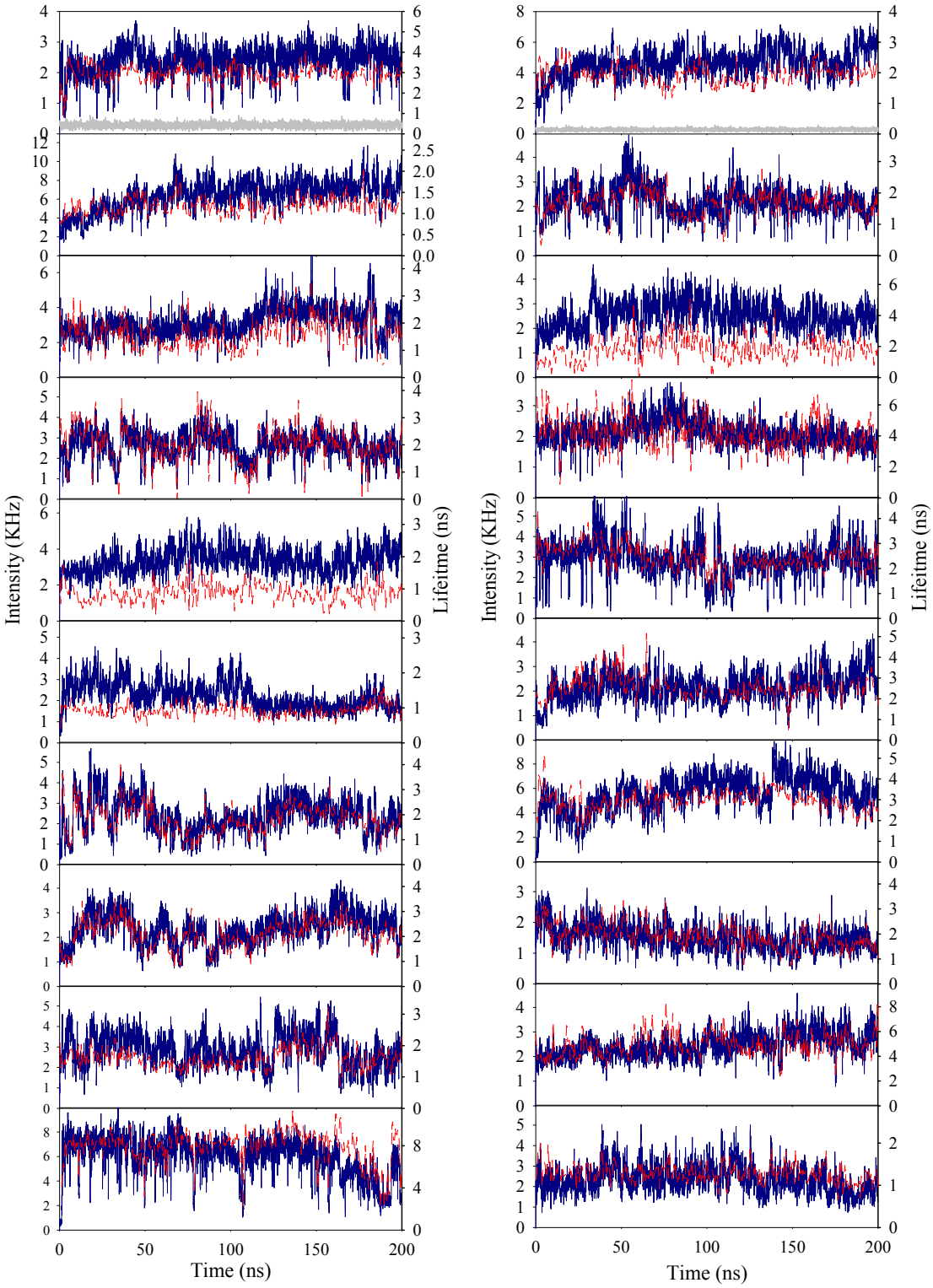

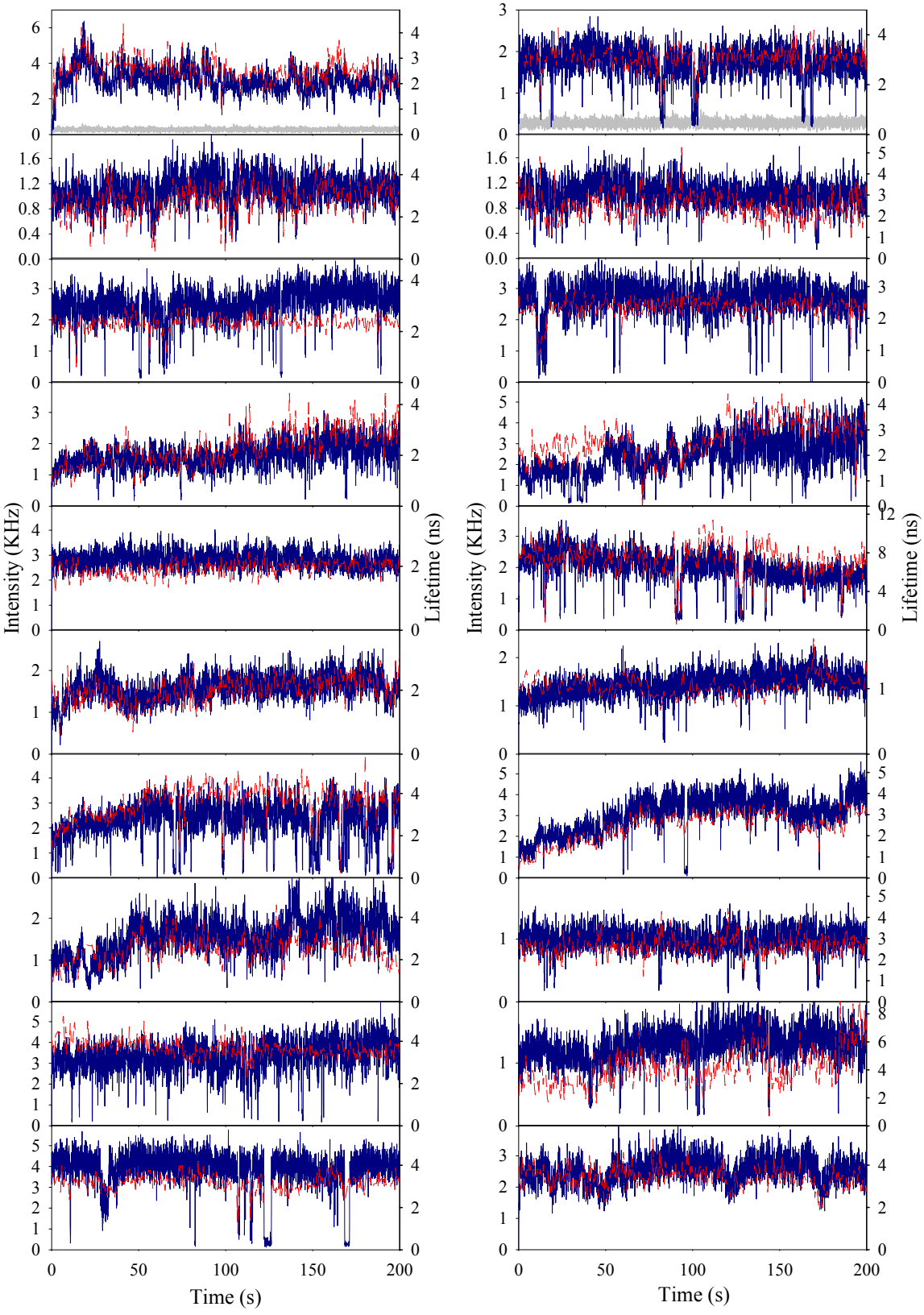
Intensity (KHz)
Lifetime (ns)
Time (s)
0
50
100
150
200

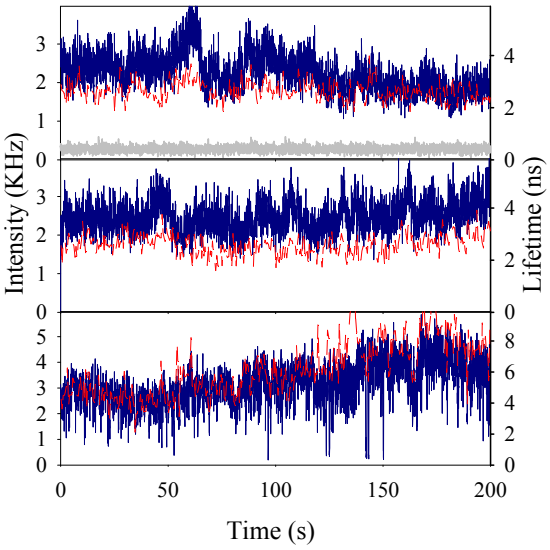
Intensity (KHz)
Lifetime (ns)
Time (s)

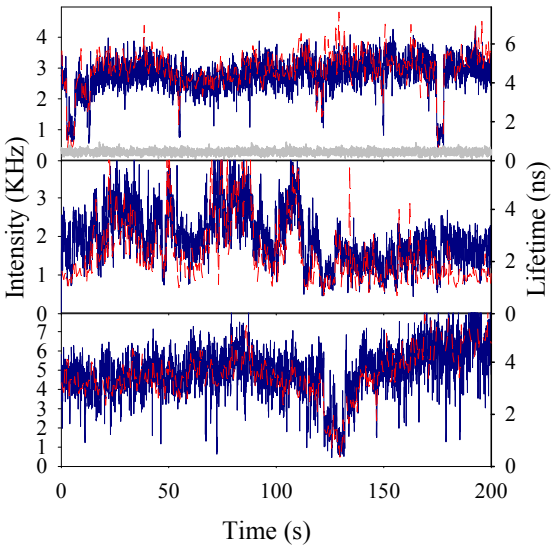
Intensity (KHz)
Lifetime (ns)
Time (s)

Appendix 2. Samples of fluorescence intensity (blue) and lifetime (red) trajectories of single QDs on In_2O_3.

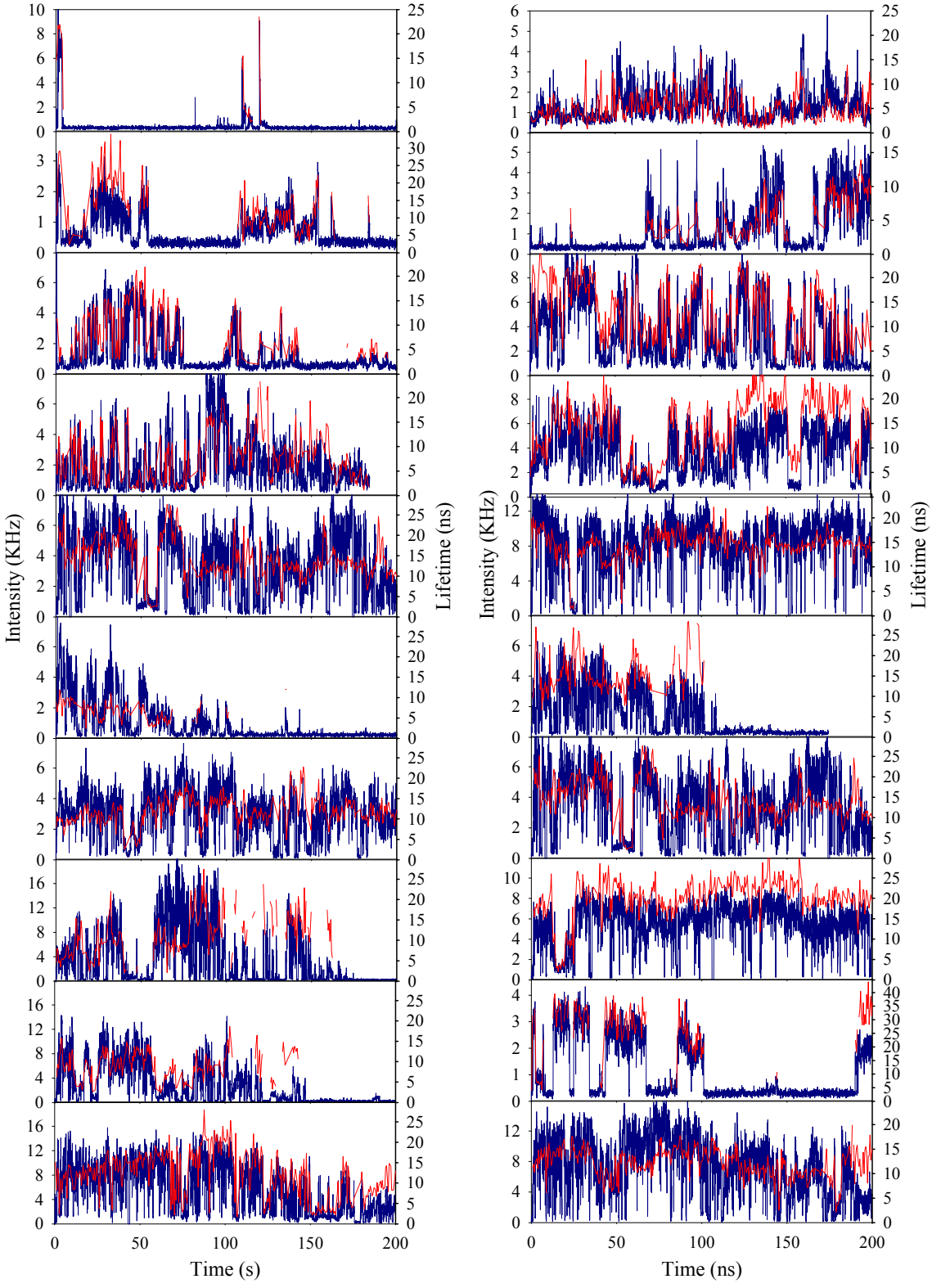

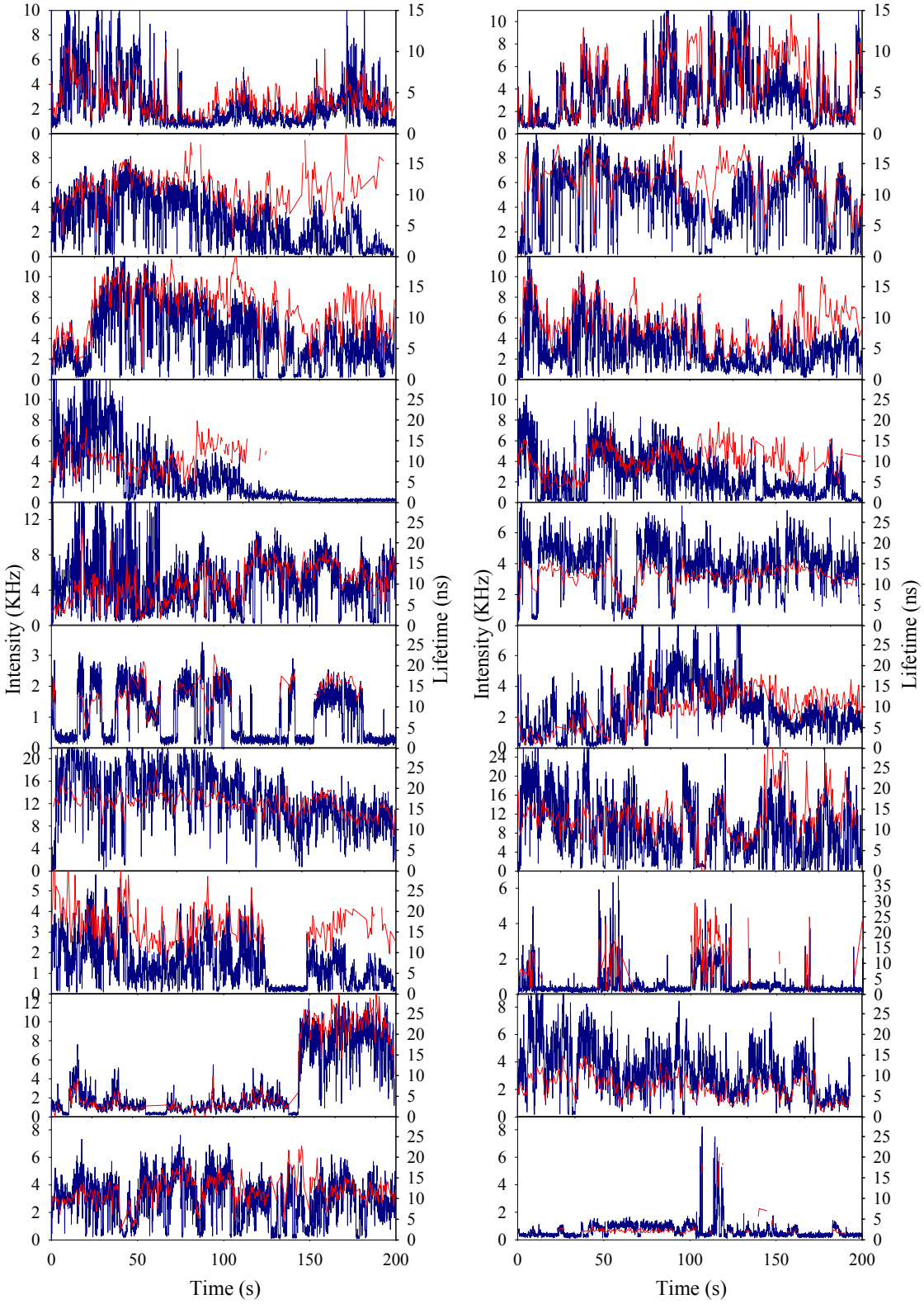
Intensity (KHz)
Lifetime (ns)
Time (s)
Intensity (KHz)
Lifetime (ns)
Time (s)

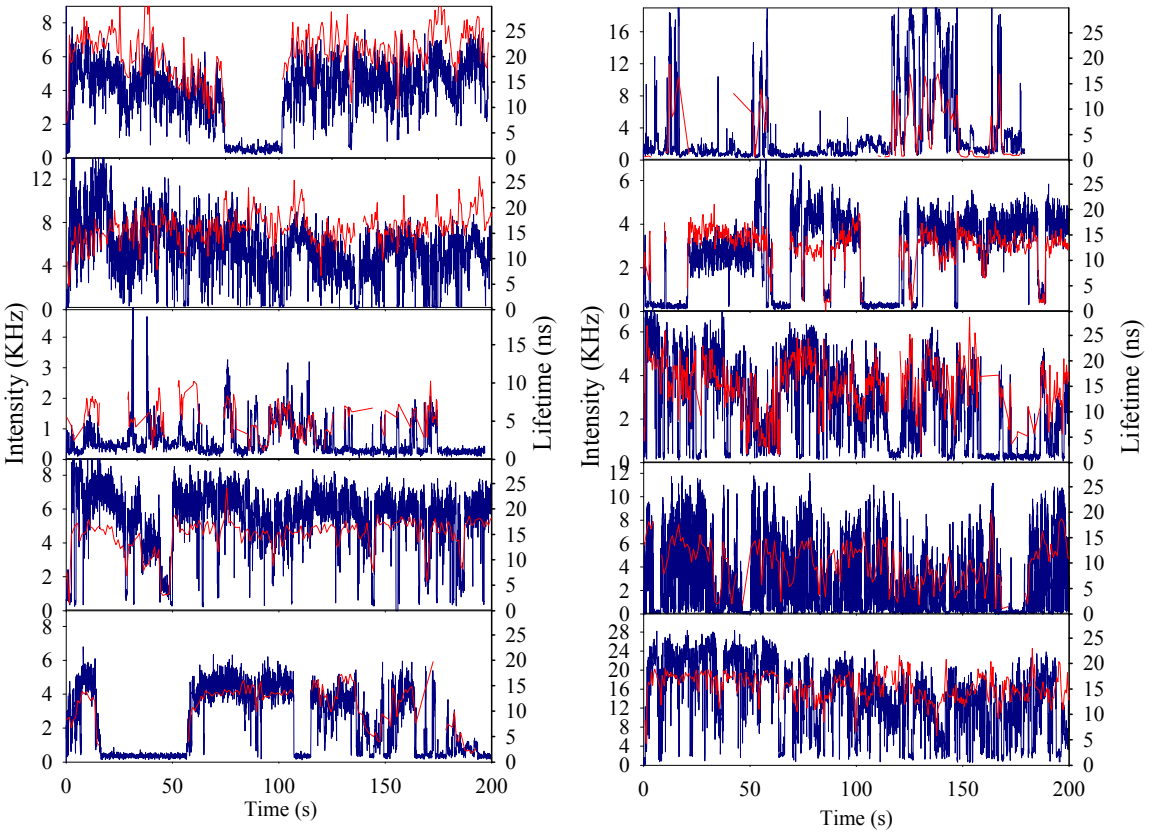
Intensity (KHz)
Lifetime (ns)
Time (s)
Intensity (KHz)
Lifetime (ns)
Time (s)